

Electronic Thesis and Dissertation Repository

---

8-18-2021 9:45 AM

## Fabrication Of Inkjet-Printed Enzyme-Based Biosensors Towards Point-Of-Care Applications

Yang Bai, *The University of Western Ontario*

Supervisor: Yang, Jun, *The University of Western Ontario*

A thesis submitted in partial fulfillment of the requirements for the Doctor of Philosophy degree in Biomedical Engineering

© Yang Bai 2021

Follow this and additional works at: <https://ir.lib.uwo.ca/etd>

---

### Recommended Citation

Bai, Yang, "Fabrication Of Inkjet-Printed Enzyme-Based Biosensors Towards Point-Of-Care Applications" (2021). *Electronic Thesis and Dissertation Repository*. 8003.  
<https://ir.lib.uwo.ca/etd/8003>

This Dissertation/Thesis is brought to you for free and open access by Scholarship@Western. It has been accepted for inclusion in Electronic Thesis and Dissertation Repository by an authorized administrator of Scholarship@Western. For more information, please contact [wlsadmin@uwo.ca](mailto:wlsadmin@uwo.ca).

## Abstract

In the recent years, point-of-care (POC) devices are continuously being demanded in the healthcare field due to the advantages of low-cost, easy-to-use, rapid and on-site detection. Among all kinds of POC devices, electrochemical biosensors are superior candidates because of the miniaturization simplicity, fast analysis and high selectivity nature to the sensing analytes. Traditional fabrication method of electrochemical biosensors by drop-casting process suffers from uneven thickness of functionalization layer and low reproducibility. Nowadays, inkjet printing has been a promising technique for biosensor fabrication. The merits, such as precise position, micro-dispensing, minimum contamination, less waste and potentiality for mass production as valuable features of inkjet printing, have attracted significant attention by researchers. However, there are still some issues that need to be addressed to promote inkjet printing technique for the POC applications. The most important problems include: 1. deficient investigation towards the effect of inkjet printing on the sensing element of biosensor, which is critical for the improvement of the sensor performance; 2. inadequate printing strategy for multi-functional layers printing, which is essential for the development of a stable and sensitive biosensor ; 3. lack of demonstration for the construction of inkjet-printed biosensor system towards point-of-care testing, which will be significant for the development of POC devices.

To bridge these gaps, I firstly studied the influence of mechanical stress on the biological materials of enzymes based on the pressure wave propagation mechanism. Then, based on the first enzyme printing study, a reagentless enzyme-based biosensor was fabricated through a novel multi-layer printing strategy. In the end, to demonstrate the inkjet-printed biosensor

for point-of-care analyte detection, a smartphone-supported biosensor system was constructed, consisting of a smartphone, an Android APP, a portable potentiostat and a functionalized screen-printed electrode (SPE) via inkjet printing.

In general, the investigation of inkjet printing technique towards fabrication of POC devices opens a door for further research and development of an increasing variety of inkjet-printed POC devices. Through the work presented in this dissertation, I thoroughly investigated the effect of printing on enzymes, and substantially build upon the multi-layer printing strategy and biosensor system for inkjet-printed POC devices. The work in this research paves a way toward creating high performance, low-cost, easy-to-use and rapid POC diagnostic devices.

## Keywords

Inkjet printing, point-of-care, enzyme activity, pyruvate oxidase, drop-on-demand printer, mechanical stress, electrochemical sensor, reagentless, screen-printed electrode, saliva phosphate.

## Summary for Lay Audience

Inkjet printing has not only been widely used in our daily life, but also been applied or demonstrated for point-of-care applications. Although some studies have been done for inkjet-printed biosensors, including the development of printing biomaterials, the optimizations of printing formula and the symbolizations of the sensor configuration, etc., issues still exist. For example, the effect of inkjet printing on the biological materials from the aspect of printing mechanism, printing strategies for multi-functional layers printing or complex sensor structure, and realization of inkjet-printed point-of-care applications are still needed to be addressed.

This thesis investigates the influence of printing parameters on the biological materials of enzymes. The results revealed that it is possible to modulate the enzyme activity through settings of printing parameters. Then, the thesis presents an inkjet-printed reagentless biosensor based on the printing strategy of multi-functional layers for analyte detection. Uniform deposition and enhanced electrochemical performance were achieved by the proposed multi-layer inkjet printing method compared to traditional drop-casting method. A linear response which covers the physiological range of serum phosphate was obtained. The proposed simple, affordable, labor-free and reagentless printing strategy can be easily applied to measure other analytes of interest by simply modulating the components of the ink. Additionally, a smartphone-supported inkjet-printed biosensor system was developed for point-of-care analyte detection. The biosensor system is extremely user-friendly that untrained individuals can easily operate. This developed prototype of biosensor system demonstrates a reliable and reproducible biosensor fabrication route for the reference of other POC applications.

## Co-Authorship Statement

This PhD thesis has been carefully prepared by Y. Bai and reviewed by Dr. J. Yang according to the regulations for an integrated article format thesis stipulated by the Faculty of Graduate and Postdoctoral Studies at Western University and has been co-authored as follows:

### **Chapter 3: Study of the enzyme activity change due to inkjet printing for biosensor fabrication**

All the experiments and data analyses were conducted by Y. Bai under the supervision of Dr. J. Yang. The initial draft and following modification of this manuscript were conducted by Y. Bai under the supervision of Dr. J. Yang. The other coauthors contributed to the formation of the final version with discussions and related characterizations. A paper co-authored Y. Bai, D.X. Zhang, Q.Q. Guo, J.F. Xiao, M.Y. Zheng and J. Yang has been published in the *ACS Biomaterials Science & Engineering*, 2021.

### **Chapter 4: An inkjet printing assisted surface functionalization method for enzyme immobilization to develop a reagentless enzyme-based biosensor**

All the experiments and data analyses were conducted by Y. Bai under the supervision of Dr. J. Yang. The initial draft and following modification of this manuscript were conducted by Y. Bai under the supervision of Dr. J. Yang. The other coauthors contributed to the formation of the final version with discussions and related characterizations. A paper co-authored Y. Bai, D.X. Zhang, J.F. Xiao, M.Y. Zheng, Q.Q. Guo and J. Yang has been submitted to *Applied Materials Interfaces*.

## **Chapter 5: Inkjet-printed smartphone-supported electrochemical biosensor system for reagentless point-of-care analyte detection**

All the experiments and data analyses were conducted by Y. Bai under the supervision of Dr. J. Yang. The initial draft and following modification of this manuscript were conducted by Y. Bai under the supervision of Dr. J. Yang. The other coauthors contributed to the formation of the final version with discussions and related characterizations. A paper co-authored Y. Bai, Q.Q. Guo, J.F. Xiao, M.Y. Zheng, D.X. Zhang and J. Yang has been accepted by *Sensors and Actuators B*.

All other chapters are drafted and revised by Y. Bai under the supervision of Dr. J. Yang.

## Acknowledgments

I would like to express my sincere thanks, appreciation and gratitude to my supervisor, Dr. Jun Yang for his unlimited support, professional guidance and exemplary supervision in this research. Thank you for your support and encouragement when I encountered challenges and roadblocks during the study.

Also, I would like to thank my advisor committes, Dr. Jin Zhang, Dr. Ana Luisa Trejos and Dr. Walter Siquera. Many thanks to Dr. Jin Zhang who took time to offer me academic suggestions about writing articles and performing experiments. Also, a lot of thanks to Dr. Ana Luisa Trejos who is really a responsible advisor committee member, any other students would be lucky to have her in the advisor committee. For Dr. Walter Siquera, I really appreciate for his valuable advises to my research.

Then, I would like to thank to my colleagues. The research presented in this thesis could not have happened without their help. I would like to appreciate all generous help from Dr. Dongxing Zhang, Dr. Qiuquan Guo, Dr. Junfeng Xiao, Dr. Xiangyu Yin, Dr. Yue Zhang, Dr. Mingyue Zheng, Dr. Xingxing Liu, Dr. Xiaobin Cai and Dr. Zhandong Huang. I would like to thank Dr. Dongxing Zhang particularly, he is such a patient and considerate man who really helped me a lot every time I was confused and struggling with my study. Other group members also deserve my gratitude for their valuable comments and suggestions. I am also grateful to Dr. Ruizhong Zhang and Dr. Mahdi Hesari to guide me in the right direction in the research. I also thank the staffs from Western Nanofab and Biomolecular Interactions & Conformations Facility for their technical assistance.

Most importantly, I would like to express my heartfelt thanks and love to my family and my friends, first to my parents Lichen and Guiyan, my grandma Wenwei and my friends Chuchu, Liying, Rong and Wei. They encouraged me in every step throughout my PhD study. I am deeply grateful to them and I would not have done it this far without them.

At last, I want to thank for my cat Wazi. She is precious for me and I am blessed to have her be my cat. She is always by my side, no matter I am depressed or happy. Though she will never know how thankful I am to her, I will always love her and take care of her until the last day of her life.



# Table of Contents

Abstract .....	ii
Summary for Lay Audience .....	iv
Co-Authorship Statement.....	v
Acknowledgments.....	vii
Table of Contents .....	ix
List of Tables .....	xiii
List of Figures .....	xiv
List of Appendices .....	xx
Chapter 1 .....	1
1 Introduction .....	1
1.1 Objectives .....	4
1.2 Outline.....	6
Chapter 2.....	10
2 Literature review .....	10
2.1 Biosensor.....	10
2.1.1 History.....	10
2.1.2 Classification of biosensors .....	11
2.1.3 Structure.....	12
2.2 Enzyme-based electrochemical biosensor .....	13
2.2.1 Enzymes .....	14
2.2.2 Enzyme immobilization .....	15
2.3 Biomarkers.....	17
2.3.1 Definition, classification, and application of biomarkers .....	17

2.3.2	Phosphate as the biomarker .....	18
2.3.3	Detection methods of inorganic phosphate.....	19
2.4	Inkjet printing as the biosensor manufacturing technique .....	20
2.4.1	Introduction to inkjet printing.....	21
2.4.2	Ink formula.....	23
2.4.3	Printing parameter.....	24
2.4.4	Inkjet printing enzymes.....	26
2.5	Biosensor system for point-of-care testing .....	28
2.5.1	Screen-printed electrodes.....	29
2.5.2	Portable potentiostat.....	30
2.5.3	APP development.....	31
Chapter 3	.....	39
3	Study of the enzyme activity change due to inkjet printing for biosensor fabrication	39
3.1	Introduction.....	39
3.2	Methods and experiments .....	45
3.2.1	Materials .....	45
3.2.2	Methods.....	46
3.3	Results and discussion .....	50
3.3.1	Effects of wave superposition under different printing frequencies .....	50
3.3.2	Effects of wave amplitude under different printing voltages.....	52
3.3.3	Secondary Structure of Protein after Printing.....	54
3.4	Conclusions.....	58
Appendices	.....	64
Chapter 4	.....	67
4	An inkjet printing assisted surface functionalization method for enzyme immobilization to develop a reagentless enzyme-based biosensor.....	67

4.1	Introduction.....	68
4.2	Materials and methods .....	70
4.2.1	Chemicals and instruments .....	70
4.2.2	Functionalization of the MWCNTs .....	72
4.2.3	Ink formulation .....	72
4.2.4	Functionalization of the working electrode by inkjet printing.....	73
4.2.5	Voltammetric experiments using the proposed biosensor .....	76
4.3	Results and discussion .....	77
4.3.1	Characterization of the functionalized MWCNTs .....	77
4.3.2	Comparison of functionalization performance between of drop-casting and inkjet-printing methods.....	80
4.3.3	Optimization of the sensor .....	85
4.3.4	Evaluation of the modified working electrode.....	94
4.3.5	Phosphate detection by cyclic voltammetry .....	97
4.4	Conclusions.....	102
	Appendices.....	108
	Chapter 5.....	110
5	An inkjet-printed smartphone-based electrochemical biosensor system for reagentless point-of-care analyte detection.....	110
5.1	Introduction.....	111
5.2	Materials and methods .....	113
5.2.1	Chemicals and reagents.....	113
5.2.2	Functionalization of the screen-printed electrode.....	115
5.2.3	APP development.....	115
5.2.4	Testing of the proposed biosensor system. ....	116
5.3	Results and discussion .....	116

5.3.1	Design of the biosensor system.....	116
5.3.2	Design and evaluation of the functionalized working electrode.....	120
5.3.3	Sensing principle and electrochemical performance of the SPE sensor .	122
5.3.4	Demonstration of the proposed biosensor system .....	127
5.4	Conclusions.....	128
	Appendices.....	134
	Chapter 6.....	155
6	Thesis summary and further direction.....	155
6.1	Thesis summary .....	155
6.2	Thesis contribution.....	157
6.3	Future direction.....	158
	Curriculum Vitae .....	160

## List of Tables

Table 2-1: Important cornerstones in the development of biosensors during the period 1970–1992. Reprinted with permission from ref. [5] .....	11
Table 2-2: Main fabrication techniques for electrochemical biosensors: advantages and challenges. Reprinted with permission from ref. [46] .....	21
Table 3-1: Physical properties of the ink at room temperature.....	46
Table 3-2: Printing parameters used in the experiments.....	47
Table 3-3: Relative secondary structure percentage change compared to unprinted enzyme ink. ....	55
Table 4-1: Comparison of electrochemical sensors reported in literature for phosphate detection.....	100
Table 4-2: Detection of phosphate in the artificial serum (n=3).....	102
Table 5-1: Comparison of sensors reported in literature for saliva phosphate detection....	127
Table 5-2: Detection of phosphate using Xenstat portable potentiostat (n=3). ....	128

## List of Figures

Figure 1-1 The overview of the POC devices. Reprinted with permission from ref. [5] .....	2
Figure 1-2 (a) Photograph of glucose biosensors inkjet-printed on paper with a loop on the device geometry/configuration. The device is comprised of 2 printed layers of PEDOT: PSS used as reference, working and counter electrode. (b) Photograph of the fully printed biosensor. (c) 3D exploded schematic of the working electrode with all the separately printed layers, namely the electrode (PEDOT: PSS), the dielectric (SunTronic EMD6415), the biological coating containing the enzyme and the mediator (glucose oxidase and ferrocene), and the encapsulation layer (nafion). (d) Cross sectional SEM image of the working electrode taken using a focused ion beam (FIB). PEDOT: PSS (1), the biological coating (2), and the encapsulation layer (3) are assembled vertically on paper. The scale bar in a and d are 1 cm and 1 $\mu$ m, respectively Reprinted with permission from ref. [8].....	3
Figure 2-1: Types of biosensors that are applied in various fields of engineering Reprinted with permission from ref. [13].....	12
Figure 2-2: Schematic representation of a biosensor. Reprinted with permission from ref. [5] .....	13
Figure 2-3: The monomeric unit of pyruvate oxidase showing the CORE (red), FAD (violet) and TPP (blue) domains. Reprinted with permission from ref. [19] .....	15
Figure 2-4: Common types of enzyme immobilization on electrode surface. Reprinted with permission from ref. [17] .....	16

Figure 2-5: Schematic diagram showing the principles of operation of a continuous inkjet (CIJ) printer. Reprinted with permission from ref. [47] .....	22
Figure 2-6: Schematic diagram showing the principles of operation of a drop-on-demand (DOD) inkjet printing system. Drops are ejected by a pressure pulse generated in a fluid-filled cavity behind the printing orifice. This pressure pulse can be generated by (a) a vapor pocket or bubble generated by a thin-film heater (thermal inkjet) or (b) a mechanical actuation, e.g., from a piezoelectric transducer (piezoelectric inkjet). Reprinted with permission from ref. [47] .....	23
Figure 2-7: Optimized jetting waveform obtained from this work in the Waveform Editor window.....	25
Figure 2-8: Stable droplets in the Drop Watcher window obtained from this work.....	25
Figure 2-9 A photo of typical benchtop instruments for electrochemical analysis. ....	28
Figure 2-10: Schematic of a Dropsens screen printed electrode. Reprinted with permission from ref. [70].....	30
Figure 2-11: The CheapStat, an inexpensive, “do-it-yourself” potentiostat. Reprinted with permission from ref.[70] .....	31
Figure 3-1: A photo of the drop-on-demand printer from FUJIFILM Dimatix, Inc.....	41
Figure 3-2: Schematic of the drop ejection mechanism. Piezoelectric crystal movement driven by the printing waveform and corresponding wave propagation in the printhead chamber. The direction of pressure wave was drawn with red arrow. Segment 1 is the ink fill	

period: ink is drawn from the reservoir to the printhead chamber; Segment 2 is the ink print period: ejection occurs upon the formation of enhanced pressure wave (pressure wave reflected from the reservoir combines with the positive pressure wave); Segment 3 is the recovery period, backward going pressure wave is reflected from the nozzle. .... 42

Figure 3-3: Structure of the printhead chamber showing the piezoelectric crystal, nozzle and ink reservoir. In the green dashed box is the shear stress at the nozzle, In the blue dashed box is the compression stress in the printhead chamber, in the yellow circle is the three-dimensional conformation of pyruvate oxidase. Reprinted with permission from ref. [15].. 43

Figure 3-4: Increase percentage of the enzyme activity and the shear rate after printing under 4, 6, 8, and 10 kHz at 23.6 V (first series). The unprinted enzyme ink was the control group. Enzyme activity was calculated based on the pyruvate oxidase activity assay. Increase percentage of enzyme activity was calculated compared to the unprinted control group. Shear rate was deducted from the droplet velocity. Results represent mean  $\pm$  SEM,  $n = 3$ . .... 51

Figure 3-5: Increase percentage of the enzyme activity and the shear rate after printing under 24, 28, 32 and 36 V at 6 kHz (second series). The unprinted enzyme ink was the control group. Enzyme activity was calculated based on the pyruvate oxidase activity assay. Increase percentage of the enzyme activity was calculated compared to the unprinted control group. Shear rate was deducted from the droplet velocity. Results represent mean  $\pm$  SEM,  $n = 3$ . .. 53

Figure 3-6: Circular dichroism spectra of unprinted pyruvate oxidase ink, sample printed at 24 V and 28 V ( $n = 10$ ). Printing frequency of 6 kHz was used..... 54

Figure 3-7: Circular dichroism spectra of unprinted glucose oxidase ink, sample printed at 24 V and 28 V ( $n = 10$ ). Printing frequency of 6 kHz was used..... 56



Figure 3-8: Circular dichroism spectra of unprinted peroxidase ink, sample printed at 24 V and 28 V (n = 10). Printing frequency of 6 kHz was used. ....	57
Figure 4-1: Schematic diagram for the cross section of the functionalized working electrode. ....	74
Figure 4-2: Schematic of the working electrode functionalization process and the sensor sensing mechanism. ....	74
Figure 4-3: (a) SEM images of the aggregated MWCNTs. (b) SEM images of the MWCNTs-COOH. (c) UV-vis absorption spectra of the MWCNTs solution and the MWCNTs-COOH solution. (d) FTIR of the MWCNTs and the MWCNTs-COOH. ....	78
Figure 4-4: Schematic of the drying process of the droplet on the electrode, side view and top view of the particle distribution status by (a) drop casting method and (b) inkjet printing method. ....	80
Figure 4-5: (a) AFM image of the “coffee ring” effect by drop casting method. (b) AFM image of an area between the center and the “coffee ring” on the working electrode by drop casting method. (c) AFM image of the same area with (b) by inkjet printing method. (d) CV curves of the functionalized electrode fabricated by drop casting method and inkjet printing method in the presence 2 mM phosphate. Scan rate: 50 mV/s. ....	82
Figure 4-6: Effects of the concentration of (a) MWCNTs-COOH, (b) PyOD, (c) FAD, (d) TPP, (e) MgCl <sub>2</sub> , (f) pyruvate, (g) BSA, (h) GLA, (i) Nafion on the oxidation peak current of the cyclic voltammogram obtained from the modified electrode. Phosphate concentration measured was 2 mM. ....	89

Figure 4-7: Effects of the (a) the concentration of the citrate buffer, (b) the pH of the citrate buffer, (c) the pH of the test solution on the oxidation peak current of the cyclic voltammogram obtained from the modified electrode. Phosphate concentration measured was 2 mM..... 93

Figure 4-8: CV curves of bare electrode (solid line), MWCNTs-COOH/substrate/cofactor electrode (dash line), MWCNTs-COOH/enzyme/substrate/cofactor electrode (dot line) in 0.1 M KCl which contained 10 mM K<sub>3</sub>Fe(CN)<sub>6</sub>. Scan rate: 50 mV/s..... 95

Figure 4-9: Potentiometric responses of the sensor to different concentration of phosphate. (a) Concentration increased with the direction of the orange arrow (0.2 to 2.0 mM). (b) Calibration curve for different concentration of phosphate. (c) Interference test. (d) Sensor stability test..... 98

Figure 5-1: User interaction with the proposed biosensor system..... 118

Figure 5-2: (a) Electrochemical measurement using wireless portable potentiostat. The biosensor system includes a smartphone displaying a dynamic curve for the real-time data received through Bluetooth, a portable potentiostat and a modified SPE for analyte detection. (b) Parameter settings for the calibration curve. (c) Settings of the data processing method for the obtained data. (d) The App displays the real-time saliva phosphate concentration on the smartphone..... 119

Figure 5-3: Schematic of the functionalized process of the screen-printed electrodes..... 122

Figure 5-4: Illustration of the detection mechanism of the proposed biosensor system for saliva phosphate detection. .... 123

Figure 5-5: (a) Amperometric responses of the sensor to different concentration of phosphate. Concentration increased with the direction of the orange arrow (from 0 mM to 2 mM). Inset is the calibration curve for different concentration of phosphate. (b) Anti-interference of the biosensor with the existence of  $\text{NO}_3^-$ , Urea, lactic acid and the mixture in the phosphate solution. (c) Different storage condition after 14 days (control group is the current response on the first day). (d) Stability study of the sensor. .... 126

## List of Appendices

Appendix 3-1: Shear rate at different printing parameter. Results represent mean $\pm$ SEM, $n =$ Jetting issues during printing .....	64
Appendix 3-2: Photo taken by the CCD camera. Blocked nozzle: nozzle 1 was blocked with no droplet jetting; satellite drop/fracted drops: droplet from nozzle 2 was fracted to several pieces immediately after jetting; droplet off the track: droplet from nozzle 3 was stable and round around 900 $\mu\text{m}$ but drift off the center line. ....	65
Appendix 3-3: Secondary structure percentage of pyruvate oxidase, glucose oxidase and peroxidase. ....	66
Appendix 4-1: Printing waveforms for enzyme layer (blue line), crosslinking layer (yellow line), and protective layer (red line).....	108
Appendix 4-2: Cost breakdown of the serum phosphate sensor (materials and reagents) ...	109
Appendix 5-1: Ink formula and composition for each printing layer. ....	134
Appendix 5-2: Stable droplet array (Nozzles are positioned at the 0-micron mark, perfect round droplets are shown at the 200-micron mark).....	135
Appendix 5-3: (a) CV curves of bare electrode (black line), enzyme/substrate/cofactor electrode (red line) and MWCNT-COOH/enzyme/substrate/cofactor electrode (blue line) in 0.1 M KCl which contained 10 mM $\text{K}_3\text{Fe}(\text{CN})_6$ . Scan rate: 50 mV/s. (b) Cyclic voltammograms of modified electrode in 0.1M KCL which contained 10 mM $\text{K}_3\text{Fe}(\text{CN})_6$ at	

scan rate of 40, 60, 80 100, 120 mV/s (inset: the plot of peak current vs. square root of scan rates).....	136
Appendix 5-4: Code of the parameter page for settings of the calibration curve .....	137
Appendix 5-5: Code for the Calculation page .....	142

## Glossary of Terms

AFM	atomic force microscope
APP	application
AUNW	gold nanowire
BSA	bovine serum albumin
CB	citrate buffer
CIJ	continuous inkjet
CV	cyclic voltammetry
EDTA	tetrasodium salt hydrate
FAD	flavin adenine dinucleotide
DI	deionized water
DOD	drop-on-demand
GLA	glutaraldehyde
GOD	glucose oxidase
HRP	horseradish peroxidase
MWCNT	multi-walled carbon nanotube
POC	point-of-care
PyOD	pyruvate oxidase
SP	saliva phosphate
SPE	screen-printed electrode
TPP	thiamine pyrophosphate

## Chapter 1

### 1 Introduction

Point-of-care (POC) testing provides the diagnostic or prognostic test on-site to offer immediate results without the requirement of expensive and complicated bench-top instrument, sample pre-treatment or skilled technician. POC biosensors as a kind of miniaturized and portable devices are designed to be used on-site by untrained individuals, providing real-time and remote health monitoring [1, 2]. Figure 1-1 shows an overview of the construction of the POC devices. Among all kinds of biosensors, enzyme-based electrochemical biosensors for POC applications have shown their great potential in the patient diagnosis and healthcare field. Significant progress has been made in POC devices during the past few years from the aspect of microfluidics integration, use of latest nanomaterials, advancement of data analysis and improved connectivity [3, 4].

However, the built-up of such POC biosensors are currently at an early stage just demonstrated in the laboratory. For instance, most of the biosensors are based on the drop-casting method to functionalize the transducer which limits the sensor reproducibility because of the inevitable coffee-ring effect. Moreover, the use of biomaterials and nanotechnology during the fabrication process of POC devices requires precise position and quantitatively functionalization of the electrode. To meet the above requirements, the use of inkjet printing technique as a key manufacturing technology for the POC biosensor fabrication is suggested in this thesis.

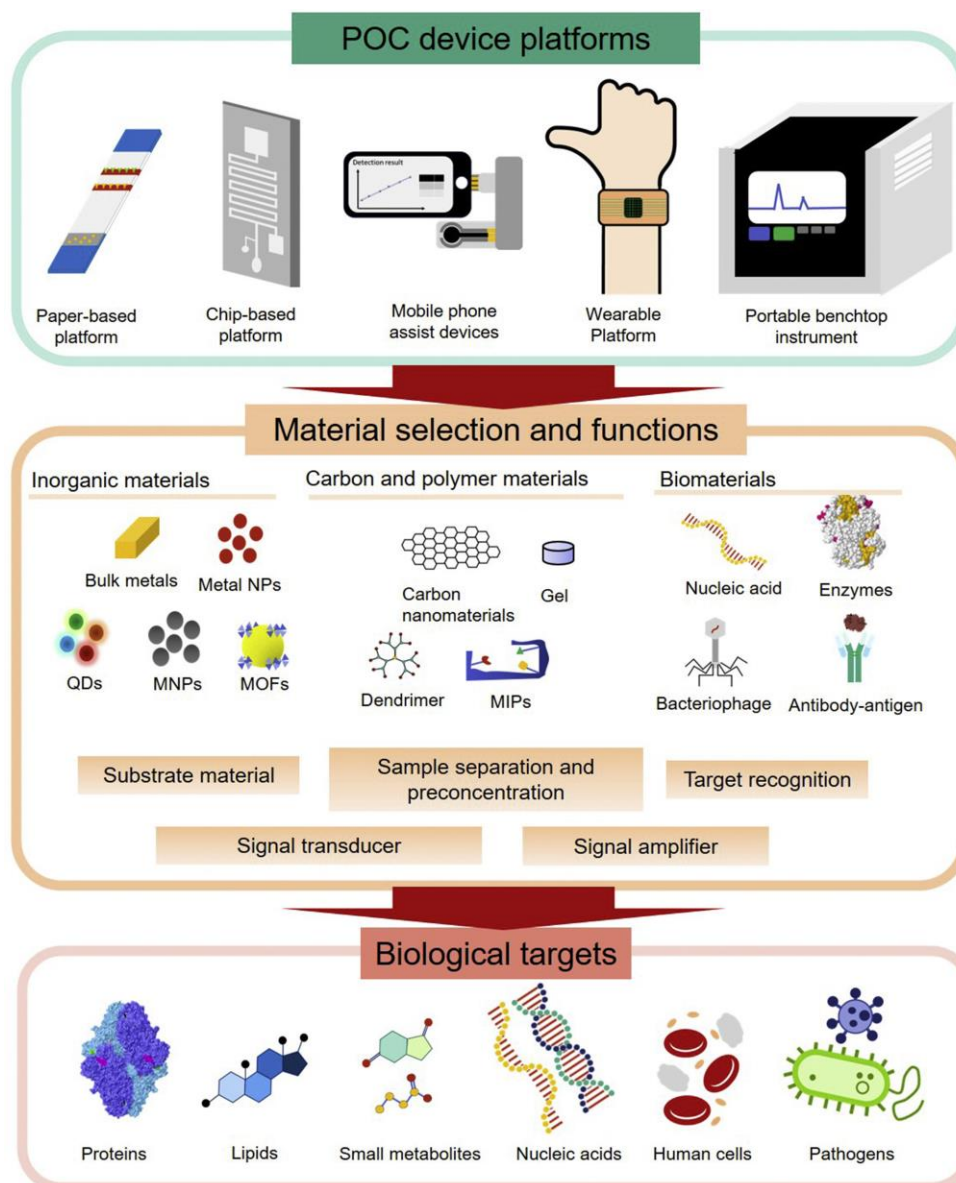


**Figure 1-1 The overview of the POC devices. Reprinted with permission from ref. [5]**

Inkjet printing as a powerful tool combines efficient and customizable manufacturing of biosensors with high resolution, miniaturization and low-cost. With the integration of microfluidic and electronics systems, inkjet-printed enzyme-based biosensors have attracted attention in the fields of POC testing [6, 7]. Till now, various kinds of inkjet-



printed biosensors have been developed. Most of the studies mainly focus on improving the performance of glucose sensor. Research has also been conducted from the aspect of inclusion of novel nanomaterials, printing strategies on different kinds of substrate electrodes, discovery of novel non-enzymatic sensing materials. Printing strategies for the construction of the glucose sensor system is relatively settled. For example, Figure 1-2 presents an all inkjet-printed glucose sensor on a paper substrate. However, a more universal inkjet printing route for the fabrication of complex enzyme-based biosensors (for instance, enzyme with cofactors and coenzymes) is demanded to serve as an example for other inkjet-printed biosensors.

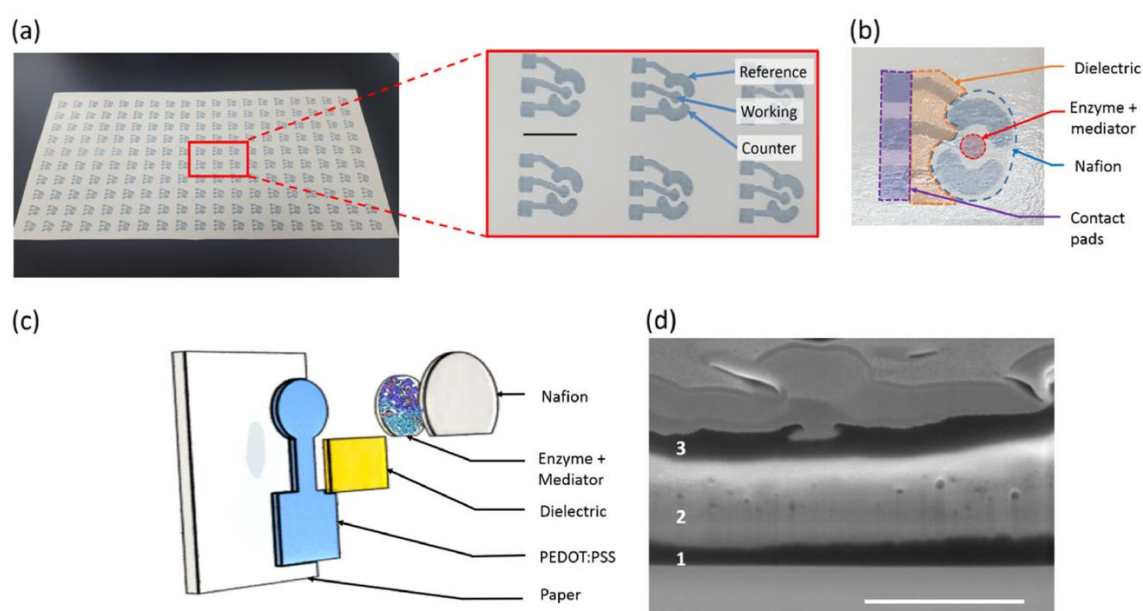


**Figure 1-2 (a) Photograph of glucose biosensors inkjet-printed on paper with a loop on the device geometry/configuration. The device is comprised of 2 printed layers of PEDOT: PSS used as reference, working and counter electrode. (b) Photograph of the fully printed biosensor. (c) 3D exploded schematic of the working electrode with all the separately printed layers, namely the electrode (PEDOT: PSS), the dielectric**

**(SunTronic EMD6415), the biological coating containing the enzyme and the mediator (glucose oxidase and ferrocene), and the encapsulation layer (nafion). (d) Cross sectional SEM image of the working electrode taken using a focused ion beam (FIB). PEDOT: PSS (1), the biological coating (2), and the encapsulation layer (3) are assembled vertically on paper. The scale bar in a and d are 1 cm and 1  $\mu\text{m}$ , respectively Reprinted with permission from ref. [8]**

Moreover, studies are highly demanded for coupling of biosensors and APPs for the built-up of smartphone-based POC biosensor system in pursuit of high reproducibility, user-friendliness, and wide applicability. General inkjet printing route for construction of biosensor system and widely applicable apps for different occasions of electrochemical analysis are of great importance and highly desirable for the development of POC devices. The implementation of such inkjet-printed biosensor system would have great references for constructions of the POC devices.

## 1.1 Objectives

Paving the way towards practical performance of the inkjet-printed biosensor system is necessary in real applications. Therefore, the ultimate goal of this research is to develop an inkjet-printed biosensor system for point-of-care applications. There are specifically three progressive sets of objectives in this thesis.

(1) To investigate the influence of inkjet printing on the biological materials of enzymes from the aspect of the printing mechanism.

- To formulate a biologically stable and reliably printable enzyme-containing bio-ink.

- To investigate the effect of mechanical stress on enzyme activity based on the pressure wave propagation in the printhead chamber.
  - To study the optimal printing parameter which less affect the enzyme activity during printing.
  - To evaluate the impact of the printing process on the secondary structure of the enzymes.
  - To analyze the mechanism that caused potential enzyme activity change.
- (2) To develop novel printing strategy and facile functionalization method for inkjet-printed biosensor fabrication.
- To formulate functional and jettable inks which enable the enzyme immobilization, substrate preloading and evenly dispersed nanomaterials.
  - To optimize the ink component for all three layers in pursuit of highest analytical response.
  - To optimize the operation printing parameters for different layer printing, specifically, printing voltage, printing frequency, drop spacing, substrate temperature, etc.
  - To investigate the morphology and analytical performance of the functionalized inkjet-printed electrode and drop-casted electrode.
  - To evaluate the electrochemical performance of the functionalized inkjet-printed electrode based on the reversible cyclic voltammetry using  $K_3Fe(CN)_6$  solution.
  - To demonstrate the proposed printing strategy by prototyping an inkjet-printed biosensor.
  - To evaluate the performance of the proposed biosensor by linear calibration,

selectivity test and stability test.

(3) to build up an inkjet-printed smartphone-supported biosensor platform for point-of-care analyte detection.

- To design a user-friendly POC biosensor system that can smoothly incorporate functionalized inkjet-printed electrode, smartphone APP and portable potentiostat.
- To develop an APP that researchers can easily adjust the codes or parameters for different occasions and untrained personnel can easily operate and read the results.
- To build up a prototype POC sensor system according to the proposed plan using artificial body fluid.
- To evaluate the analytical performance of the POC biosensor system through linear calibration, selectivity test, stability test and recovery test.

## 1.2 Outline

In what follows, the dissertation will be organized in an outline as six chapters.

In chapter 1, I briefly introduced the background of the study, identified the research opportunities and the motivation of the project. The objectives of the thesis are identified.

In chapter 2, the background information which are necessary for understanding point-of-care biosensing is reviewed, including the basics of biosensors and biomarkers, fundamental information about point-of-care testing.

Chapter 3 presents the change pattern of enzyme activity based on printing mechanism in the bioprinting process. This study investigated the effects of pressure wave propagation

on enzyme activity from the aspects of wave superposition, wave amplitude, resulting mechanical stress, and protein conformation change using pyruvate oxidase as the model enzyme. Mechanical stress increased the activity of pyruvate oxidase during the inkjet printing process. A shear rate of  $3 \times 10^5 \text{ s}^{-1}$  enhanced the activity by around 14%. The enhancement mechanism was proposed that the mechanical activation or mild proteolysis was the major cause to change the enzyme conformation and enzyme activity. The obtained results have also been compared with previously reported bioprinting practices. A comparison of circular dichroism spectra results on different enzymes revealed that the protein structural change varied due to the structure or component of specific protein.

Chapter 4 describes a reagentless biosensor fabricated through inkjet printing functionalization strategy on a screen-printed electrode for biosensing. Three functional layers, consisting of enzyme layer, crosslinking layer and protective layer were subsequently printed on the working electrode after careful optimization of the ink formula and printing parameters to pursue the best optimal sensor performance. A comparison of morphology and analytical performance between traditional drop-casted electrode and our inkjet-printed electrode was presented, more uniform deposition and enhanced electrochemical performance were achieved by inkjet printing method. The analytical results of the proposed sensor have been compared with various biosensors that reported previously. This sensor is applied to demonstrate the detection of inorganic phosphate in the artificial serum.

Chapter 5 demonstrates an inkjet-printed electrochemical enzyme-based biosensor system which can work with the smartphone for the point-of-care analyte detection. Four components of a smartphone, an Android APP, a portable potentiostat and a

functionalized screen-printed electrode form the proposed biosensing system. A prototyping biosensor system for detection of phosphate in artificial saliva is presented. The proposed biosensor system demonstrates a reliable and reproducible biosensor fabrication route that has meaningful reference for similar biosensor systems.

Chapter 6 provides conclusions and a summary of all the results reported in the thesis, as well as directions of future research.

## References

1. Narayan, R.J., *Medical Biosensors for Point of Care (POC) Applications*. 2016: Woodhead Publishing.
2. Wang, C., M. Liu, Z. Wang, S. Li, Y. Deng, and N.J.N.T. He, *Point-of-care diagnostics for infectious diseases: From methods to devices*. *Nano Today*, 2021. **37**: p. 101092.
3. Zarei, M., *Portable biosensing devices for point-of-care diagnostics: Recent developments and applications*. *TrAC Trends in Analytical Chemistry*, 2017. **91**: p. 26-41.
4. Rusling, J.F. and R.J.J.B. Forster, *Biosensors Designed for Clinical Applications*. *Biomedicines*, 2021. **9**(7): p. 702.
5. Manmana, Y., T. Kubo, and K.J.T.T.i.A.C. Otsuka, *Recent developments of point-of-care (POC) testing platform for biomolecules*. *TrAC Trends in Analytical Chemistry*, 2020: p. 116160.
6. Sardini, E., M. Serpelloni, and S. Tonello, *Printed Electrochemical Biosensors: Opportunities and Metrological Challenges*. *Biosensors*, 2020. **10**(11).
7. Costa-Rama, E. and M.T.J.B. Fernández-Abedul, *Paper-Based Screen-Printed Electrodes: A New Generation of Low-Cost Electroanalytical Platforms*. *Biosensors*, 2021. **11**(2): p. 51.
8. Bihar, E., S. Wustoni, A.M. Pappa, K.N. Salama, D. Baran, and S. Inal, *A fully inkjet-printed disposable glucose sensor on paper*. *npj Flexible Electronics*, 2018. **2**(1): p. 30.

## Chapter 2

### 2 Literature review

In this chapter, the background information of the point-of-care biosensors is introduced, including basics of the biosensors, the use of biomarkers, the fabrication methods of biosensors and latest technical support for point-of-care applications. The purpose of this literature review is to provide sufficient information for the analysis and discussions in the following chapters.

#### 2.1 Biosensor

##### 2.1.1 History

Biosensors are the devices that detect the biological or chemical signals and convert them into the measurable electrical signals [1]. It is commonly acknowledged that Leland C. Clark, Jr developed the first biosensor in 1956 for the detection of oxygen [2]. It is until 1975 that the first commercial biosensor was developed by a company named Yellow Spring Instrument (YSI). Various kinds of biosensors were invented during the period of 1970 and 1992 (see in Table 2-1), and they are the foundation for the biosensors nowadays. Remarkable achievements have been made in the field of biosensor since the creation of the i-STAT sensor [3]. Now the field of biosensor is an interdisciplinary research area that covers the subjects of physics, chemistry, materials, biology and engineering [4]. It also involves the fundamentals of nanotechnology, electronics and applicatory medicine [5]. For the past 10 years (2010-2020), there are over 47 000 reports on the topics of biosensors in the database of Web of Science.



**Table 2-1: Important cornerstones in the development of biosensors during the period 1970–1992. Reprinted with permission from ref. [5]**

Year	Development of biosensors
1970	Discovery of ion-sensitive field-effect transistor (ISFET) by Bergveld [6]
1975	Fibre-optic biosensor for carbon dioxide and oxygen detection by Lubbers and Opitz [7]
1975	First commercial biosensor for glucose detection by YSI [8]
1975	First microbe-based immunosensor by Suzuki et al. [9]
1982	Fibre-optic biosensor for glucose detection by Schultz [10]
1983	Surface plasmon resonance (SPR) immunosensor by Liedberg et al. [11]
1984	First mediated amperometric biosensor: ferrocene used with glucose oxidase for glucose detection [12]
1990	SPR-based biosensor by Pharmacia Biacore [7]
1992	Handheld blood biosensor by i-STAT [7]

### 2.1.2 Classification of biosensors

The two most fundamental and widely used categorizations of sensors are physical sensors and chemical sensors. To be more specific, based on the mode of reception, the area of application and the analyte that is measured, biosensors can be classified in magnetic sensors, thermometric sensors, optical sensors, radiation detecting sensors, electrical sensors and electrochemical sensors, etc. They have been extensively studied by researchers [1]. The figure 2-1 demonstrates different types of biosensors that are applied in various engineering fields.

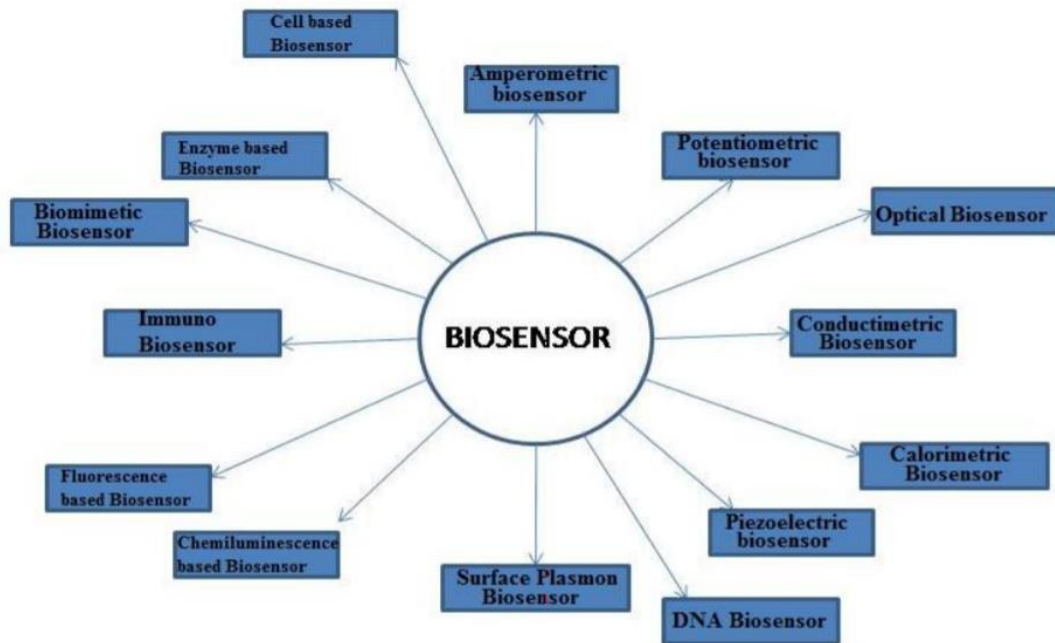


**Figure 2-1: Types of biosensors that are applied in various fields of engineering**  
 Reprinted with permission from ref. [13]

### 2.1.3 Structure

The figure 2-2 shows the schematic representation of a biosensor structure. It mainly includes four parts, namely bioreceptor, transducer, electronics and display. The bioreceptor (enzymes, cells, aptamers, deoxyribonucleic acid, antibodies, etc.) responds to the analyte and generates a signal (light, heat, pH, mass change, etc.) upon their interaction. The transducer connects with the bioreceptor and converts the generated signal into a measurable form. The electronics usually consist of complex electronic circuitry which amplify and convert the transduced signal from analogue into digital form. The output signals will then be presented on the display in the form of numbers, curves, images, etc.

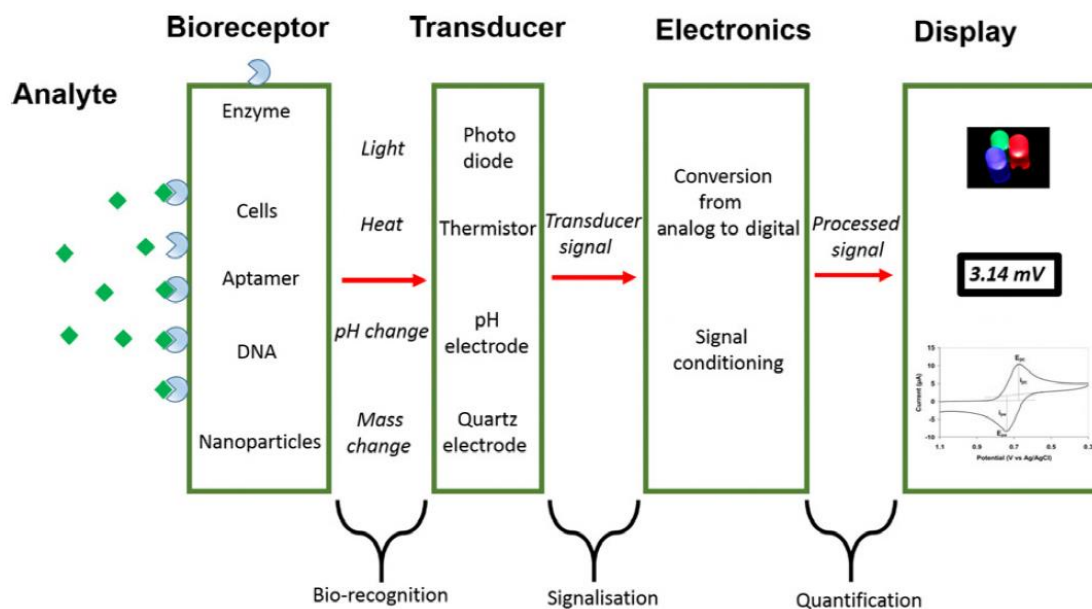


**Figure 2-2: Schematic representation of a biosensor. Reprinted with permission from ref. [5]**

## 2.2 Enzyme-based electrochemical biosensor

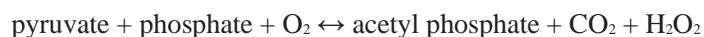
Electrochemical biosensors are the sensing devices that transduce the biochemical events to electrical signals through electron movement on an electrode with immobilized biomolecules [14]. Enzyme-based electrochemical biosensors are the sensors that employ enzymes as the bioreceptors. Enzymes are highly specific toward particular molecules which decide the selectivity of the biosensor. Enzyme-based electrochemical biosensors with the advantages of high selectivity, fast response, easy-to-use and possibility of miniaturization have been widely used in various fields such as health care, clinical diagnosis, environmental assessment, etc [15, 16].

## 2.2.1 Enzymes

Enzymes mainly consist of proteins which are folded into complicated three-dimensional shapes. Enzymes are biological catalysts which can convert specific substances into products. For some enzymes, additional components of cofactors (inorganic or organic compounds) and coenzymes (organic molecules) are required to realized full enzyme activity. Various kinds of enzyme [17] have been used in the enzyme-based biosensors, including the following:

- Oxidoreductases: catalysing oxidation or reduction reactions which can be detected electrochemically
- Transferases: transferring a functional group from one molecule to another
- Hydrolases: catalysing the hydrolysis of various bonds
- Lyases: cleaving various bonds (C-C, C-O or C-N bonds) by means other than hydrolysis and oxidation
- Isomerases: catalysing the addition of a functional group to a molecule to form an isomeric form
- Ligases: catalysing the coupling of two molecules

The model enzyme that I used in the thesis is pyruvate oxidase (PyOD), which belongs to the family of oxidoreductases. PyOD as a multi-substrate, multi-cofactor enzyme catalyzes the following chemical reaction:



PyOD is a tetrameric flavoprotein consisting of thiamine pyrophosphate (TPP), flavin adenine dinucleotide (FAD), a divalent metal ion. The two active sites of the enzymes

located in the interfaces of TPP domain and CORE domain. PyOD-based biosensors have been widely employed in detecting the analyte of inorganic phosphate in the environment and human body fluid [18, 19].

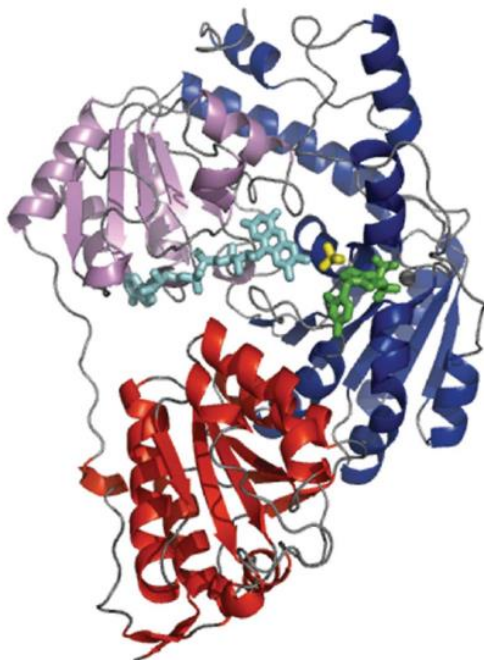


**Figure 2-3: The monomeric unit of pyruvate oxidase showing the CORE (red), FAD (violet) and TPP (blue) domains. Reprinted with permission from ref. [19]**

### 2.2.2 Enzyme immobilization

The enzymes used in the biosensor should be in close association to the transducer. Different enzyme immobilization approaches have been developed to improve the performance of the biosensors [20-22]. The figure 2-4 presents common immobilization strategies, including adsorption, covalent bonding, entrapment/encapsulation, and cross-linking.

- Adsorption

Adsorption bonds the enzymes to the surface of the support/electrode through weak interaction such as van der Waals forces, electrostatic force or hydrophobic forces.

- Covalent bonding

Covalent bonding immobilizes the enzymes onto the support via covalent bonds with functional groups such as amino groups, carboxyl groups, sulfhydryl groups, hydroxyl groups, phenolic groups, and thiol groups.

- Entrapment/encapsulation

Entrapment is usually achieved by physical entrapment of enzymes in the three-dimensional structure of polymeric gel.

- Cross-linking

Cross-linking is realized via strong chemical binding between enzymes with crosslinking agents like glutaraldehyde. Sometimes additional proteins like bovine serum albumin are utilized as mediators.

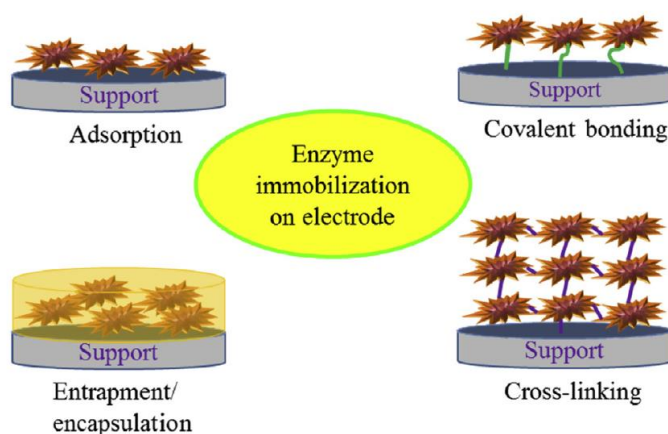


**Figure 2-4: Common types of enzyme immobilization on electrode surface.**

**Reprinted with permission from ref. [17]**

## 2.3 Biomarkers

### 2.3.1 Definition, classification, and application of biomarkers

A biomarker is defined as a specific characteristic that is measured as an indicator of normal biologic processes, pathogenic processes, or responses to an exposure or intervention [23]. Biomarkers are classified into different categories according to their respective applications in patient care, clinical study, and therapeutic development [24].

- Diagnostic biomarkers

A diagnostic biomarker detects or identifies the presence of a disease or condition, or redefine the subtype of the disease [23].

- Monitoring biomarkers

A monitoring biomarker can be measured serially to detect the condition of a disease or evidence of exposure to a medical product or environmental element, or assess the effect of a medical product or biological agent.

- Pharmacodynamic/response biomarkers

The level of pharmacodynamic/response biomarkers changes with the exposure to a medical product or environmental element.

- Predictive biomarkers

The presence or change in the predictive biomarkers predicts an individual or group of individuals more likely to experience a favorable or unfavorable effect from the exposure to a medical product or environmental element [23].

- Prognostic biomarkers

Prognostic biomarkers are used to assess the probability of a clinical event, disease recurrence, or disease progression in patients with a disease or medical condition [24].

- Safety biomarkers

A safety biomarker is measured before or after an exposure to a medical product or environmental element to indicate probability, presence, or extent of a toxicity as an adverse event [24].

Rapid evaluation of biomarkers by point-of-care testing is critical for disease diagnosis or monitoring of the progression of the diseases.

### 2.3.2 Phosphate as the biomarker

The biomarker used in this thesis is inorganic phosphate. Measurement of phosphate concentration in the body fluid is clinically significant to human body. Inorganic phosphate in the serum is usually used to quantify the phosphate level in the body with a reference range of 25 to 45 mg/l (0.81-1.45 mM) for adults [17]. The deficiency of serum phosphate (less than 25 mg/l) indicates the condition of malnutrition, while the excess of phosphate (more than 45 mg/l) is considered as a disease indicator for hyperphosphatemia, cardiovascular and chronic kidney disease [15].

As one of the constituents of saliva, inorganic phosphate has become a vital analyte in various dental and oral studies along with other scientific fields. Research has been conducted on the concentration of saliva phosphate at the conditions of stimulation [25], different salivary flow rate [26], pH [27] and buffering capacity [28], and the relationships between the phosphate contents and oral health [29]. The fluctuations of saliva phosphate have been investigated as indicators of hyperphosphatemia [30, 31],



ovulation [32], uremic state [33] and risk of developing dental caries and forming of dental calculus [29].

### 2.3.3 Detection methods of inorganic phosphate

Current standard method to measure inorganic phosphate is the colorimetric method [34]. However, the disadvantages of complicity, inclusion of carcinogenic reagent, use of the expensive instruments and weak anti-interference performance limited its usage for on-site measurement. Till now, various biosensors including optical sensors, chemical sensors and electrochemical sensors have been developed for phosphate measurement in the body fluid.

Various mono-enzymatic biosensors, bi-enzymatic biosensors and multi-enzymatic biosensors for phosphate measurement have also been developed [35-40]. Among them, mono-enzymatic is superior to other kinds because of cost-effectiveness, simple enzyme immobilization procedure and high sensor stability. Kwan *et.al* [36] immobilized pyruvate oxidase through gel-entrapment on the screen-printed electrode (SPE) and a linear range of 7.5-625  $\mu\text{M}$  was achieved. Gilbert *et.al* [41] crosslinked pyruvate oxidase through glutaraldehyde on a cobalt phthalocyanine screen-printed electrode, which achieved a linear range of 2.5-130  $\mu\text{M}$ . Through the incorporation of nanomaterials, substantial increase of linear range has been achieved by Orgabiela *et.al* [42] and Cui *et.al* [43] using AuNWs (12.5-1000  $\mu\text{M}$ ) and Pt/Au alloy nanowire arrays (0.248-1.456 mM).

Gunin Saikia and Parameswar K. Iyer made an optical sensor to detect  $\text{Fe}^{3+}$  and inorganic phosphate simultaneously [44]. It is a highly sensitive and highly selective approach,

while the time for measurements are 30 mins, and a pre-treatment procedure is required. Suzanne L. Tobey and Eric V. Anslyn developed a chemical sensor to determine the phosphate concentrations in both horse serum and human saliva at biological pH [45].

## 2.4 Inkjet printing as the biosensor manufacturing technique

Various techniques have been adopted to fabricate electrochemical biosensors, including subtractive manufacturing, thin film, lithography, electrospray/electrospinning and printing technology. Their advantages and challenges have been listed in the table 2-3. Compared to the other techniques, printing technologies provide potentialities for device miniaturization, compatibility in complex systems and ease of customization [46].

Two types of printing technologies have been employed in the biosensor manufacturing, namely, contact printing and non-contact printing. Though contact printing (gravure, flexographic, offset, micro-contact dispensing and screen printing) is a high throughput and low-cost method, the problems of low resolution and high material waste cannot be ignored. In the other hand, non-contact printing technique, especially inkjet printing technique has attracted the attention in the biosensor manufacturing field due to its advantages of minimum material waste, high resolution and more complex patterns [46].

**Table 2-2: Main fabrication techniques for electrochemical biosensors: advantages and challenges. Reprinted with permission from ref. [46]**

Techniques	Advantages	Challenges
Bulk Electrodes	Higher stability, larger surface	No possibility of miniaturization, large volumes of sample needed, low customization possibility
Printing technologies	Miniaturization, low cost, wide range of inks and substrates available, integrability, complex geometries, possible combination with nanostructures, with bio-receptors	Stability, repeatability, compatibility among materials
Thin Film (Vacuum-Based, Spin Coating)	Fine control of the thickness, low costs, high repeatability	High temperatures, vacuum needed, non-compatible with low- melting point substrates, no complex geometries
Lithography	High resolution, high accuracy, high repeatability	Long process needed particular materials mask based high costs limited available substrates
Electrospray Electrospinning	Good control of fibers, control of porosity possibility to combine multiple materials	Low lateral resolution, no complex geometries

### 2.4.1 Introduction to inkjet printing

Inkjet printing is a prevailing tool for its accurate positioning and elaborate manufacture, taking advantages over other techniques, and performs as a promising tool of handling biological fluid. According to the mechanisms of droplet generation, inkjet printing can be classified into continuous inkjet (CIJ) printing and drop-on-demand (DOD) inkjet printing [47].

CIJ printing produces a continuous stream of liquid drops. The drops not required for printing are deflected into a gutter and recycled. The schematic diagram of working mechanism for the CIJ printing is shown in Figure 2-5. The recycling process also increases the possibility of ink contamination because the ink is exposed to the environment.

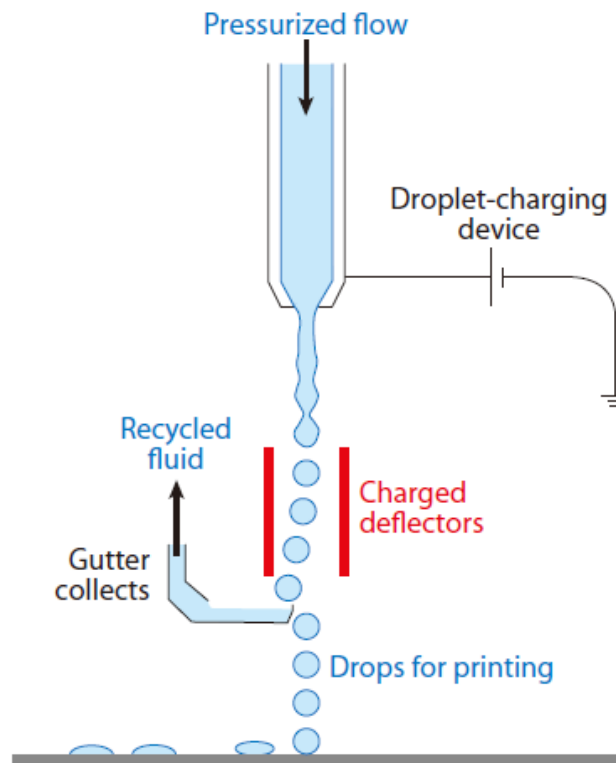


**Figure 2-5: Schematic diagram showing the principles of operation of a continuous inkjet (CIJ) printer. Reprinted with permission from ref. [47]**

DOD printing, in the other hand, only deposit droplets when it is required. There are mainly two subtypes of DOD printing, thermal DOD printing and piezoelectric printing. The schematic diagram for the working mechanism of them is presented in Figure 2-6.

Compared to thermal DOD printing, piezoelectric printing is more frequently used in the research and industry due to the convenience to monitor the drop size and velocity of fluid.

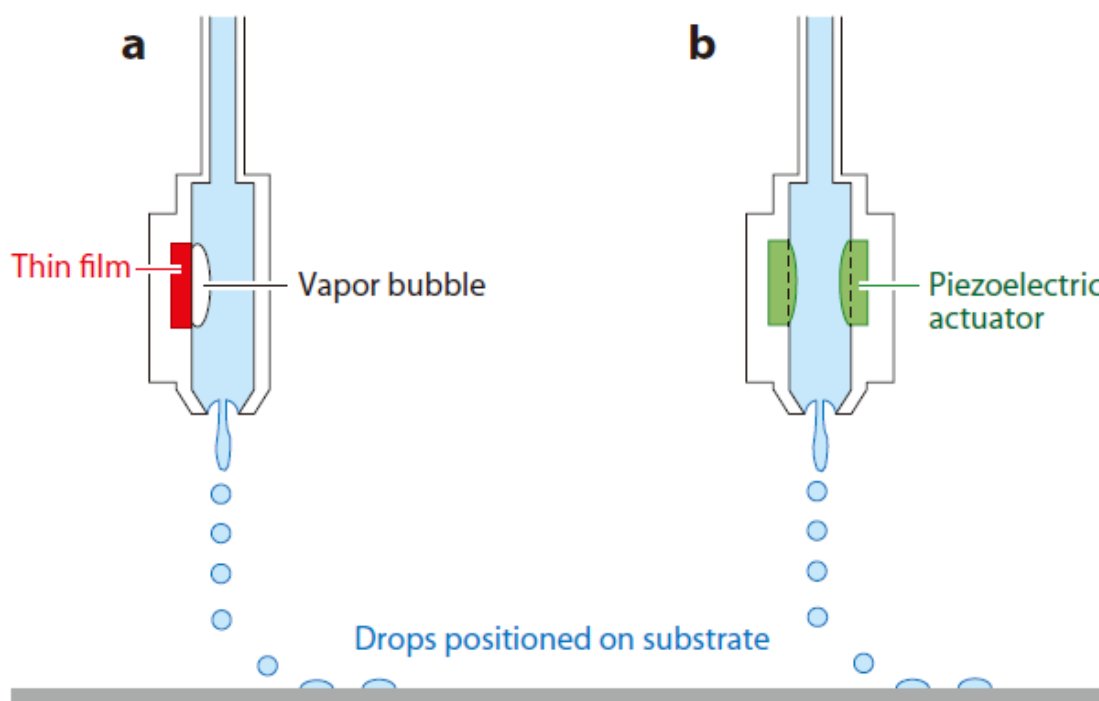


**Figure 2-6: Schematic diagram showing the principles of operation of a drop-on-demand (DOD) inkjet printing system. Drops are ejected by a pressure pulse generated in a fluid-filled cavity behind the printing orifice. This pressure pulse can be generated by (a) a vapor pocket or bubble generated by a thin-film heater (thermal inkjet) or (b) a mechanical actuation, e.g., from a piezoelectric transducer (piezoelectric inkjet). Reprinted with permission from ref. [47]**

#### 2.4.2 Ink formula

For the ink that contains biomaterials (here as enzymes), the ink should satisfy the requirement of good rheological property and ability to stabilize the biomaterial.

For the rheological property, the enzyme ink is carefully adjusted to guarantee of the dimensionless number  $Z$  of the ink is between 1 to 10 according to the equation [48]:

$$Z = \frac{1}{Oh} = \frac{Re}{\sqrt{We}} = \frac{\sqrt{\gamma\rho a}}{\eta}$$

where  $Oh$ ,  $Re$ , and  $We$  are the Ohnesorge, Reynolds, and Weber numbers, respectively,  $\gamma$ ,  $\rho$ , and  $\eta$  are the surface tension, density, and dynamic viscosity of the fluid, respectively, and  $a$  is the characteristic length, here taken as the diameter of the printer orifice.

According to the Fujji Dimatix Material Printer User Manual, the viscosity and surface tension should be adjusted within the range of 2-30 cp and 32-42 dynes/cm for the printer to form stable drops. Glycerol and Triton x100 are commonly selected to adjust the viscosity and surface tension of the ink separately.

For the enzyme ink stability, stabilizing reagent is suggested to be included in the ink. For example, BSA is added as an enzyme stabilizer and sacrificial agent in the ink for glucose sensor printing [49].

### 2.4.3 Printing parameter

According to the Fujji Dimatix Material Printer User Manual, waveform should be finely regulated with the duration time, slew rate and level parameter for each segment until stable and round drop is seen at the 1000-micron mark on the drop watcher window. Printing voltage and printing frequency of the waveform should also be optimized to achieve fast and stable droplet ejection, as shown in Figure 2-7 and Figure 2-8.

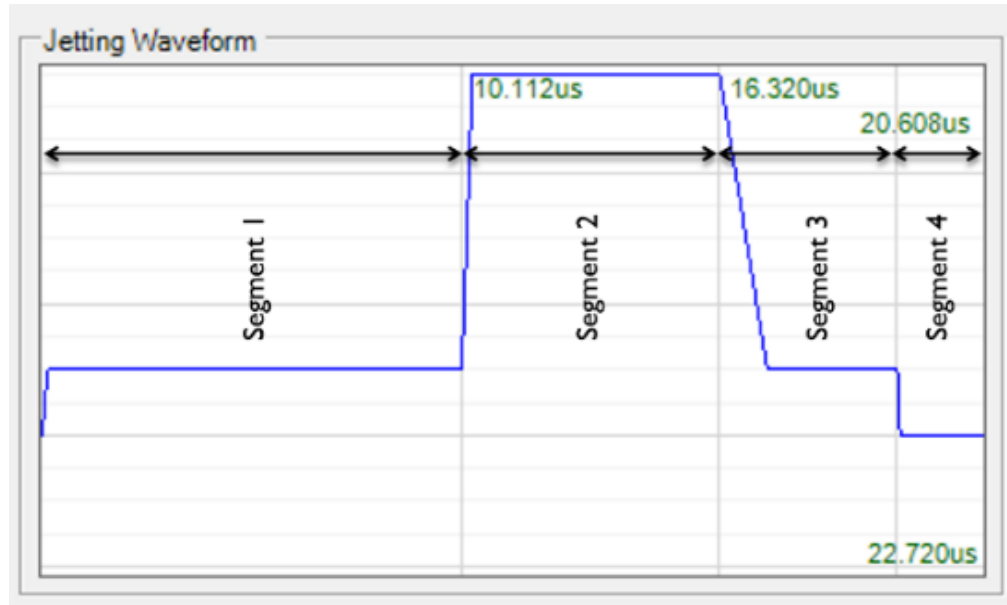


**Figure 2-7: Optimized jetting waveform obtained from this work in the Waveform Editor window.**

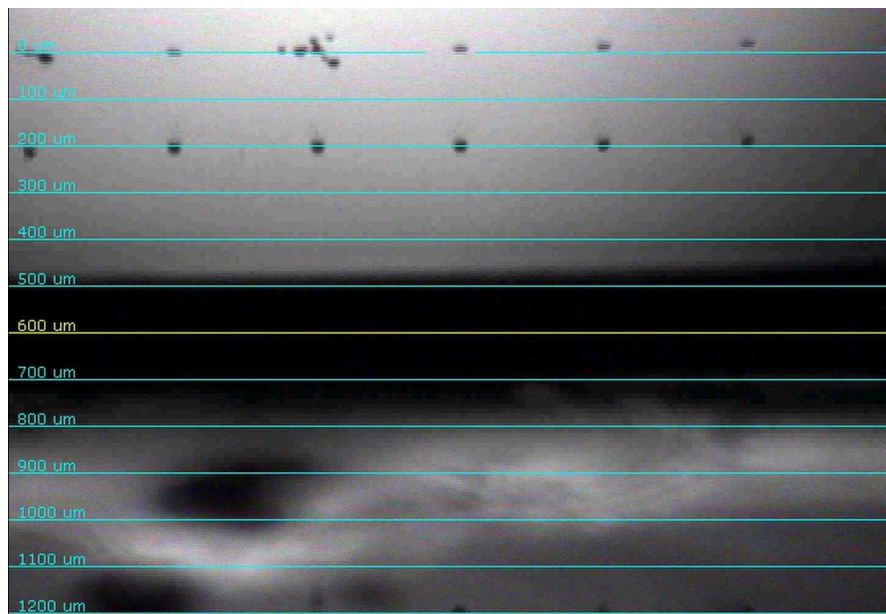


**Figure 2-8: Stable droplets in the Drop Watcher window obtained from this work.**

#### 2.4.4 Inkjet printing enzymes

The most frequently studied enzymes for printing are HRP [50-53] and GOD [51, 53-61], either from mechanism or application. Some other kinds of enzyme that have been printed are xanthine oxidase [62], acetylcholinesterase [63], lactic oxidase [63], lipase [63], glycerol kinase [63], L- $\alpha$ -glycerophosphate oxidase [63] and  $\beta$ -galactosidase [64], etc.

For the investigation of ink formula, Sabina Di Risio *et al.* investigated the effect of ink viscosity modifiers on the HRP activity during the printing process [52]. They found that the percentage change of the HRP activity before and after the printing was less than 2%. Different viscosity modifiers were tested during the experiment regarding to the dosing and effect in the ink formula.

In respect to the influence of different printing parameters on enzymes, Nishioka *et al.* worked on the effect of varying the compression rate of the nozzle (by modifying the waveform by applying a fixed voltage over different time ranges) on the HRP activity using drop-on-demand printing [50]. They found that HRP activity was compromised by increasing the compression rate up to  $5.48 \mu\text{m}^3/\mu\text{s}$ , but by adding sugar to the enzyme solution, the damage could be mitigated. However, this is hard to be achieved in the practical applications. The droplet speed is quite slow at 0.3-0.4 m/s, while the velocity of commercial inkjet printers is usually higher, ranging from 1-10 m/s. In this study, no other additives (viscosity modifiers or surfactants) are included in the HRP solution except for the fluorescein sodium-salt and sugar.



To investigate whether change of protein conformation occurred during printing, C. Cook *et al.* evaluated the changes of the GOD structure under different printing conditions. Light scattering, analytical ultra-centrifugation and circular dichroism are used to characterize the protein. They found no significant difference in the molecular weight and secondary structure of enzyme, suggesting no protein conformation occurred during the printing process. They also investigated GOD printed at 5 kHz with different printing voltages (40 V, 60 V, 80 V), and found that with the increasing of printer actuation voltage, the enzyme activity decreased. It indicated that more subtle alteration of the protein structure might occur during printing [65]. One year earlier, Tianming Wang *et al.* compared the retained activity of GOD printed at 1 kHz with the same voltage group of 40 V, 60 V, 80 V by the change of fluorescence intensity before and after printing and found no loss of activity and little change in the protein tertiary structure after printing [56]. This observation suggests that the printing frequency is the cause for the subtle protein structures that influence enzyme activity.

When applying the enzyme printing technique into the biosensor fabrication, L. Setti *et al.* found no enzyme activity loss for the GOD during the thermal inkjet printing process for fabricating glucose sensor [57]. The GOD activity was evaluated after printing, and the results show that there was no activity reduction during the printing. The enzyme activity values before and after the printing were 210.3 and 238.0 U/mL, respectively. This may be due to the decreasing gradient of temperature from the heater surface to the bulk ink solution, which allows the enzyme to feel temperatures lower than the nozzle heater surface. In their study, viscosity regulators and surfactant agents are added in the

biological ink to acquire better printing performance. The glycerol used in the ink formula may act as a stabilizing agent protecting the enzyme against the thermal shock.

## 2.5 Biosensor system for point-of-care testing

Point-of-care testing (POCT) is one of the most important application of biosensors and most of POC devices are based on the electrochemical detection [66]. POCT performs the diagnostic or prognostic test near the patient to offer immediate results without the requirement of expensive and complicated bench-top instrument, sample pre-treatment, skilled technician, etc. [67]

Conventional benchtop devices are designed for research that can perform a wide variety of electrochemical analysis and are only available in the research lab, healthcare facilities or hospitals. However, it is expensive, complex and bulky for point-of-care testing. Figure 2-9 is a photo of typical benchtop biosensor system including the electrochemical cell, potentiostat and a laptop.



**Figure 2-9 A photo of typical benchtop instruments for electrochemical analysis.**

Currently there is an increasing demand for inexpensive, handheld, user-friendly and customizable biosensors, which can obtain the results onsite. This pursuit of a portable efficient, affordable POC biosensor system now can be realized based on the progress of nanotechnology, additive manufacturing, miniaturization technologies, internet technology, smartphones, APP development, etc. [68]

### 2.5.1 Screen-printed electrodes

Screen-printed electrodes are widely used in the electrochemical biosensor system due to its low-cost and reproducibility for mass production. Electroanalysis combined with screen-printed electrodes can offer inexpensive, accurate, sensitive, fast, quantitative information and laboratory equivalent results [69]. With the help of screen-printed electrodes, the requirement of sample transportation and preparation to the laboratory is greatly reduced. Through modifying the materials on the working electrode, the biosensor can be easily customized and suit for different measurement requirement. Figure 2-10 is a typical screen-printed electrode fabricated by DropSenses.

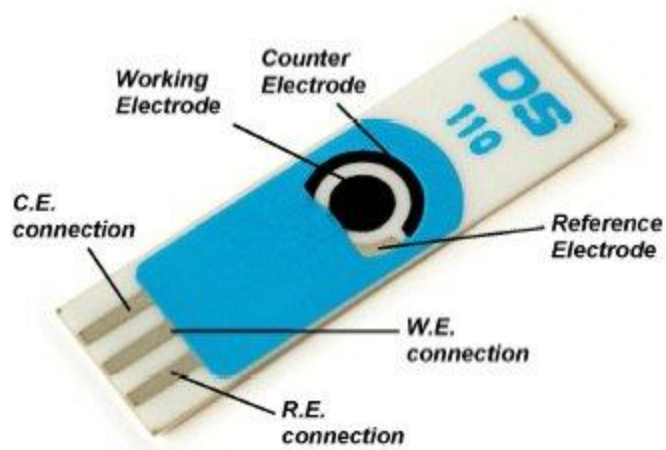


**Figure 2-10:** Schematic of a Dropsens screen printed electrode. Reprinted with permission from ref. [70]

### 2.5.2 Portable potentiostat

The use of potentiostat is essential to control and measure the parameters (time, current and voltage) of the electrochemical experiments. With the development of electronics, bulky, heavy and expensive benchtop potentiostats have evolved to inexpensive and portable potentiostats that are suitable for point-of-care testing [71].

Till now, various portable potentiostats have been developed [71-74]. Coupling with the screen-printed electrodes, smartphones and wireless transmission technique, rapid diagnosis results can be easily obtained. Figure 2-11 demonstrates an open-source portable potentiostat which can be easily adjusted to tailor the experimental needs.

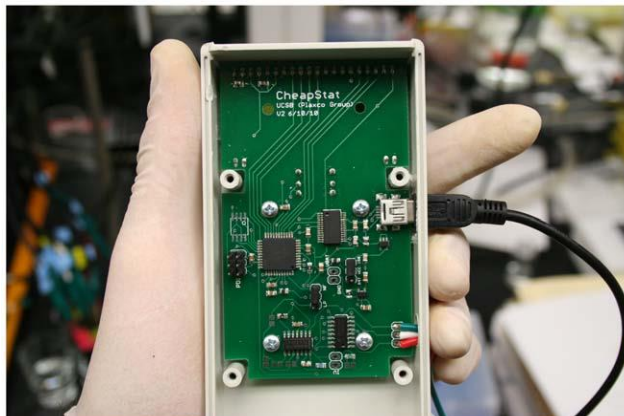


**Figure 2-11: The CheapStat, an inexpensive, “do-it-yourself” potentiostat. Reprinted with permission from ref.[70]**

### 2.5.3 APP development

In recent years, smartphones with software applications (APP) have been integrated into POC biosensor systems for imaging and signal analysis. Customized and easy-to-use APP enables any user to perform rapid and easy analysis anywhere and anytime. Till now, many biosensor systems have been equipped with customized APP for specific electrochemical analysis [75-78]. The real-time control, monitoring and signal imaging on the APP efficiently improve the user experience and greatly help the researchers to perform the analysis.

## References

1. Ali, J., J. Najeeb, M. Asim Ali, M. Farhan Aslam, and A. Raza, *Biosensors: Their Fundamentals, Designs, Types and Most Recent Impactful Applications: A Review*. Journal of Biosensors & Bioelectronics, 2017. **08**(01).
2. Heineman, W.R., W.B.J.B. Jensen, and Bioelectronics, *Leland c. clark jr.(1918–2005)*. 2006. **8**(21): p. 1403-1404.
3. Vestergaard, M.J.N. and Nanobioanalyses, 373© Springer Japan 2015 MC Vestergaard et al.(eds.), *Nanobiosensors and Nanobioanalyses*. 2015: p. 373.
4. Hinze, S.J.S., *Bibliographical cartography of an emerging interdisciplinary discipline: The case of bioelectronics*. 1994. **29**(3): p. 353-376.
5. Bhalla, N., P. Jolly, N. Formisano, and P. Estrela, *Introduction to biosensors*. Essays in biochemistry, 2016. **60**(1): p. 1-8.
6. Bai, Y., D. Zhang, Q. Guo, J. Xiao, M. Zheng, and J. Yang, *Study of the Enzyme Activity Change due to Inkjet Printing for Biosensor Fabrication*. ACS Biomaterials Science & Engineering, 2021.
7. Mun'delanji, C.V., K. Kerman, I.-M. Hsing, and E. Tamiya, *Nanobiosensors and nanobioanalyses*. 2015: Springer.
8. Yoo, E.-H. and S.-Y.J.S. Lee, *Glucose biosensors: an overview of use in clinical practice*. 2010. **10**(5): p. 4558-4576.
9. Suzuki, S., F. Takahashi, I. Satoh, and N.J.B.o.t.C.S.o.J. Sonobe, *Ethanol and Lactic Acid Sensors Using Electrodes Coated with Dehydrogenase—Collagen Membranes*. 1975. **48**(11): p. 3246-3249.
10. Schultz, J.S., *Optical sensor of plasma constituents*. 1982, Google Patents.
11. Liedberg, B., C. Nylander, I.J.S. Lunström, and actuators, *Surface plasmon resonance for gas detection and biosensing*. 1983. **4**: p. 299-304.
12. Cass, A.E., G. Davis, G.D. Francis, H.A.O. Hill, W.J. Aston, I.J. Higgins, E.V. Plotkin, L.D. Scott, and A.P.J.A.c. Turner, *Ferrocene-mediated enzyme electrode for amperometric determination of glucose*. 1984. **56**(4): p. 667-671.
13. Kaur, H., A. Bhosale, and S.J.I.J.H.S.R. Shrivastav, *Biosensors: classification, fundamental characterization and new trends: a review*. 2018. **8**: p. 315-333.
14. Cho, I.-H., D.H. Kim, and S. Park, *Electrochemical biosensors: perspective on functional nanomaterials for on-site analysis*. Biomaterials Research, 2020. **24**(1): p. 6.

15. Rahman, M.A., D.-S. Park, S.-C. Chang, C.J. McNeil, and Y.-B. Shim, *The biosensor based on the pyruvate oxidase modified conducting polymer for phosphate ions determinations*. *Biosensors and Bioelectronics*, 2006. **21**(7): p. 1116-1124.
16. Kimmel, D.W., G. LeBlanc, M.E. Meschievitz, and D.E. Cliffel, *Electrochemical Sensors and Biosensors*. *Analytical Chemistry*, 2012. **84**(2): p. 685-707.
17. Navaee, A. and A. Salimi, *Chapter 7 - Enzyme-based electrochemical biosensors*, in *Electrochemical Biosensors*, A.A. Ensafi, Editor. 2019, Elsevier. p. 167-211.
18. Risse, B., G. Stempfer, R. Rudolph, H. Möllering, and R. Jaenicke, *Stability and reconstitution of pyruvate oxidase from Lactobacillus plantarum: dissection of the stabilizing effects of coenzyme binding and subunit interaction*. *Protein Science*, 1992. **1**(12): p. 1699-1709.
19. Juan, E.C.M., M.M. Hoque, M.T. Hossain, T. Yamamoto, S. Imamura, K. Suzuki, T. Sekiguchi, and A. Takénaka, *The structures of pyruvate oxidase from Aerococcus viridans with cofactors and with a reaction intermediate reveal the flexibility of the active-site tunnel for catalysis*. *Acta crystallographica. Section F, Structural biology and crystallization communications*, 2007. **63**(Pt 11): p. 900-907.
20. Rocchitta, G., A. Spanu, S. Babudieri, G. Latte, G. Madeddu, G. Galleri, S. Nuvoli, P. Bagella, M.I. Demartis, V. Fiore, R. Manetti, and P.A. Serra, *Enzyme Biosensors for Biomedical Applications: Strategies for Safeguarding Analytical Performances in Biological Fluids*. *Sensors (Basel, Switzerland)*, 2016. **16**(6): p. 780.
21. Walter, P., B. Podsiadły, B. Wałpuski, and M. Jakubowska. *Common configurations and challenges in screen-printed enzymatic electrochemical biosensors*. in *Photonics Applications in Astronomy, Communications, Industry, and High-Energy Physics Experiments 2018*. 2018. SPIE.
22. Mohamad, N.R., N.H.C. Marzuki, N.A. Buang, F. Huyop, and R.A. Wahab, *An overview of technologies for immobilization of enzymes and surface analysis techniques for immobilized enzymes*. *Biotechnology, biotechnological equipment*, 2015. **29**(2): p. 205-220.
23. Group, F.-N.B.W., *BEST (Biomarkers, endpoints, and other tools) resource [Internet]*. 2016.
24. Califf, R.M., *Biomarker definitions and their applications*. *Experimental biology and medicine (Maywood, N.J.)*, 2018. **243**(3): p. 213-221.
25. Becks, H. and W. Wainwright, *Human saliva: XI. The effect of activation on salivary calcium and phosphorus content*. *Journal of Dental Research*, 1941. **20**(6): p. 637-648.

26. Dawes, C., *Rhythms in salivary flow rate and composition*. Int. J. Chronobiol., 1974. **2**: p. 253.
27. Mukherjee, S., *The state of calcium and phosphate in saliva*. Journal of periodontal research, 1968. **3**(3): p. 236-247.
28. Kavanagh, D.A. and G. Svehla, *Variation of salivary calcium, phosphate and buffering capacity in adolescents*. Archives of Oral Biology, 1998. **43**(12): p. 1023-1027.
29. Larsen, M. and E. Pearce, *Saturation of human saliva with respect to calcium salts*. Archives of Oral Biology, 2003. **48**(4): p. 317-322.
30. Savica, V., L.A. Calo, A. Granata, R. Caldarera, A. Cavaleri, D. Santoro, P. Monardo, R. Savica, U. Muraca, and G. Bellinghieri, *A new approach to the evaluation of hyperphosphatemia in chronic kidney disease*. Clin Nephrol, 2007. **68**(4): p. 216-21.
31. Savica, V., L.A. Calo, R. Caldarera, A. Cavaleri, A. Granata, D. Santoro, R. Savica, U. Muraca, A. Mallamace, and G. Bellinghieri, *Phosphate salivary secretion in hemodialysis patients: implications for the treatment of hyperphosphatemia*. Nephron Physiol, 2007. **105**(3): p. p52-5.
32. Ben-Aryeh, H., S. Filmar, D. Gutman, R. Szargfl, and E. Paldi, *Salivary phosphate as an indicator of ovulation*. American Journal of Obstetrics & Gynecology, 1976. **125**(6): p. 871-874.
33. Blum, M., S. Zurkowsky, J. Gilad, and A. Aviram, *Salivary phosphate and calcium concentrations in uremia*. Clinical nephrology, 1979. **12**(4): p. 191-192.
34. Murphy, J. and J.P. Riley, *A modified single solution method for the determination of phosphate in natural waters*. Analytica Chimica Acta, 1962. **27**: p. 31-36.
35. Gilbert, L., S. Browning, A.T. Jenkins, and J.P.J.M.A. Hart, *Studies towards an amperometric phosphate ion biosensor for urine and water analysis*. 2010. **170**(3-4): p. 331-336.
36. Kwan, R.C.H., H.F. Leung, P.Y.T. Hon, H.C.F. Cheung, K. Hirota, and R. Renneberg, *Amperometric biosensor for determining human salivary phosphate*. Analytical Biochemistry, 2005. **343**(2): p. 263-267.
37. Adeloju, S.B. and A.T. Lawal, *Fabrication of a bilayer potentiometric phosphate biosensor by cross-link immobilization with bovine serum albumin and glutaraldehyde*. Analytica Chimica Acta, 2011. **691**(1): p. 89-94.



38. Lawal, A.T. and S.B. Adeloju, *Polypyrrole based amperometric and potentiometric phosphate biosensors: A comparative study B*. Biosensors and Bioelectronics, 2013. **40**(1): p. 377-384.
39. Fernández, J.J., J.R. López, X. Correig, and I. Katakis, *Reagentless carbon paste phosphate biosensors: preliminary studies*. Sensors and Actuators B: Chemical, 1998. **47**(1): p. 13-20.
40. Mousty, C., S. Cosnier, D. Shan, and S. Mu, *Trienzymatic biosensor for the determination of inorganic phosphate*. Analytica chimica acta, 2001. **443**(1): p. 1-8.
41. Gilbert, L., A.T.A. Jenkins, S. Browning, and J.P. Hart, *Development of an amperometric, screen-printed, single-enzyme phosphate ion biosensor and its application to the analysis of biomedical and environmental samples*. Sensors and Actuators B: Chemical, 2011. **160**(1): p. 1322-1327.
42. Ogabiela, E., S.B. Adeloju, J. Cui, Y. Wu, and W. Chen, *A novel ultrasensitive phosphate amperometric nanobiosensor based on the integration of pyruvate oxidase with highly ordered gold nanowires array*. Biosensors and Bioelectronics, 2015. **71**: p. 278-285.
43. Cui, J., E.E. Ogabiela, J. Hui, Y. Wang, Y. Zhang, L. Tong, J. Zhang, S.B. Adeloju, X. Zhang, and Y. Wu, *Electrochemical Biosensor based on Pt/Au Alloy Nanowire Arrays for Phosphate Detection*. Journal of The Electrochemical Society, 2015. **162**(3): p. B62-B67.
44. Saikia, G. and P.K. Iyer, *A Remarkable Superquenching and Superdequenching Sensor for the Selective and Noninvasive Detection of Inorganic Phosphates in Saliva*. Macromolecules, 2011. **44**(10): p. 3753-3758.
45. Tobey, S.L. and E.V. Anslyn, *Determination of Inorganic Phosphate in Serum and Saliva Using a Synthetic Receptor*. Organic Letters, 2003. **5**(12): p. 2029-2031.
46. Sardini, E., M. Serpelloni, and S. Tonello, *Printed Electrochemical Biosensors: Opportunities and Metrological Challenges*. Biosensors, 2020. **10**(11).
47. Derby, B., *Inkjet Printing of Functional and Structural Materials: Fluid Property Requirements, Feature Stability, and Resolution*. Annual Review of Materials Research, 2010. **40**(1): p. 395-414.
48. Derby, B., *Bioprinting: inkjet printing proteins and hybrid cell-containing materials and structures*. Journal of Materials Chemistry, 2008. **18**(47): p. 5717-5721.
49. Delaney, J.T., P.J. Smith, and U.S. Schubert, *Inkjet printing of proteins*. Soft Matter, 2009. **5**(24): p. 4866-4877.

50. Nishioka, G.M., A.A. Markey, and C.K. Holloway, *Protein damage in drop-on-demand printers*. J Am Chem Soc, 2004. **126**(50): p. 16320-1.
51. Zhang, Y., F. Lyu, J. Ge, and Z. Liu, *Ink-jet printing an optimal multi-enzyme system*. Chemical Communications, 2014. **50**(85): p. 12919-12922.
52. Di Risio, S. and N. Yan, *Piezoelectric Ink-Jet Printing of Horseradish Peroxidase: Effect of Ink Viscosity Modifiers on Activity*. Macromolecular Rapid Communications, 2007. **28**(18 - 19): p. 1934-1940.
53. Gainey Wilson, K., P. Ovington, and D. Dean, *A Low-Cost Inkjet-Printed Glucose Test Strip System for Resource-Poor Settings*. Journal of diabetes science and technology, 2015. **9**(6): p. 1275-1281.
54. Liu, C.-C., *Applications of Thick Film Screen Printing and Ink Jet Printing for the Manufacturing of Single Use, Disposable Biosensors*. ECS Transactions, 2008. **16**(11): p. 3-13.
55. Newman, J.D., A.P.F. Turner, and G. Marrazza, *Ink-jet printing for the fabrication of amperometric glucose biosensors*. Analytica Chimica Acta, 1992. **262**(1): p. 13-17.
56. Wang, T., C. Cook, and B. Derby. *Fabrication of a Glucose Biosensor by Piezoelectric Inkjet Printing*. in *2009 Third International Conference on Sensor Technologies and Applications*. 2009.
57. Setti, L., A. Fraleoni-Morgera, B. Ballarin, A. Filippini, D. Frascaro, and C. Piana, *An amperometric glucose biosensor prototype fabricated by thermal inkjet printing*. Biosens Bioelectron, 2005. **20**(10): p. 2019-26.
58. Bihar, E., S. Wustoni, A.M. Pappa, K.N. Salama, D. Baran, and S. Inal, *A fully inkjet-printed disposable glucose sensor on paper*. npj Flexible Electronics, 2018. **2**(1): p. 30.
59. Yun, Y.H., B.K. Lee, J.S. Choi, S. Kim, B. Yoo, Y.S. Kim, K. Park, and Y.W. Cho, *A Glucose Sensor Fabricated by Piezoelectric Inkjet Printing of Conducting Polymers and Bionzymes*. Analytical Sciences, 2011. **27**(4): p. 375-375.
60. Cook, C.C., T. Wang, and B. Derby, *Inkjet delivery of glucose oxidase*. Chemical Communications, 2010. **46**(30): p. 5452-5454.
61. Wang, T., C. Cook, and B. Derby, *Inkjet printing glucose oxidase for biosensor applications*. ECS Transactions, 2008. **16**(11): p. 15-20.
62. Lee, J., A.A.S. Samson, and J.M. Song, *Inkjet-Printing Enzyme Inhibitory Assay Based on Determination of Ejection Volume*. Analytical Chemistry, 2017. **89**(3): p. 2009-2016.

63. Hossain, S.M.Z., R.E. Luckham, A.M. Smith, J.M. Lebert, L.M. Davies, R.H. Pelton, C.D.M. Filipe, and J.D. Brennan, *Development of a Bioactive Paper Sensor for Detection of Neurotoxins Using Piezoelectric Inkjet Printing of Sol–Gel-Derived Bioinks*. *Analytical Chemistry*, 2009. **81**(13): p. 5474-5483.
64. Creran, B., X. Li, B. Duncan, C.S. Kim, D.F. Moyano, and V.M. Rotello, *Detection of Bacteria Using Inkjet-Printed Enzymatic Test Strips*. *ACS Applied Materials & Interfaces*, 2014. **6**(22): p. 19525-19530.
65. Cook, C., T. Wang, and B. Derby, *Inkjet Printing of Enzymes for Glucose Sensors*. *MRS Online Proceedings Library Archive*, 2009. **1191**.
66. Montes-Cebrián, Y., A. Álvarez-Carulla, G. Ruiz-Vega, J. Colomer-Farrarons, M. Puig-Vidal, E. Baldrich, and P.L.J.S. Miribel-Català, *Competitive USB-powered hand-held potentiostat for POC applications: An HRP detection case*. 2019. **19**(24): p. 5388.
67. Narayan, R.J., *Medical Biosensors for Point of Care (POC) Applications*. 2016: Woodhead Publishing.
68. Zarei, M., *Portable biosensing devices for point-of-care diagnostics: Recent developments and applications*. *TrAC Trends in Analytical Chemistry*, 2017. **91**: p. 26-41.
69. García-Miranda Ferrari, A., S.J. Rowley-Neale, and C.E. Banks, *Screen-printed electrodes: Transitioning the laboratory in-to-the field*. *Talanta Open*, 2021. **3**: p. 100032.
70. Cheng, W., E. Stuart, K. Tschulik, J. Cullen, and R.J.N. Compton, *A disposable sticky electrode for the detection of commercial silver NPs in seawater*. 2013. **24**(50): p. 505501.
71. Ainla, A., M.P. Mousavi, M.-N. Tsaloglou, J. Redston, J.G. Bell, M.T. Fernández-Abedul, and G.M. Whitesides, *Open-source potentiostat for wireless electrochemical detection with smartphones*. *Analytical chemistry*, 2018. **90**(10): p. 6240-6246.
72. Rowe, A.A., A.J. Bonham, R.J. White, M.P. Zimmer, R.J. Yadgar, T.M. Hobza, J.W. Honea, I. Ben-Yaacov, and K.W.J.P.o. Plaxco, *CheapStat: an open-source, “Do-It-Yourself” potentiostat for analytical and educational applications*. 2011. **6**(9): p. e23783.
73. Jenkins, D.M., B.E. Lee, S. Jun, J. Reyes-De-Corcuera, and E.S. McLamore, *ABE-Stat, a Fully Open-Source and Versatile Wireless Potentiostat Project Including Electrochemical Impedance Spectroscopy*. *Journal of The Electrochemical Society*, 2019. **166**(9): p. B3056-B3065.

74. Shen, X., F. Ju, G. Li, and L.J.S. Ma, *Smartphone-Based Electrochemical Potentiostat Detection System Using PEDOT: PSS/Chitosan/Graphene Modified Screen-Printed Electrodes for Dopamine Detection*. *Sensors*, 2020. **20**(10): p. 2781.
75. Giordano, G.F., M.B. Vicentini, R.C. Murer, F. Augusto, M.F. Ferrão, G.A. Helfer, A.B. da Costa, A.L. Gobbi, L.W. Hantao, and R.S.J.E.A. Lima, *Point-of-use electroanalytical platform based on homemade potentiostat and smartphone for multivariate data processing*. 2016. **219**: p. 170-177.
76. Zhu, X., Y. Ju, J. Chen, D. Liu, and H. Liu, *Nonenzymatic Wearable Sensor for Electrochemical Analysis of Perspiration Glucose*. *ACS Sensors*, 2018. **3**(6): p. 1135-1141.
77. Zhang, L., W. Yang, Y. Yang, H. Liu, and Z. Gu, *Smartphone-based point-of-care testing of salivary  $\alpha$ -amylase for personal psychological measurement*. *Analyst*, 2015. **140**(21): p. 7399-7406.
78. Aronoff-Spencer, E., A.G. Venkatesh, A. Sun, H. Brickner, D. Looney, and D.A. Hall, *Detection of Hepatitis C core antibody by dual-affinity yeast chimera and smartphone-based electrochemical sensing*. *Biosens Bioelectron*, 2016. **86**: p. 690-696.

## Chapter 3

### 3 Study of the enzyme activity change due to inkjet printing for biosensor fabrication

Enzymes, the most commonly used biosensing element, have a great influence on the performance of biosensors. Recently, drop-on-demand (DOD) printing technique has been widely employed for the fabrication of biosensors due to its merits of noncontact, less waste, and rapid deposition. However, enzyme printing studies were rarely conducted on the effect of printing parameters from the aspect of the pressure wave propagation mechanism. This study investigated the effects of pressure wave propagation on enzyme activity from the aspects of wave superposition, wave amplitude, resulting mechanical stress, and protein conformation change using pyruvate oxidase as the model enzyme. We found that the mechanical stress increased the activity of pyruvate oxidase during the inkjet printing process. A shear rate of  $3 \times 10^5 \text{ s}^{-1}$  enhanced the activity by around 14%. The enhancement mechanism was investigated, and the mechanical activation or mild proteolysis was found to change the conformation of pyruvate oxidase and improve its activity. This study is fundamental to understand the effect of both printing mechanism and induced mechanical stress on the properties of biomolecules and plays an important role in modulating the activity of other enzyme-based inks, which is crucial for the development of biosensors.

#### 3.1 Introduction

Nowadays biosensors are widely used in a broad range of areas such as biomedical diagnosis, point-of-care monitoring, environmental monitoring, food quality control, biomedical research, etc. [1]. Enzymes as the bioreceptor are extensively used to

fabricate biosensors [2]. Currently developed manufacturing practice, especially inkjet printing technology, provides flexible fabrication methods for biosensors by precisely positioning a small amount of materials, and takes advantages of controlling unnecessary wastage of enzymes and potential contamination [2]. Inkjet printing has attracted a high attention in the research community, and is becoming the most feasible technique to deposit enzymes [3]. In recent years, a number of enzyme-based glucose sensors have been developed for diabetes diagnosis [4-7]. It is believed inkjet printing technique will be routinely used for the development of other enzyme-based biosensors.

When printing the enzyme-contained ink, the enzymes will be affected during the drop formation process, especially by the variable pressure wave in the printhead (see Figure 3-1). Herein, pressure wave is the direct acoustic response induced by the displacement of piezoelectric crystal, it drives the fluid flow in the printhead chamber and drops eject from the nozzle. Pressure waves are indirectly driven by the printing parameter settings, as the displacement of piezoelectric crystal is controlled by printing frequency, voltage and slew rate of an electrical waveform, which decides the magnitude and rate of the volume change [8]. Drop ejection occurs through generating sufficient magnitude pressure pulses by superposition of two or more consecutive pressure wave [9, 10]. Superposition of pressure waves can be complicated under different printing parameter settings. Basically, higher printing frequency means decreased distance of adjacent waveform, more complicated wave superposition. Higher voltage results in larger wave amplitude and correspondingly higher drop velocity at the printhead nozzle. Muhammad *et. al* [11] studied the change profile of pressure in the printhead chamber and the velocity response at the printhead nozzle exit for a single pulse printing. It was found that

both chamber pressure and orifice velocity varied extensively. At the time of drop ejection, the chamber pressure reached as high as 280 kPa and the velocity at nozzle inlet reached about 4 m/s. It indicated that nonnegligible mechanical stress (compression stress in the printhead chamber and shear stress at the nozzle) are induced by the alteration of printing parameters.



**Figure 3-1: A photo of the drop-on-demand printer from FUJIFILM Dimatix, Inc.**

When involving multi-pulses printing process, pressure and velocity change will be more complicated. Several studies investigated the dependency of the drop velocity on the printing frequency, and wave-like velocity fluctuation was observed [9, 12]. It was found both wave amplitude and compression/shear stress (reflected by shear rate and drop velocity) also increased with the applied voltage. Thus, it is fundamental to study the alteration of the above-mentioned printing parameters and then investigate the effect of mechanical stress on the enzyme ink.

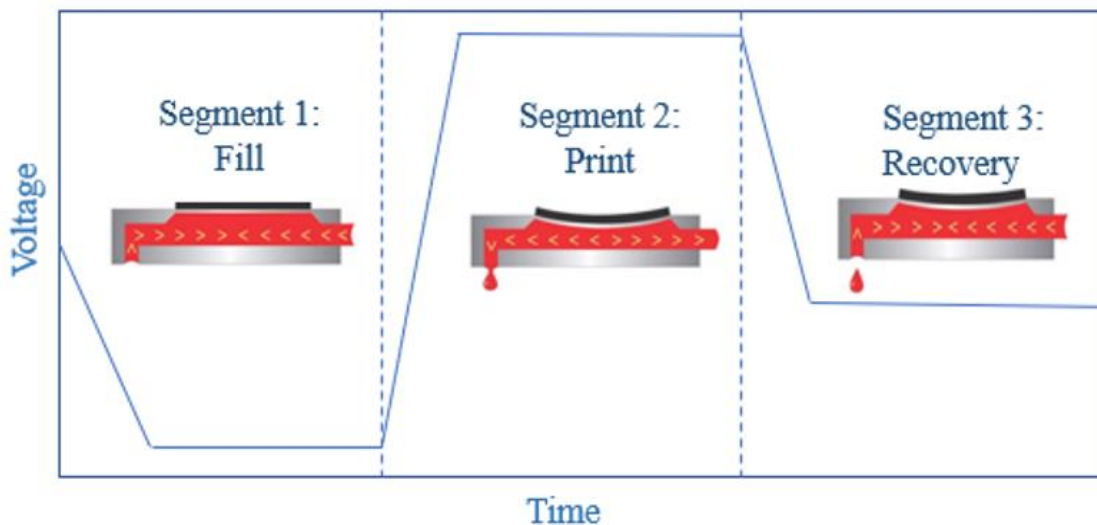


**Figure 3-2: Schematic of the drop ejection mechanism. Piezoelectric crystal movement driven by the printing waveform and corresponding wave propagation in the printhead chamber. The direction of pressure wave was drawn with red arrow. Segment 1 is the ink fill period: ink is drawn from the reservoir to the printhead chamber; Segment 2 is the ink print period: ejection occurs upon the formation of enhanced pressure wave (pressure wave reflected from the reservoir combines with the positive pressure wave); Segment 3 is the recovery period, backward going pressure wave is reflected from the nozzle.**

Several experimental studies investigated the effect of printing parameters on enzymes' activity. Nishioka *et al.* [13] studied the effect of displacement rate of piezoelectric crystal (by applying a fixed voltage on piezo-element over different time range) on peroxidase using DOD printing. A printing frequency of 100 Hz was used to avoid adjacent pressure wave superposition. Also drop velocity was restricted below 0.3 m/s to avoid shear stress at the nozzle. Enzyme activity loss was found with higher compression rate. In another study, Tianming *et al.* [6] studied the effect of printing voltage on the



glucose oxidase. In their study, a printing frequency of 1 kHz was applied and printing voltage of 40 V, 60 V and 80 V were used. They suggested that protein tertiary structure and glucose oxidase activity were not affected by shear stress at the nozzle. From the same research group, Christopher *et al.* [14] investigated the effect of waveform slew rate on the glucose oxidase. Glucose oxidase activity was found to be slightly decreased with increased slew rate. They also repeated the experiment of varied voltage amplitude using a higher printing frequency of 5 kHz. Different from the study of Christopher, they found glucose oxidase activity decreased as the printer actuation voltage increases. As printing frequency is the major variable between the above studies, it is suspected that protein damage may occur at higher printing frequency due to increased wave superposition.

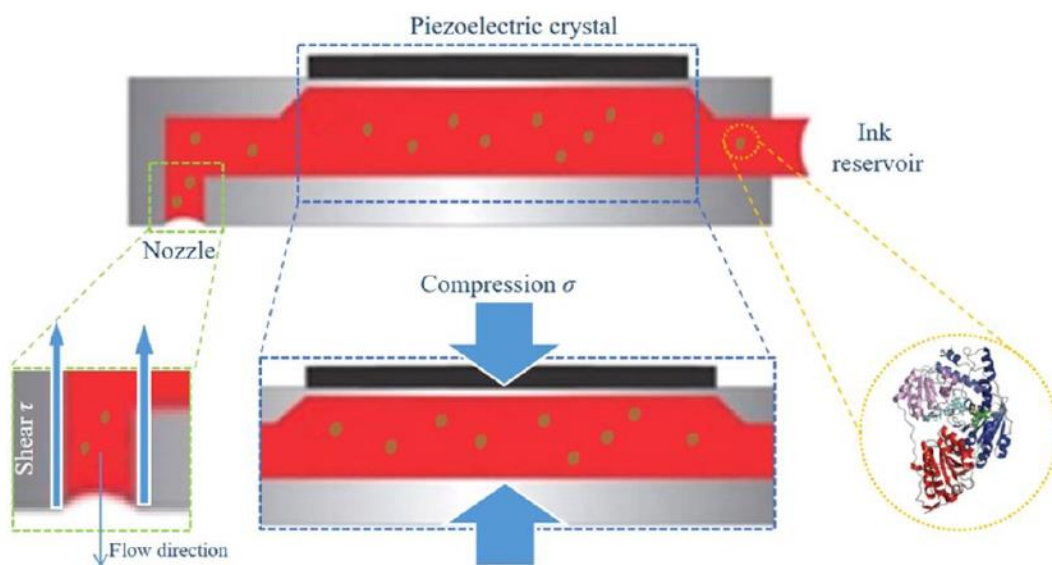


**Figure 3-3: Structure of the printhead chamber showing the piezoelectric crystal, nozzle and ink reservoir. In the green dashed box is the shear stress at the nozzle, In the blue dashed box is the compression stress in the printhead chamber, in the**

**yellow circle is the three-dimensional conformation of pyruvate oxidase. Reprinted with permission from ref. [15].**

To our best knowledge, the effect of wave superposition on enzyme activity was rarely involved. Additionally, commercial printers usually work under resonance conditions, where pressure waves are timed to reinforce each other, resulting in even higher compression on the ink solution [13]. Current studies [6, 13, 14] about printing enzyme mainly focus on low frequency printing which cannot be transformed to the industrial fabrication practice of biosensors. Thus, it is necessary to systematically investigate the probable effect of specific mechanical stress on enzymes from the aspect of wave propagation to understand the mechanism of enzyme activity change, and it is also practical to study the change pattern of enzyme activity under different printing frequency to facilitate the fabrication process for future biosensor.

So far, there are contradictory findings about the effect of compression stress and shear stress on the activity of different enzyme or on the three-dimensional conformation of enzyme protein [16]: on the one hand, higher compression rate has negative effect on enzyme activity due to the damaged peroxidase structure by compression stress [13]; on the other hand, increased compression had minimal effect on the glucose oxidase activity and corresponding protein structure [6]. In addition, the threshold of shear rate to denature the protein remains controversial [17-20]. Further investigation is imperative to understand the effect of mechanical stress on the enzyme activity and protein structure of different enzymes.

In this study, in order to compare with parallel printing studies of enzymes with different size and structure [4-6, 21-25], pyruvate oxidase was employed [26-29]. A piezo-driven

DOD printer (seen in Figure 3-1) was used to investigate the effect of wave superposition on the activity change of pyruvate oxidase under different printing frequencies and voltages. Drop velocity was measured for each printing group. Shear rate was calculated based on the observed mean drop velocity to reflect corresponding shear stress status at the nozzle. A full statistical study of enzyme activity change was presented. Protein structure changes of three different kinds of enzymes (pyruvate oxidase, glucose oxidase and peroxidase) were examined before and after printing.

## 3.2 Methods and experiments

### 3.2.1 Materials

Pyruvate oxidase from microorganism (PyOD, E.C.1.2.3.3) was purchased from Toyobo (New York, USA). Peroxidase from horseradish (E.C. 1.11.1.7), Glucose Oxidase from *Aspergillus niger* (GOx, E.C.1.1.3.4), bovine serum albumin (BSA), Triton X-100 and glycerol were obtained from Sigma-Aldrich. 4-Aminoantipyrine, n-ethyl-n-(2-hydroxy-3-sulfopropyl)-m-toluidine (EHSPT), thiamine pyrophosphate (TPP), flavin adenine dinucleotide (FAD), tetrasodium salt hydrate (EDTA) and  $MgSO_4$  were purchased from TCI. All other reagents used were of analytical grade and used as received. All solutions were prepared in double distilled water. Citrate buffer (ionic strength 0.02 M, pH 5.7) and phosphate buffer (ionic strength 0.04 M, pH 5.9) were prepared according to normal lab procedures.

### 3.2.2 Methods

#### Bio-ink preparation

Pyruvate oxidase was prepared in citrate buffer. Ink formula was developed to satisfy the rheological requirement and to stabilize the enzyme. According to manufacturer's data supplied with the printhead, the suitable viscosity and surface tension range for dispensing fluids are 2-30 centipoises (cps) and 28-42 dynes/cm separately. Additives were used to modify the physical property of the ink. Specifically, 20% w/v glycerol was added to adjust the viscosity. To modify the ink surface tension, 0.075% Triton $\times$ -100 was included. 0.05% w/v bovine serum albumin (BSA) has been added as an enzyme stabilizer and sacrificial agent to minimize protein absorption on the polypropylene bag of the ink cartridge [30]. Density of the ink was calculated by weighing the mass divided by its volume. Physical properties of the ink are shown in Table 3-1.

**Table 3-1: Physical properties of the ink at room temperature.**

Viscosity/(cp)	Surface tension/(dynes/cm)	Density/(g/cm <sup>3</sup> )
3.26	32.6	1.02

#### Printing experiments

The level, slew rate and duration of the waveform that defines the displacement of piezoelectric actuator will highly influence the droplet formation process and the fluid mechanical stress (figure 3-2 and figure 3-3). A printing waveform was optimized based on drop formation requirements of stable round droplet and no satellite drop (see

supporting video: stable drop). Same waveform settings were employed in all experiments.

**Table 3-2: Printing parameters used in the experiments.**

Name	Number	Printing frequency/kHz	Printing voltage/V
Control	0	none	none
First series	1	4	23.6
	2	6	23.6
	3	8	23.6
	4	10	23.6
Second series	5	6	24
	6	6	28
	7	6	32
	8	6	36

Velocity of droplet in flight was determined by stroboscopic images captured by CCD camera. Average drop velocity was calculated by measuring the spacing between droplets and the printing frequency. Shear rate  $\epsilon$  during drop generation, as a reflect of shear stress at the nozzle, is given by the equation

$$\epsilon = v/r \quad (1)$$

where  $v$  and  $r$  are drop velocity and radius respectively [31]. Shear rates of printing voltage of 24 V to 36 V at a 2 V interval with printing frequency of 5, 6, 7 and 8 kHz were calculated and plotted in Appendix 3-1.

Ink was directly printed from a 21.5  $\mu\text{m}$  diameter printhead onto a clean storage pan to get approximately 120  $\mu\text{l}$  printed sample. Pipetted ink was used as unprinted control group against the printed sample, to ensure that any observed effects can be solely attributed to the printing process. All printed ink groups were gathered and stored in a refrigerator immediately after printing. All printing groups were repeated in triplicates the same as other enzyme printing experiments [25].

To acquire satisfied printing performance for precise positioning of the ink and avoid the occurrence of jetting issue (see Appendix 3-2), only printing setting that drives the droplet as a round drop at the 1000  $\mu\text{m}$  mark at the drop watcher window will be retained to analyze the enzyme activity. After screening the printing performance, performed experiments with different printing parameters were finalized and listed in Table 3-2. Specifically, printing frequency of 4 to 10 kHz with an interval of 2 kHz (Group 1 to 4, first series) at a constant voltage of 23.6 V (most stable droplet ejecting performance was observed at 23.6 V) were chosen to investigate the wave superposition effect in the printhead cartridge. Printing voltage of 24 V to 36 V with an interval of 4 V (Group 5 to 8, second series) at a frequency of 6 kHz (based on timed meniscus oscillation) were used to investigate the effect of wave amplitude on the enzyme activity.

The selection of printing voltage for three kinds of enzymes was based on overall drop formation performance (see example supporting video: stable drop and unstable drop). The printing parameter of the stable drop and unstable drop video is 6 kHz 24 V and 6 kHz 32 V separately using peroxidase ink. From the stable drop video, it is clear to see that round and stable droplets ejecting from 0  $\mu\text{m}$  to 1200  $\mu\text{m}$  mark for all the nozzle. This ensures the precise and stable deposition of the ink. For unstable drop video,

droplets from all nozzles were found broken to pieces since 100  $\mu\text{m}$  mark. Due to the requirement of printing performance, we only choose 24 V and 28 V at 6 kHz for all three kinds of the enzyme ink after careful screening the droplet quality.

### Enzyme activity determination

Pyruvate oxidase activity was determined using a modified method reported by B. Sedewitz [32]. The principle of this assay relies on the oxidative coupling among  $\text{H}_2\text{O}_2$ , 4-Aminoantipyrine and EHSPT. 0.2 mL 4-Aminoantipyrine solution (0.15%, w/v), 0.2 ml EHSPT solution (0.3%, w/v), 0.2 ml TPP solution (3 mM), 0.2 ml FAD solution (0.15 mM), 0.2ml EDTA solution (15 mM), 0.2ml  $\text{MgSO}_4$  solution (0.15 mM) and 0.3 ml Peroxidase (50 U/ml) were added into 1 ml of phosphate buffer (0.15 M). The obtained buffer was mixed with 0.5 ml pyruvate solution (0.3 M) and equilibrated at  $37^\circ\text{C}$  for 5 min, resulting in the working solution. Then 0.1 ml of diluted pyruvate oxidase ink solution (0.1-0.5 U/ml) was added in the aforementioned working solution and mixed by gentle inversion. The absorbance of the resultant quinoneimine dye at 550 nm was immediately recorded for 4 min. Measurements were carried out against the reagent blank, containing all the component of the ink but the enzyme. The extinction coefficient of quinoneimine dye under the assay condition was  $36.88 \text{ cm}^3/\mu\text{mol}$  [33]. Enzyme activity experiments were conducted on all the printed samples and unprinted control group.

### Characterization and apparatus

SNB-1 Viscosimeter (Karoht Shanghai, China) was used to measure the viscosity at room temperature under steady shear at 12 rpm. BZY101 Automatic Surface Tensiometer (Vetus Anhui, China) was used to characterize the surface tension. Printing experiments

were carried out using Fujifilm DIMATIX Materials Printer Dmp-2831 (FUJIFILM Dimatix, Inc., USA) with the customized ink cartridge DMC-11610. Driving waveform of printhead piezo-element was controlled through Graphical User Interface application software (DMP-2800). Cary 100 UV-visible spectrophotometer (Agilent, USA) was used to conduct enzyme activity experiments. Circular dichroism assays were carried out using a Jasco J-810 spectrometer (Jasco, USA).

## Data analysis

All statistical analyses were conducted in GraphPad Prism 8.0. The Shapiro-Wilk test was used to investigate the normal distribution status of all data set. Repeated measures one-way ANOVA was used for multiple comparisons. Tukey's post hoc comparisons were performed to determine whether there are significant differences between groups. Regression analysis were performed for different data groups. All results are expressed as average and standard error of the mean for three replicates (if not mentioned otherwise). A  $p < 0.05$  was considered statistically significant.

## 3.3 Results and discussion

### 3.3.1 Effects of wave superposition under different printing frequencies

Four printing frequency (first series) were used to investigate the effect of pressure wave superposition on enzyme. The increase of enzyme activity and shear rate response were depicted in Figure 3-4. Evident improvement was observed after printing compared with the unprinted control group ( $p < 0.05$ ). The quantified enhancement of pyruvate oxidase activity ranged from 10.84% to 14.10%. It is deduced the protein conformation was changed during the printing process. Thus, inside regions of enzyme protein was exposed



and the accessibility of substrate was enhanced resulting in an improvement of the enzyme activity. The enhancement phenomenon of enzyme activity was also reported by other researchers through ultrasound treatment [34, 35] or single-molecule fluorescence-magnetic tweezers microscopy [36]. To further verify the assumption of potential protein structure change, characterization of protein secondary structure after printing was performed and presented in section 3.3.

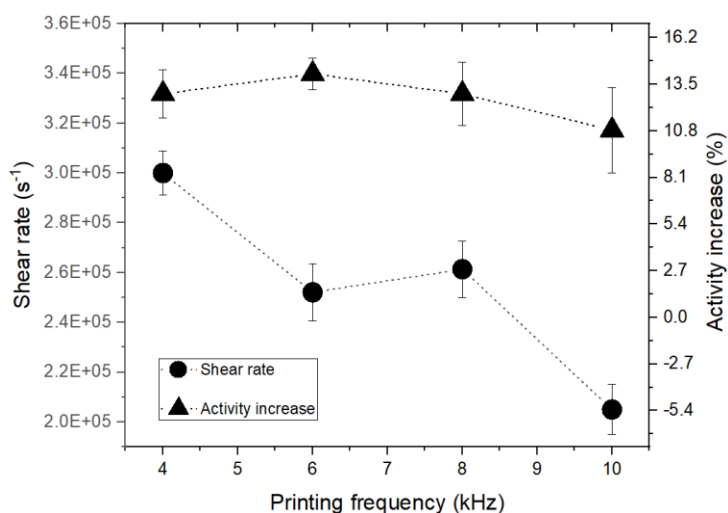


**Figure 3-4: Increase percentage of the enzyme activity and the shear rate after printing under 4, 6, 8, and 10 kHz at 23.6 V (first series). The unprinted enzyme ink was the control group. Enzyme activity was calculated based on the pyruvate oxidase activity assay. Increase percentage of enzyme activity was calculated compared to the unprinted control group. Shear rate was deduced from the droplet velocity. Results represent mean  $\pm$  SEM,  $n = 3$ .**

Although significant improvement was observed between printing groups and control groups, less effect was found between the different printing frequencies ( $p > 0.05$ ). This suggests that pressure wave superposition through variance of printing frequency has less

effect on the pyruvate oxidase activity. An explanation is that low wave amplitude will constrain the compression wave due to the pursuit of a stable ejection performance in the first series; thus, superposition of multiple compression waves hardly produce sufficient mechanical stress on pyruvate oxidase [13]. To further verify this hypothesis and investigate the role of increased wave amplitude, second series of printing voltage were executed in the later section (section 3.2).

The correlation between shear rate and printing frequencies was plotted to establish the relationship between shear rate and enzyme activity. Although the activity varied from 10.84% to 14.10% with the shear rate from  $2.05 \times 10^5 \text{ s}^{-1}$  to  $3 \times 10^5 \text{ s}^{-1}$ , no correlation was identified ( $p = 0.3894$ ) between shear rate and enzyme activity for the first series. It is deduced, in our case, that wave superposition was not significant enough to intensify the shear force on enzyme ink.

### 3.3.2 Effects of wave amplitude under different printing voltages

As wave amplitude is proportional to the printing voltage, different printing voltages were used to investigate the effects of wave amplitude on pyruvate oxidase activity (second series). Statistical differences ( $p < 0.05$ ) were observed for the enzyme activity increase among printing groups in the second series in Figure 3-5. It is verified wave amplitude had significant effects on the catalytic activity of pyruvate oxidase. Less improvement was obtained when further increasing the voltage to 32 V or even 36 V group, because large wave amplitude was induced by high fluid shear, resulting in partial enzyme denaturation [17]. Under this circumstance, activity enhancement brought by the printing process was mitigated by the enzyme structure deformation. Normally, higher printing voltage is suggested in inkjet printing process since higher voltage will

prominently increase the efficiency. However, excessive mechanical force induced by high wave amplitude can be detrimental to the enzymes.

A negative correlation was found between shear rate and enzyme activity (second series,  $r = -0.59$ ,  $p < 0.05$ ): lowest shear rate of  $2.52 \times 10^6 \text{ s}^{-1}$  increased the activity by 13.55% ( $p < 0.05$ ) whereas highest shear rate of  $5.11 \times 10^6 \text{ s}^{-1}$  can only enhance the activity by no more than 5%. That is because, mechanical activation dominated the change at the situation of lower shear force. However, denaturation occurred when higher shear rate was reached [2]. The effects of enzyme denaturation were also found by other researchers through fluid shear on bovine insulin [20] and lysozyme [37]. Further verification for the assumption of enzyme structure change was performed by circular dichroism and presented in section 3.3.

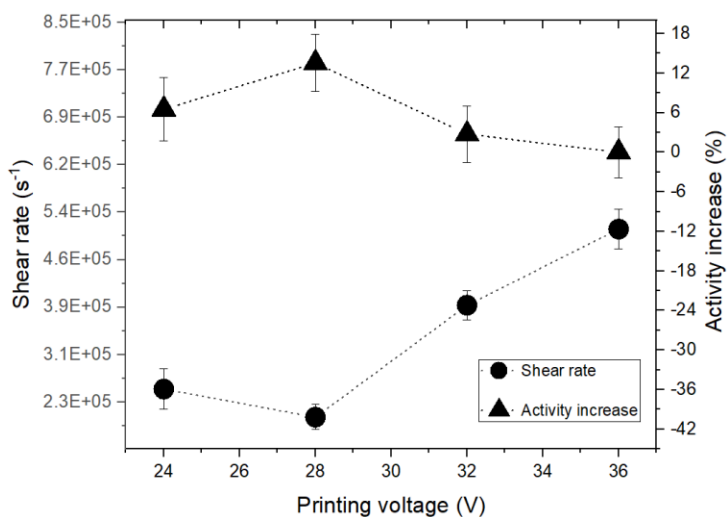


**Figure 3-5: Increase percentage of the enzyme activity and the shear rate after printing under 24, 28, 32 and 36 V at 6 kHz (second series). The unprinted enzyme ink was the control group. Enzyme activity was calculated based on the pyruvate oxidase activity assay. Increase percentage of the enzyme activity was calculated**

compared to the unprinted control group. Shear rate was deduced from the droplet velocity. Results represent mean  $\pm$  SEM,  $n = 3$ .

### 3.3.3 Secondary Structure of Protein after Printing

To verify the hypothesis that mechanical stress will induce a change of protein's secondary structure, circular dichroism was performed to characterize enzyme's secondary structure before and after printing. Glucose oxidase and peroxidase were also printed using the same ink formula as a comparison. Figure 3-6, figure 3-7 and figure 3-8 show the CD spectra of different enzyme ink exposed to shear rates driven by different printing voltage. Percentages of different secondary structures were calculated and listed in the supporting information (see Table S1).

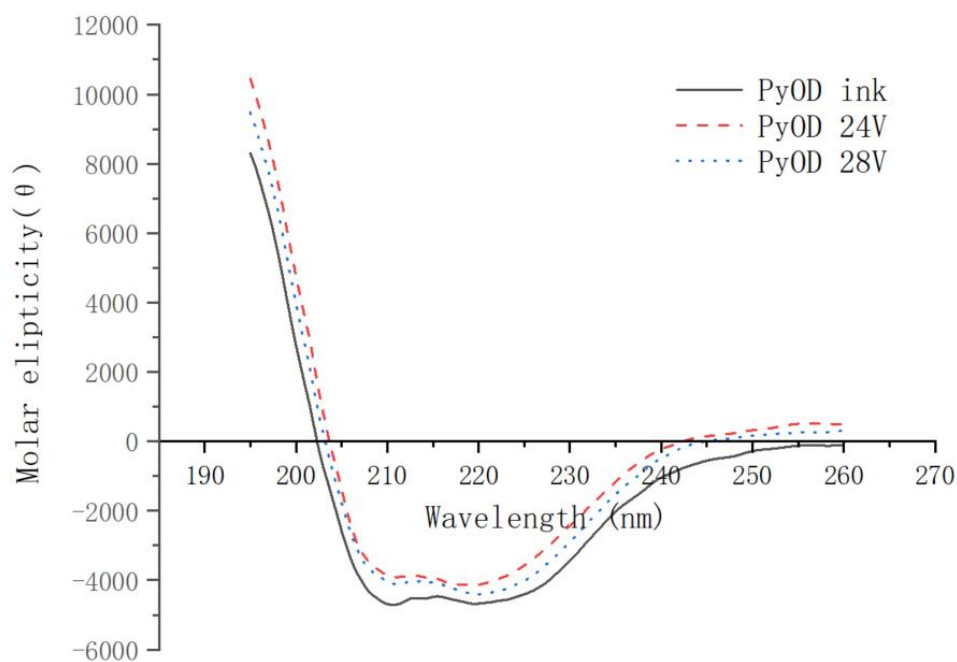


**Figure 3-6: Circular dichroism spectra of unprinted pyruvate oxidase ink, sample printed at 24 V and 28 V ( $n = 10$ ). Printing frequency of 6 kHz was used.**

**Table 3-3: Relative secondary structure percentage change compared to unprinted enzyme ink.**

Enzyme	6 kHz 24 V		6 kHz 28 V	
	$\alpha$ -helix	$\beta$ -sheet	$\alpha$ -helix	$\beta$ -sheet
Pyruvate oxidase	72.3%	100.5%	68.1%	110.5%
Glucose oxidase	111.8%	95.8%	89.8%	102.3%
Peroxidase	101.6%	103.2%	103.5%	100.5%

Negative bands at 208 nm, 216 nm and 222 nm presented in all the spectrums indicated  $\alpha$ -helices and  $\beta$ -sheets existed in all the enzyme structure. For pyruvate oxidase,  $\alpha$ -helix content decreased prominently with the increasing of the printing voltage/shear rate. Especially for the group printed at 6 kHz 28 V, a decrease percentage of 31.9% was identified compared to the unprinted group. However,  $\beta$ -sheet content of pyruvate oxidase barely changed in the 6 kHz 24 V group and increased 10.5% compared to the control group. This showed that  $\beta$ -sheet structure was more stable than  $\alpha$ -helix for pyruvate oxidase. In pyruvate oxidase, six parallel  $\beta$ -sheets were surrounded by  $\alpha$ -helices and the active sites were buried in the region interface and uncovered by the C-terminal domain [28, 29]. It can be interpreted by the decrease of  $\alpha$ -helix content at the region interface in the printing process facilitate the entrance of substrate, which improved the catalytic activity of pyruvate oxidase. When considering further the proteolysis occurred during printing process, higher improvement was obtained [38, 39]. Thus, according to

the results shown in Figure 3-6, the change of protein secondary structure and potential proteolysis under pressure wave has positive effect on the activity of pyruvate oxidase.

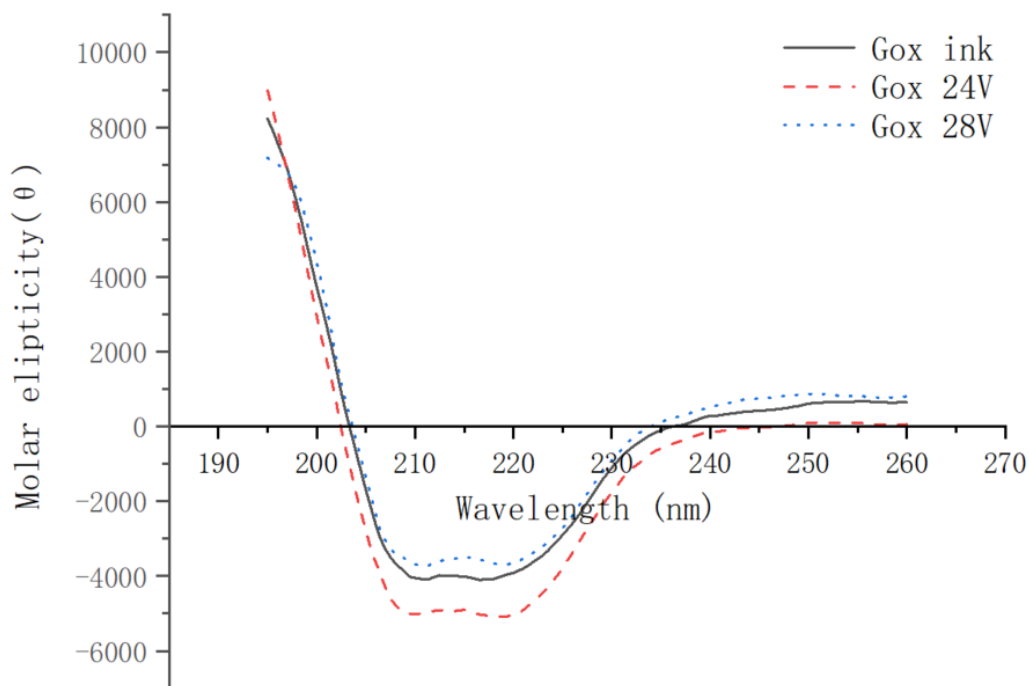


**Figure 3-7: Circular dichroism spectra of unprinted glucose oxidase ink, sample printed at 24 V and 28 V (n = 10). Printing frequency of 6 kHz was used.**

The secondary structures of both glucose oxidase and peroxidase had smaller change of overall percentage ( $\leq 12\%$ ) after printing compared to that of pyruvate oxidase ( $\sim 31\%$ ), as shown in Table 3-3. For glucose oxidase, content of  $\beta$ -sheet was less than 5% for both printing group, indicating glucose oxidase secondary structure was stable under pressure wave, which maintained its activity after printing. Similar conclusions were obtained by other researchers about the glucose printing and sensor fabrication process [7, 40].

For peroxidase, minimal protein unfolding phenomenon was observed from the increased percentage ( $\leq 5\%$ ) of  $\alpha$ -helices and  $\beta$ -sheets for both printing condition. The stable

performance of peroxidase's secondary structure suggests its potential application of inkjet printing peroxidase sensor.

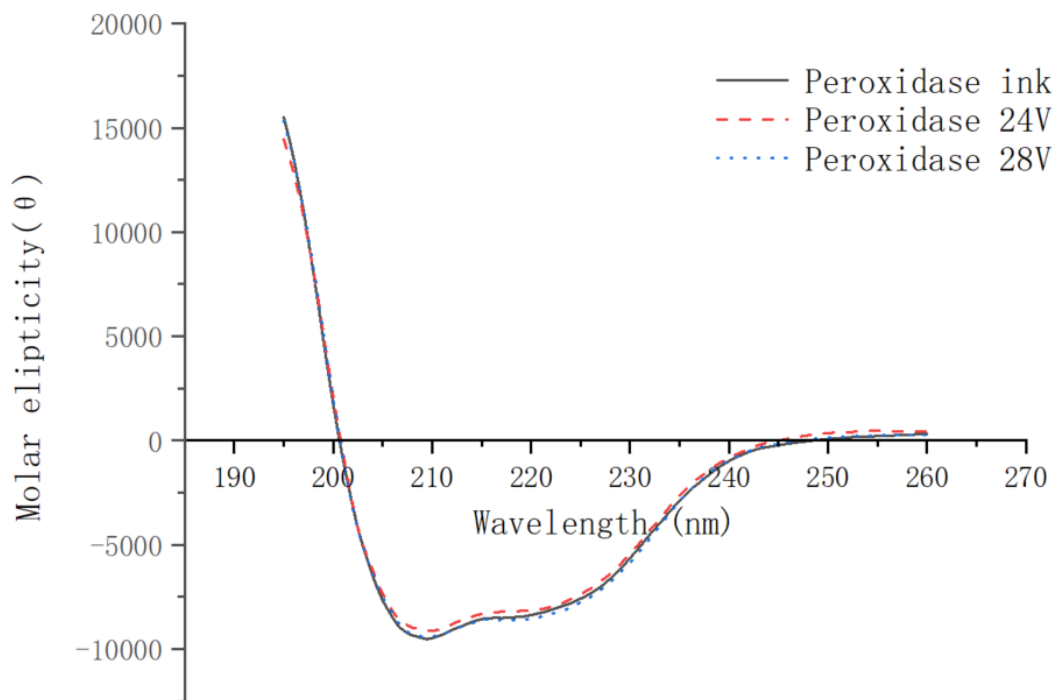


**Figure 3-8: Circular dichroism spectra of unprinted peroxidase ink, sample printed at 24 V and 28 V (n = 10). Printing frequency of 6 kHz was used.**

It is suggested that the change difference of secondary structure between pyruvate oxidase and other enzymes result from the shape, size, structure stability of the enzyme. Glucose oxidase is composed of two identical subunits. Each subunit includes 587 amino acids and has a molecular weight of 66.7 kDa [41]. Peroxidase has 309 amino acids with a molecular weight of 44 kDa [42]. Pyruvate oxidase consists of four identical subunits (603 amino acids) with a molecular weight of 265 kDa [27, 28]. According to the circular dichroism result, we deduced that secondary structure of the enzyme with larger size, more amino acids and more subunits was more instable during the printing procedure. As

pyruvate oxidase activity increased due to the instability nature against printing procedure, the activity-stability trade-off phenomenon on pyruvate oxidase is surprisingly favorable in the inkjet printing process [43]. The change difference of secondary structure between different enzymes suggests that printing parameters should be properly regulated accordingly to modulate the pressure wave and obtain optimum enzyme activity performance for specific enzyme printing.

### 3.4 Conclusions

In this study, we investigated the effect of wave propagation on the activity of pyruvate oxidase. This is the first study to investigate the change of enzyme activity based on the printing mechanism in the bioprinting process. Pyruvate oxidase activity was positively influenced due to the pressure wave induced mechanical forces, and the change of protein conformation induced by mechanical activation or mild proteolysis. It is found, printing frequency had less effect on the variation of pyruvate oxidase catalytic ability, since a limited change of wave superposition was induced; the mechanical stress induced by printing voltage had significant effect on the catalytic efficiency of pyruvate oxidase, and low shear stress tended to create higher enhancement for the activity. That is because partial denaturation and mechanical activation of the enzymes occurred simultaneously when elevated mechanical stress was induced. Comparison of CD spectra results on different enzymes revealed that protein structure change varied due to the property of specific protein.

The results of this paper are favorable for the fabrication of future biosensors to increase their sensitivity and stability. Ink formula and printing parameters need to be adjusted based on not only the requirement of drop formation, but also the performance of the



enzyme ink. The practice of correlating the pressure wave propagation and corresponding mechanical stress with the enzyme activity alteration is meaningful for other researches of enzyme printing.

## References

1. Bhalla, N., P. Jolly, N. Formisano, and P. Estrela, *Introduction to biosensors. Essays in biochemistry*, 2016. **60**(1): p. 1-8.
2. Derby, B., *Bioprinting: inkjet printing proteins and hybrid cell-containing materials and structures. Journal of Materials Chemistry*, 2008. **18**(47): p. 5717-5721.
3. Delaney, J.T., P.J. Smith, and U.S. Schubert, *Inkjet printing of proteins. Soft Matter*, 2009. **5**(24): p. 4866-4877.
4. Bihar, E., S. Wustoni, A.M. Pappa, K.N. Salama, D. Baran, and S. Inal, *A fully inkjet-printed disposable glucose sensor on paper. npj Flexible Electronics*, 2018. **2**(1): p. 30.
5. Yun, Y.H., B.K. Lee, J.S. Choi, S. Kim, B. Yoo, Y.S. Kim, K. Park, and Y.W. Cho, *A Glucose Sensor Fabricated by Piezoelectric Inkjet Printing of Conducting Polymers and Bionzymes. Analytical Sciences*, 2011. **27**(4): p. 375-375.
6. Wang, T., C. Cook, and B. Derby. *Fabrication of a Glucose Biosensor by Piezoelectric Inkjet Printing. in 2009 Third International Conference on Sensor Technologies and Applications. 2009.*
7. Setti, L., A. Fraleoni-Morgera, B. Ballarin, A. Filippini, D. Frascaro, and C. Piana, *An amperometric glucose biosensor prototype fabricated by thermal inkjet printing. Biosens Bioelectron*, 2005. **20**(10): p. 2019-26.
8. Wijshoff, H. *Manipulating drop formation in piezo acoustic inkjet. in NIP & Digital Fabrication Conference. 2006. Society for Imaging Science and Technology.*
9. Bogy, D.B. and F. Talke, *Experimental and theoretical study of wave propagation phenomena in drop-on-demand ink jet devices. IBM Journal of research and development*, 1984. **28**(3): p. 314-321.
10. Reis, N., C. Ainsley, and B. Derby, *Ink-jet delivery of particle suspensions by piezoelectric droplet ejectors. Journal of Applied Physics*, 2005. **97**(9): p. 094903.
11. Shah, M.A., D.-G. Lee, and S. Hur, *Design and Characteristic Analysis of a MEMS Piezo-Driven Recirculating Inkjet Printhead Using Lumped Element Modeling. Micromachines*, 2019. **10**(11): p. 757.
12. Ezzeldin, M., P. Van Den Bosch, A. Jokic, and R. Waarsing. *Model-free optimization based feedforward control for an inkjet printhead. in 2010 IEEE International Conference on Control Applications. 2010. IEEE.*

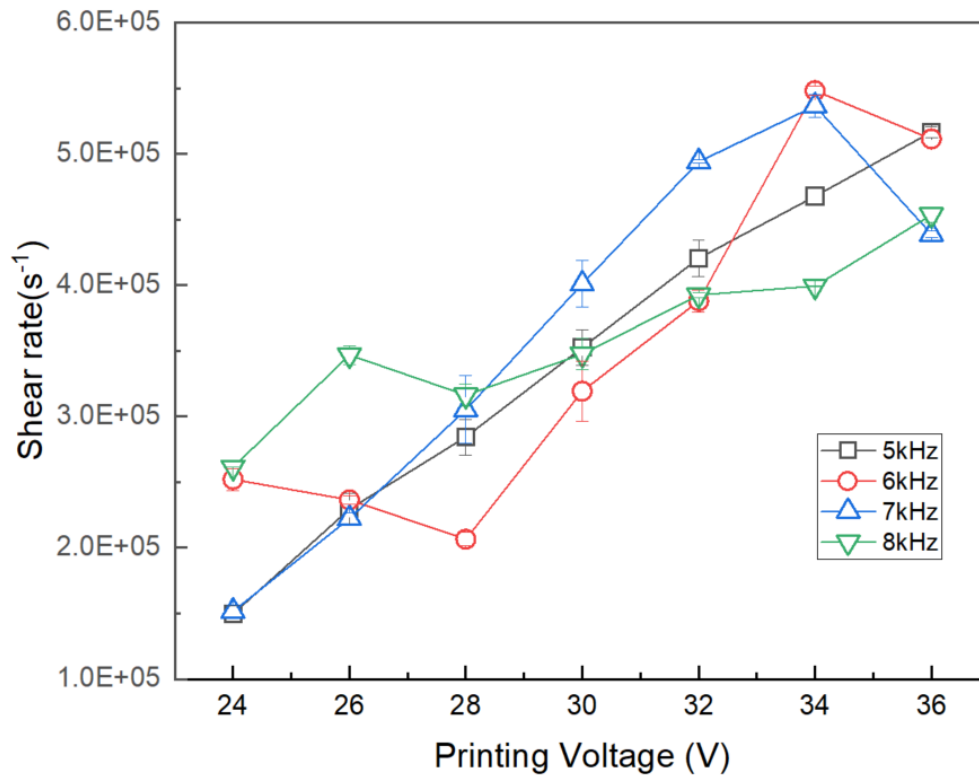
13. Nishioka, G.M., A.A. Markey, and C.K. Holloway, *Protein damage in drop-on-demand printers*. J Am Chem Soc, 2004. **126**(50): p. 16320-1.
14. Cook, C.C., T. Wang, and B. Derby, *Inkjet delivery of glucose oxidase*. Chemical Communications, 2010. **46**(30): p. 5452-5454.
15. Juan, E.C., M.M. Hoque, M.T. Hossain, T. Yamamoto, S. Imamura, K. Suzuki, T. Sekiguchi, and A. Takenaka, *The structures of pyruvate oxidase from Aerococcus viridans with cofactors and with a reaction intermediate reveal the flexibility of the active-site tunnel for catalysis*. Acta Crystallogr Sect F Struct Biol Cryst Commun, 2007. **63**(Pt 11): p. 900-7.
16. Biswas, T.T., J. Yu, and V.A. Nierstrasz, *Effects of ink characteristics and piezoelectric inkjetting parameters on lysozyme activity*. Scientific Reports, 2019. **9**(1): p. 1-11.
17. Di Stasio, E. and R. De Cristofaro, *The effect of shear stress on protein conformation: Physical forces operating on biochemical systems: The case of von Willebrand factor*. Biophysical chemistry, 2010. **153**(1): p. 1-8.
18. Thomas, C. and D. Geer, *Effects of shear on proteins in solution*. Biotechnology letters, 2011. **33**(3): p. 443-456.
19. Dickinson, E., R. Miller, and P. Walstra, *Effects of agitation on proteins*, in *Food Colloids*. 2001. p. 245-254.
20. Bekard, I.B. and D.E. Dunstan, *Shear-induced deformation of bovine insulin in Couette flow*. The Journal of Physical Chemistry B, 2009. **113**(25): p. 8453-8457.
21. Li, L., L. Pan, Z. Ma, K. Yan, W. Cheng, Y. Shi, and G. Yu, *All Inkjet-Printed Amperometric Multiplexed Biosensors Based on Nanostructured Conductive Hydrogel Electrodes*. Nano Letters, 2018. **18**(6): p. 3322-3327.
22. Newman, J.D., A.P.F. Turner, and G. Marrazza, *Ink-jet printing for the fabrication of amperometric glucose biosensors*. Analytica Chimica Acta, 1992. **262**(1): p. 13-17.
23. Risio, S.D., *Fundamental investigation of inkjet deposition and physical immobilization of horseradish peroxidase on cellulosic substrates*. 2009.
24. Hering, K., S. Björklund, S. Klein, V. Kocherbitov, and T. Ruzgas. *Inkjet printing of surfactants, proteins and enzymes for biomedical applications*. in *Student Conference Proceedings 2016: 5th Conference on Medical Engineering Science, 1st Conference on Medical Informatics*. 2016. Infinite Science Publishing.
25. Di Risio, S. and N. Yan, *Piezoelectric Ink-Jet Printing of Horseradish Peroxidase: Effect of Ink Viscosity Modifiers on Activity*. Macromolecular Rapid Communications, 2007. **28**(18 - 19): p. 1934-1940.

26. Muller, Y.A. and G.E. Schulz, *Structure of the thiamine- and flavin-dependent enzyme pyruvate oxidase*. Science, 1993. **259**(5097): p. 965.
27. Risse, B., G. Stempfer, R. Rudolph, H. Möllering, and R. Jaenicke, *Stability and reconstitution of pyruvate oxidase from Lactobacillus plantarum: dissection of the stabilizing effects of coenzyme binding and subunit interaction*. Protein Science, 1992. **1**(12): p. 1699-1709.
28. Juan, E.C.M., M.M. Hoque, M.T. Hossain, T. Yamamoto, S. Imamura, K. Suzuki, T. Sekiguchi, and A. Takénaka, *The structures of pyruvate oxidase from Aerococcus viridans with cofactors and with a reaction intermediate reveal the flexibility of the active-site tunnel for catalysis*. Acta crystallographica. Section F, Structural biology and crystallization communications, 2007. **63**(Pt 11): p. 900-907.
29. Neumann, P., A. Weidner, A. Pech, M.T. Stubbs, and K. Tittmann, *Structural basis for membrane binding and catalytic activation of the peripheral membrane enzyme pyruvate oxidase from Escherichia coli*. Proceedings of the National Academy of Sciences, 2008. **105**(45): p. 17390-17395.
30. Delehanty, J.B. and F.S. Ligler, *Method for printing functional protein microarrays*. Biotechniques, 2003. **34**(2): p. 380-385.
31. Saunders, R.E., J.E. Gough, and B. Derby, *Delivery of human fibroblast cells by piezoelectric drop-on-demand inkjet printing*. Biomaterials, 2008. **29**(2): p. 193-203.
32. Sedewitz, B., K.H. Schleifer, and F. Götz, *Purification and biochemical characterization of pyruvate oxidase from Lactobacillus plantarum*. Journal of bacteriology, 1984. **160**(1): p. 273-278.
33. TOYOBO, *PYRUVATE OXIDASE from Microorganism*.
34. Dalagnol, L.M., V.C. Silveira, H.B. da Silva, V. Manfroi, and R.C. Rodrigues, *Improvement of pectinase, xylanase and cellulase activities by ultrasound: Effects on enzymes and substrates, kinetics and thermodynamic parameters*. Process Biochemistry, 2017. **61**: p. 80-87.
35. Wang, Z., X. Lin, P. Li, J. Zhang, S. Wang, and H. Ma, *Effects of low intensity ultrasound on cellulase pretreatment*. Bioresource technology, 2012. **117**: p. 222-227.
36. Guo, Q., Y. He, and H.P. Lu, *Interrogating the activities of conformational deformed enzyme by single-molecule fluorescence-magnetic tweezers microscopy*. Proceedings of the National Academy of Sciences, 2015. **112**(45): p. 13904-13909.

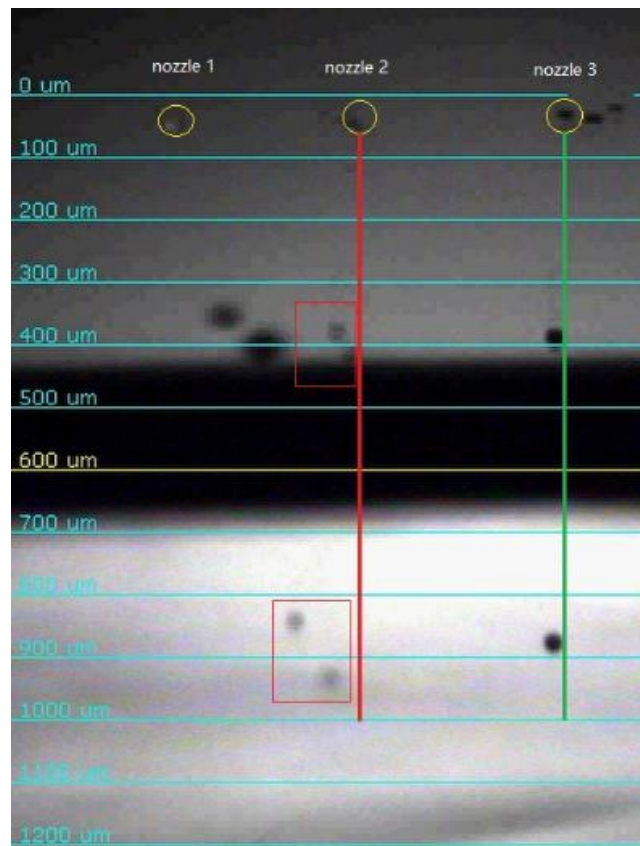
37. Ashton, L., J. Dusting, E. Imomoh, S. Balabani, and E.W. Blanch, *Shear-induced unfolding of lysozyme monitored in situ*. *Biophysical journal*, 2009. **96**(10): p. 4231-4236.
38. Gennis, R.B. and L.P. Hager, *Pyruvate oxidase*, in *The Enzymes of Biological Membranes*. 1976, Springer. p. 493-504.
39. Pill, M.F., A.L. East, D. Marx, M.K. Beyer, and H.J.A.C.I.E. Clausen - Schaumann, *Mechanical Activation Drastically Accelerates Amide Bond Hydrolysis, Matching Enzyme Activity*. 2019. **58**(29): p. 9787-9790.
40. Cook, C., T. Wang, and B. Derby, *Inkjet Printing of Enzymes for Glucose Sensors*. *MRS Online Proceedings Library Archive*, 2009. **1191**.
41. Janati-Fard, F., M.R. Housaindokht, and H. Monhemi, *Investigation of structural stability and enzymatic activity of glucose oxidase and its subunits*. *Journal of Molecular Catalysis B: Enzymatic*, 2016. **134**: p. 16-24.
42. Gajhede, M., D.J. Schuller, A. Henriksen, A.T. Smith, and T.L. Poulos, *Crystal structure of horseradish peroxidase C at 2.15 Å resolution*. *Nature Structural Biology*, 1997. **4**(12): p. 1032-1038.
43. Siddiqui, K.S., *Defying the activity–stability trade-off in enzymes: taking advantage of entropy to enhance activity and thermostability*. *Critical reviews in biotechnology*, 2017. **37**(3): p. 309-322.

## Appendices

**Appendix 3-1: Shear rate at different printing parameter. Results represent mean  $\pm$  SEM,  $n =$  Jetting issues during printing**



**Appendix 3-2: Photo taken by the CCD camera. Blocked nozzle: nozzle 1 was blocked with no droplet jetting; satellite drop/fracted drops: droplet from nozzle 2 was fractured to several pieces immediately after jetting; droplet off the track: droplet from nozzle 3 was stable and round around 900  $\mu\text{m}$  but drift off the center line.**



**Appendix 3-3: Secondary structure percentage of pyruvate oxidase, glucose oxidase and peroxidase.**

Enzyme	Unprinted ink			6 kHz 24 V			6 kHz 28 V		
	$\alpha$ -helix	$\beta$ -sheet	random coil	$\alpha$ -helix	$\beta$ -sheet	random coil	$\alpha$ -helix	$\beta$ -sheet	random coil
Pyruvate oxidase	14.1%	37.2%	49.7%	10.2%	37.4%	49.6%	9.6%	41.1%	49.9%
Glucose oxidase	5.9%	40.0%	53.5%	6.6%	38.3%	58.2%	5.3%	40.9%	50.4%
Peroxidase	31.2%	18.8%	49.5%	31.7%	19.4%	48%	32.3%	18.9%	48.5%



## Chapter 4

### 4 An inkjet printing assisted surface functionalization method for enzyme immobilization to develop a reagentless enzyme-based biosensor

Most enzyme-based biosensors are constructed by a drop-casting method due to its simplicity for surface modification. However, the reproducibility of the drop-casted surface and coffee ring effect have confined the development of drop-casted biosensors. Here, a simple and universal surface functionalization strategy for reagentless enzyme-based biosensor was developed through a novel inkjet printing assisted enzyme crosslinking method. Nanomaterials and a substrate preloading strategy were incorporated during the inkjet printing procedure. Three functional layers, namely enzyme layer, crosslinking layer and protective layer, were printed on the screen-printed electrode to fabricate the biosensor. The biosensor exhibits high sensitivity and a wide linear response which covers the physiological serum phosphate level. Compared with the traditional drop-casted electrodes, the inkjet-printed electrodes in this study present more uniform deposition of functional layers, allowing high reproducibility and enhanced electrochemical performance. The applicability of this surface functionalized method for sensor fabrication was demonstrated through measuring the phosphate concentration using artificial serum samples. The experimental conditions such as printing parameters, concentrations of ink components and buffers, pH of the buffer and test solutions were investigated for optimal sensor performance. This study demonstrates a simple, affordable, labour-free and reagentless manufacturing approach of biosensor. Furthermore, the developed strategy can be easily leveraged to fabricate other enzyme-based biosensors by simply modulating the components of the functional layers.

## 4.1 Introduction

Electrochemical biosensors have becoming a trending topic in the current research of point-of-care testing [1]. Compared with other kinds of electrochemical biosensors, enzyme-based biosensors based on screen-printed electrode have attracted more attention by the researchers due to the merits of high specificity, portability, low cost and possibilities of miniaturization for mass production [2]. As the sensing unit in the enzyme-based biosensors, enzymes are required to be sensitive to the analyte of interest as well as stable and strongly bided to the receptor/working electrode [3]. Thus, to improve the performance of enzyme-based biosensors, enzyme immobilization strategies are essential during the sensor fabrication process [4]. Commonly used immobilization methods are gel entrapment, physical adsorption and cross-linking [5]. The first two approaches are more frequently used in the studies due to the simplicity in the immobilization process. However, drawbacks such as significant diffusion barrier, possible enzyme leakage and weak bond to the electrode surface have confined the stability and reproducibility of the biosensors. To overcome the aforementioned problems, crosslinking method was developed to immobilize the enzyme aiming to create strong binding; this method is usually realized by applying glutaraldehyde or other bifunctional agents with or without the presence of a functionally inert protein such as bovine serum albumin [6]. Currently, the crosslinking process is usually enabled through drop casting technique because of its operation simplicity and rapid reaction. However, the reproducibility of the drop casted surface, coffee ring effect and possibility of mass production have confined the development of drop-casted biosensors [7].

Inkjet printing technique is emerging as a prevailing fabrication approach of biosensors in recent years due to the merits of contactless, efficient use of materials and ease of customization. Various biosensors, such as glucose sensors [8], hydrogen peroxide sensors [9], ascorbic acid sensors [8], lysozyme sensors [10] and cholesterol sensors [11] have been fabricated using inkjet printing technique. Compared with drop casting technique, inkjet printing as a drop-on-demand manufacturing technology can achieve more uniform deposition and higher producibility. To overcome the problem of clogged printhead due to high viscosity of the crosslinked glutaraldehyde and enzymes gel solution, approaches have been taken to incorporate with inkjet printing process, for instance, immobilizing enzymes through the approach of exposure to the vapor of glutaraldehyde [12-14]. The immobilized enzymes retained their activity after printing and crosslinking procedure. However, managed to bypass the viscosity problem, the fabrication this hybrid method is naturally complexed. A more straightforward way for enzyme immobilization during the printing process is demanded and the one-step inkjet printing surface functionalization strategy for enzyme crosslinking will be demonstrated in this work. In addition, the dependence of electrochemical cell is another concern which still limits the further on-site use of the sensor. Enlightened by a preloading strategy [15], the required substrates for enzyme catalyzed reaction can be preloaded via inkjet printing on the screen-printed electrodes, resulting in a reagentless biosensor.

In this study, a surface functionalization method for crosslinking the enzymes through inkjet printing technique was developed to fabricate reagentless enzyme-based biosensor, which preload the reagents on the sensing area to eliminate the requirement of electrochemical cell. Herein, the enzymes can be immobilized through inkjet printing

enzyme layer and crosslinking layer, which simplifies the two-step crosslinking procedure of printing enzymes and exposure to the glutaraldehyde vapor. To be specific, the enzyme layer consists of pyruvate oxidase and cofactors as the reaction catalyst, while the subsequent printing layer of glutaraldehyde helps to crosslink the enzyme layer on the sensing electrode. Crosslinking agent bovine serum albumin and conducting nanomaterials (carboxylic multi-walled carbon nanotubes) are introduced to strengthen the enzyme immobilization and sensing property. A final layer serves as a protective and ion-selective membrane is also printed to cover the enzyme layer and crosslinking layer. Herein, pyruvate oxidase has been chosen as the model enzyme because pyruvate oxidase is the sensing element for the mono-enzyme phosphate sensor, and the level of phosphate in the biofluids of serum is important for the clinical diagnosis of hyperphosphatemia, cardiovascular and chronic kidney disease [16, 17]. The proposed ink printing surface functionalization strategy offers a new alternative for efficient fabrication of the highly reproducible enzyme-based biosensors.

## 4.2 Materials and methods

### 4.2.1 Chemicals and instruments

Pyruvate oxidase from *microorganism* (PyOD, E.C.1.2.3.3, 10 U/mg) was purchased from Toyobo (New York, USA). Multiwall carbon nanotubes (5-15  $\mu\text{m}$ ) were purchased from Shenzhen Nanotech Port Co., Ltd (Shenzhen, China) and functionalized before use. Bovine serum albumin (BSA), Triton X-100, hydrochloric acid, nitric acid, sulfuric acid, potassium ferricyanide (III) ( $\text{K}_3\text{Fe}(\text{CN})_6$ ), glutaraldehyde (GLA), Nafion<sup>®</sup> (5 wt.%), magnesium sulfate, sodium bicarbonate, citric acid and sodium citrate dihydrate were obtained from Sigma-Aldrich. Thiamine pyrophosphate (TPP), flavin adenine

dinucleotide (FAD), magnesium chloride ( $\text{MgCl}_2$ ) and pyruvic acid were purchased from TCI. All reagents were used as received unless otherwise stated.

All solutions were prepared in the deionized water ( $18.2 \text{ M}\Omega\cdot\text{cm}^{-1}$ ). 50 mM phosphate stock solution (pH 6.0) and 25 mM citrate buffer (CB, pH 5.6) were prepared according to normal lab procedures and stored at  $4^\circ\text{C}$ . Basic artificial serum solution for sensor validity study was made by mixing 0.68 g sodium chloride, 0.02 g calcium chloride, 0.04 g potassium chloride, 0.01 g magnesium sulfate, and 0.22 g sodium bicarbonate together in 0.1 liter DI water and stored in  $4^\circ\text{C}$  [18]. Then, different concentration of phosphate solution was dissolved in the basic artificial serum solution.

Screen printed electrode (C10) were purchased from Mxense Bio-Tech Co., Ltd. (Shanghai, China) with a three electrode system: a working electrode (material: carbon, geometry area:  $0.053 \text{ cm}^2$ ), a counter electrode (material: carbon), and a reference electrode (material:  $\text{Ag}/\text{AgCl}$ ). SNB-1 Viscosimeter (Karoht Shanghai, China) was used to measure the viscosity at room temperature. BZY101 Automatic Surface Tensiometer (Vetus Anhui, China) was used to characterize the surface tension. A Fujifilm DIMATIX Materials Printer DMP-2831 (FUJIFILM Dimatix, Inc., USA) was used to carry out printing experiments. UV-vis absorption spectra were recorded with Cary 100 UV-visible spectrophotometer (Agilent, USA). A Nicolet 6700 spectrophotometer (Thermo Nicolet) was used to record the Fourier transform infrared (FTIR) spectra under transmittance mode. Scanning electron microscopy (SEM, Hitachi S-4500) was used to observe the morphology at a 10 kV accelerating voltage. Atomic force microscope (AFM, Dimension V AFM) was performed to examine the surface roughness of the working electrode.

Cyclic voltammetry (CV) measurements were conducted with CHI potentiostat (1200C, Shanghai Chen Hua Instrument Co., Ltd., Shanghai, China).

#### 4.2.2 Functionalization of the MWCNTs

To improve the solubility of MWCNTs in the water-based ink and enhance their affinity with enzymes, MWCNTs were functionalized with -COOH group by modifying the oxidation method reported by Yu-Chun Chiang *et.al.* [19, 20]. First, MWCNTs were soaked in the hydrochloric acid for 24 h. Then precipitating the MWCNTs from solution by centrifuging for 15 mins and rinsing with deionized water three times. After that, MWCNTs were dried in the air and 100 mg of MWCNTs were added in 40 ml nitric acid and sulfuric acid solution with a weight ratio of 1: 3. The obtained mixture was heated and stirred at 50°C for 24 h. After that, 100 mL of distilled water was added into the mixture. Next, the mixture was centrifuged, washed with distilled water until the dispersion turned neutral. Then the dispersion was dried in vacuum at 50 °C over night. Finally, the obtained functionalized MWCNTs were stored dry at room temperature.

#### 4.2.3 Ink formulation

To prepare the printing ink of enzyme layer (enzyme ink), we prepared a solution containing 16 U/ml pyruvate oxidase, 25  $\mu$ M TPP, 6  $\mu$ M FAD, 2 mM MgCl<sub>2</sub>, 2 mM pyruvic acid, 0.5 mg/ml functionalized MWCNTs (filtered by 0.2  $\mu$ m filter before use), 2.4% w/v BSA and 0.0075% v/v Triton X-100 using the prepared stock solutions. The enzyme ink was gently mixed and left for 30 minutes before use. For the ink of crosslinking layer (GLA ink), 2.5 % w/v GLA and 0.006% v/v Triton X-100 was prepared in deionized water. The ink for top protective layer (Nafion ink) consisted of 1.5% w/v Nafion and 0.005 % v/v Triton X-100.

Different concentration of Triton $\times$ -100 were used to modulate ink surface tension according to the printing performance and droplet surface wetting. Viscosities were also optimized within the range of ink printability suggested by the printer manufacturer.

#### 4.2.4 Functionalization of the working electrode by inkjet printing

The printing waveforms (see Appendix 4-1) and printing parameters were optimized based on our previous studies to ensure stable printing while maintaining high enzyme activity [21]. Fiducial camera was used to ensures the uniform deposition of the pattern by observing the relative position of adjacent drops during the printing process [22]. The drop spacing was set as 20  $\mu\text{m}$ . The screen-printed electrode was heated to 30  $^{\circ}\text{C}$  while printing for quick evaporation of the printed ink. Droplet counts of different layers were programmed through Pattern Editor Module to ensure defined amount of material deposition. The schematic diagram for the cross section of the functionalized working electrode is shown in Figure 4-1. Specifically, 20 layers of enzyme ink (459,330 counts) were firstly printed in the working electrode, followed by 10 layers of GLA ink (229,665 counts). The first two layers reacted to form a crosslinking composite. In the end, 10 layers of Nafion ink (229,665 counts) were printed on top of it to form a protective and selective membrane.

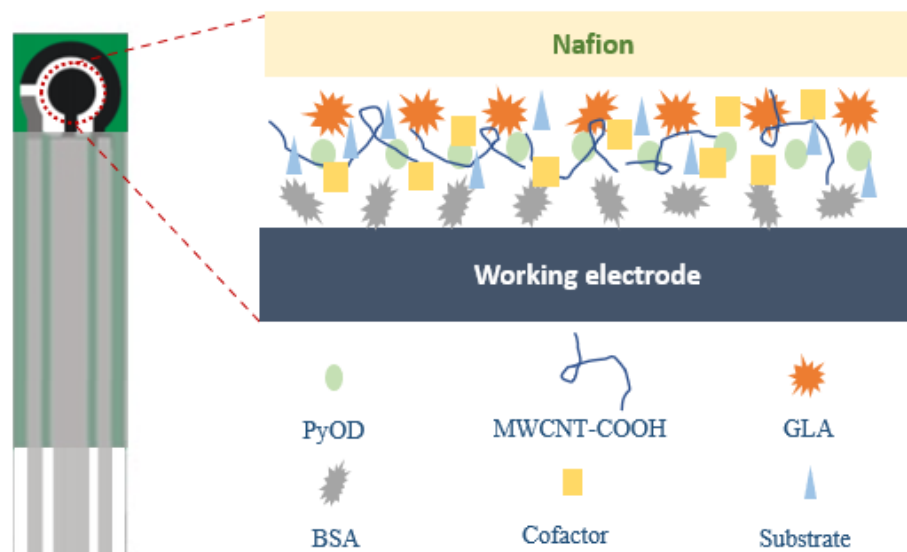


**Figure 4-1: Schematic diagram for the cross section of the functionalized working electrode.**

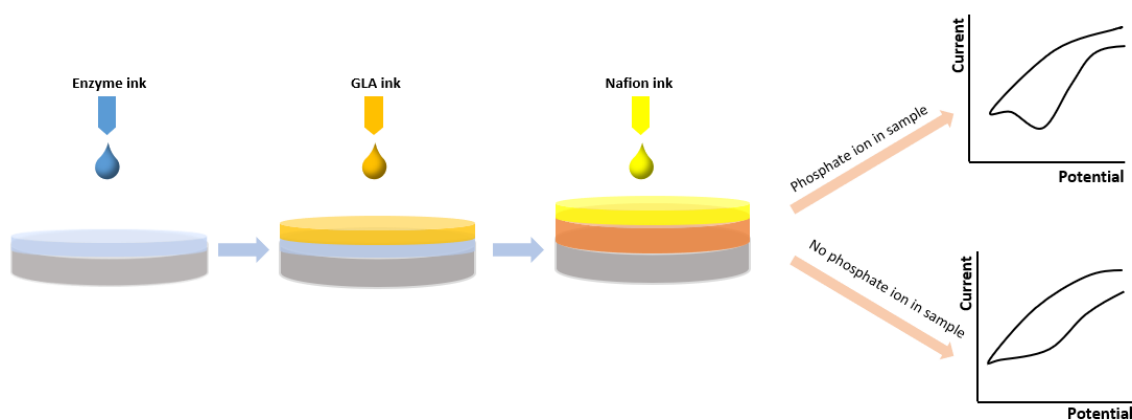


**Figure 4-2: Schematic of the working electrode functionalization process and the sensor sensing mechanism.**

Figure 4-2 shows the functionalization process of the working electrode and the working mechanism of the proposed phosphate sensor. The bottom layer (blue layer) represents the MWCNTs-COOH/enzyme/cofactor/substrate/BSA composite. The bottom layer



includes the necessary cofactors and substrates for the analyte reaction aiming to eliminate the process of reagent addition which is usually adopted in common electrochemical measurements. MWCNTs with carboxyl group were chosen because of their high affinity to the enzyme protein, high surface area for more enzyme loading and superior electrochemical property [20, 23]. BSA as the stabilizing and sacrificial agent in the printing and crosslinking process was included in the enzyme layer [6, 24, 25]. The screen-printed electrode was heated throughout the whole printing process to facilitate the droplet evaporation and decrease the tendency of liquid extension for higher deposition precision and uniformity on the working electrode. GLA (orange layer) was printed subsequently to form a crosslinking composite (red layer) together with the bottom layer by using the reaction between the amino groups of lysine residues on the external surface of BSA/enzyme with the GLA [24]. The printing of the semipermeable nafion layer (yellow layer) serves as a protective and ion selective membrane. The biosensor can detect the oxidation current of reaction product  $\text{H}_2\text{O}_2$  when the sample with phosphate ion is dropped onto the sensing area, because of the following reactions:



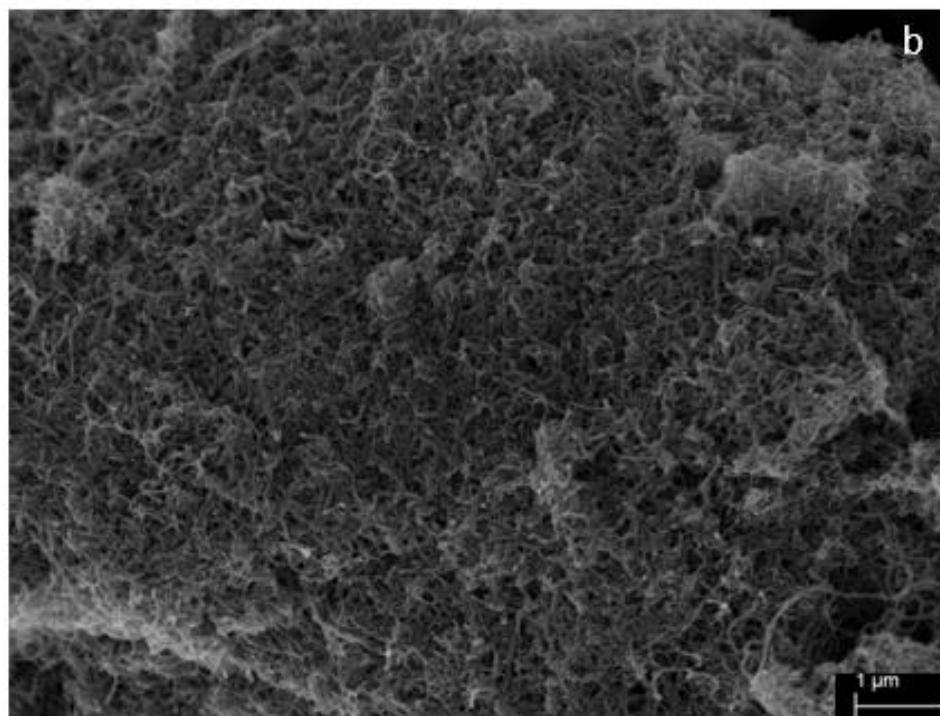
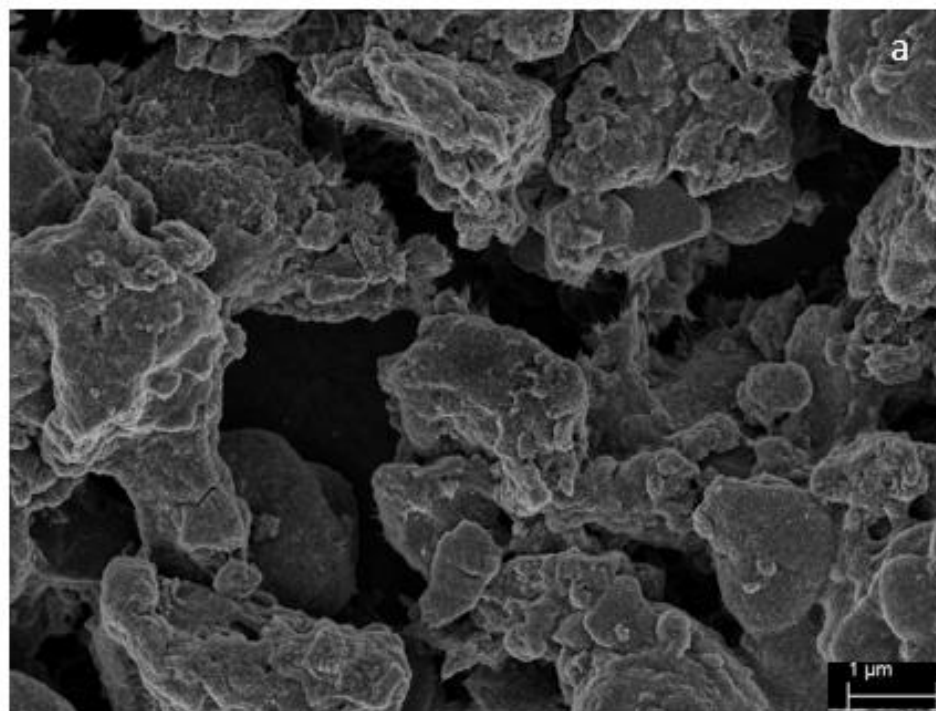
At that time, anodic peak (oxidation of the hydrogen peroxide) can be observed upon sweeping of the potential on the working electrode.

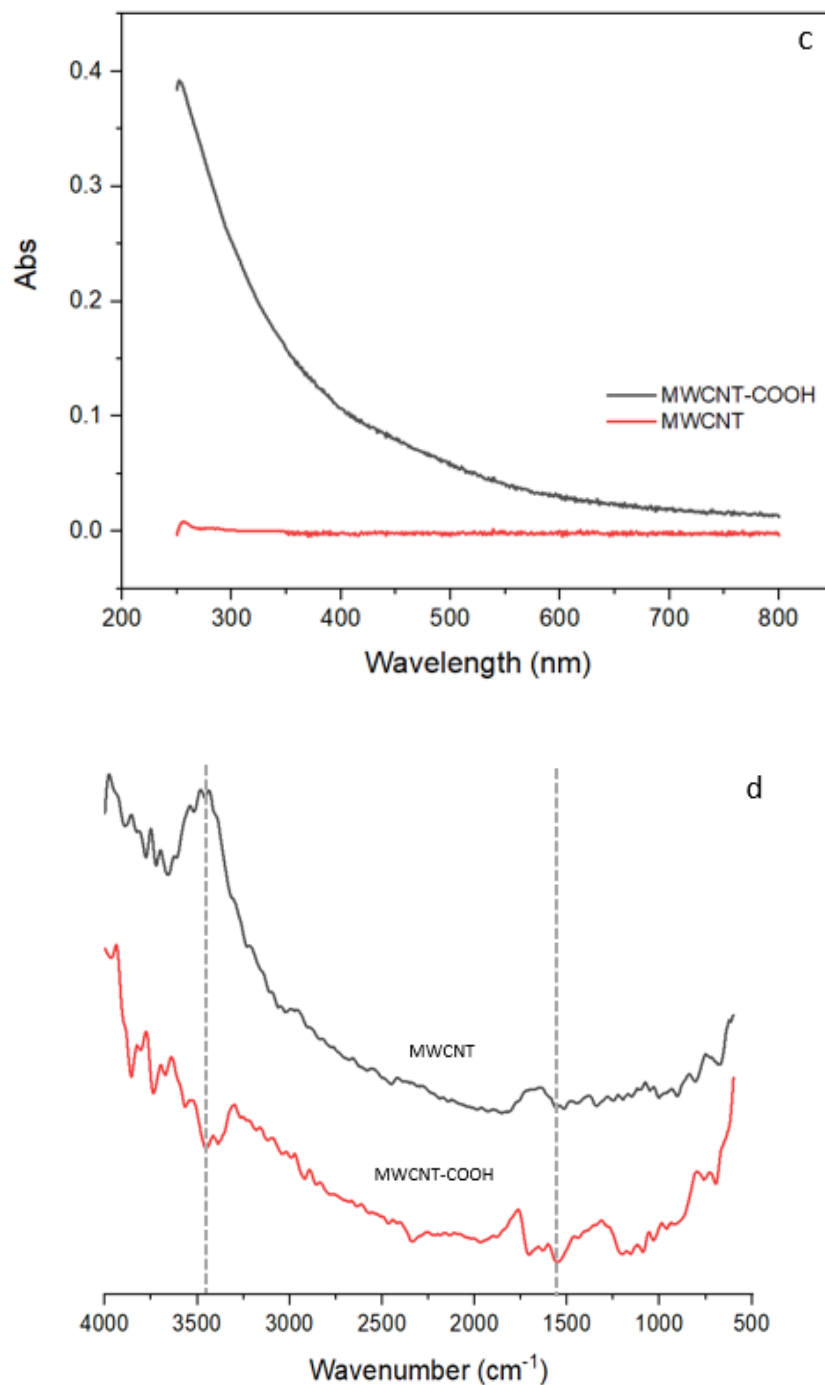
#### 4.2.5 Voltammetric experiments using the proposed biosensor

30  $\mu\text{l}$  of prepared phosphate solution or artificial serum solution was dropped onto the sensing area of the biosensor. Potential range was set between 0 and 0.6 V at a scan rate of 50 mV/s. All electrochemical responses were measured three times to obtain the average. All experiments were performed based on the above settings unless otherwise stated.

## 4.3 Results and discussion

### 4.3.1 Characterization of the functionalized MWCNTs

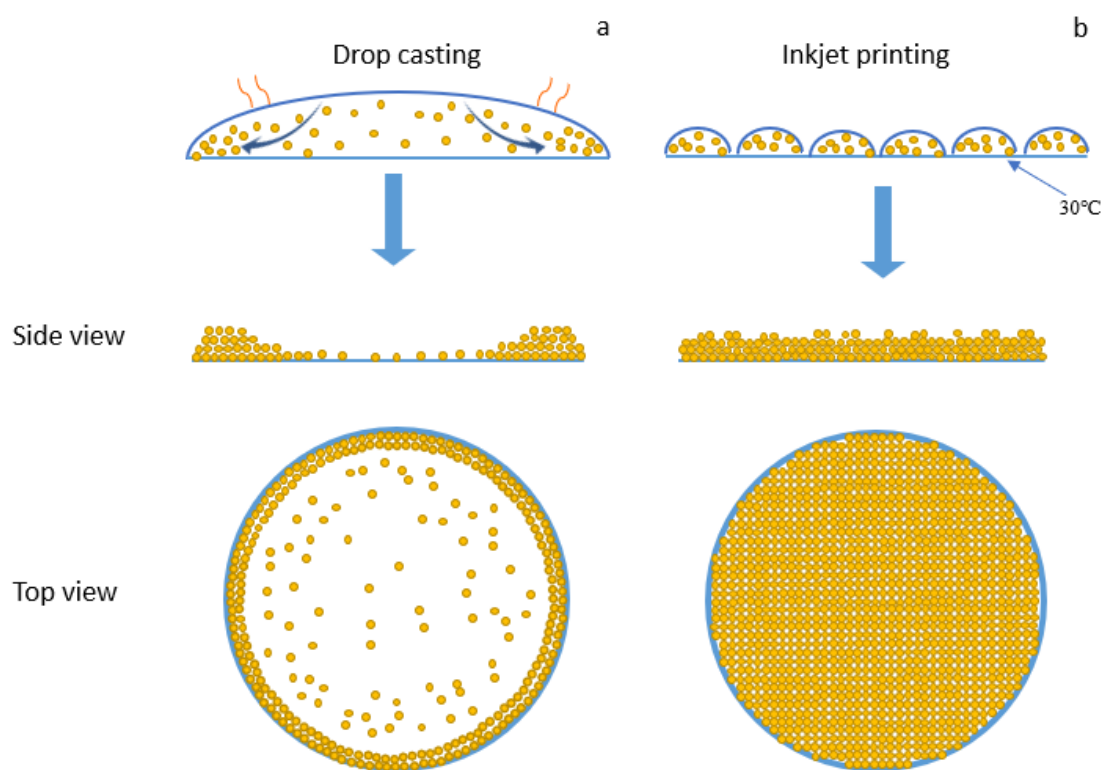




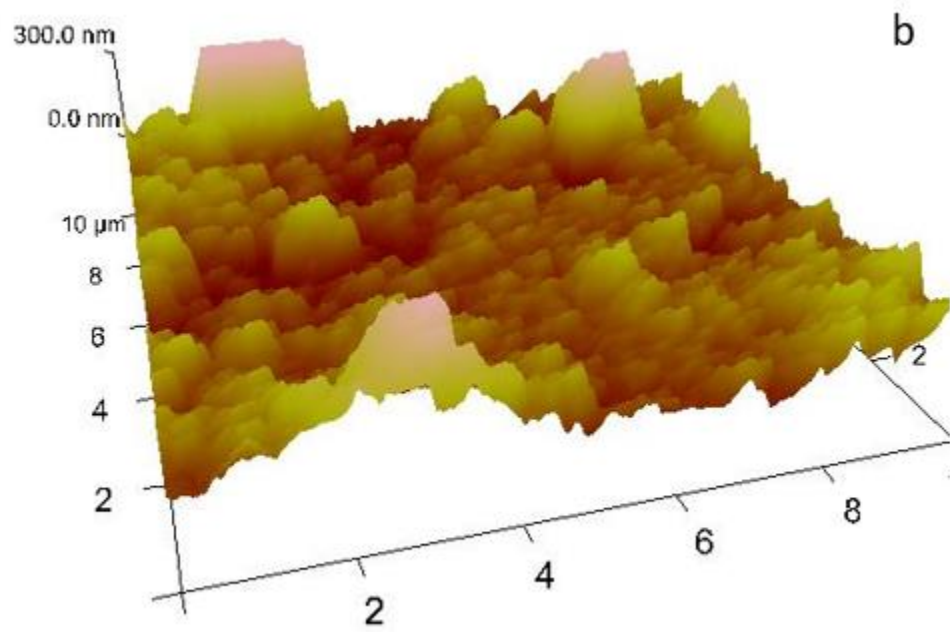
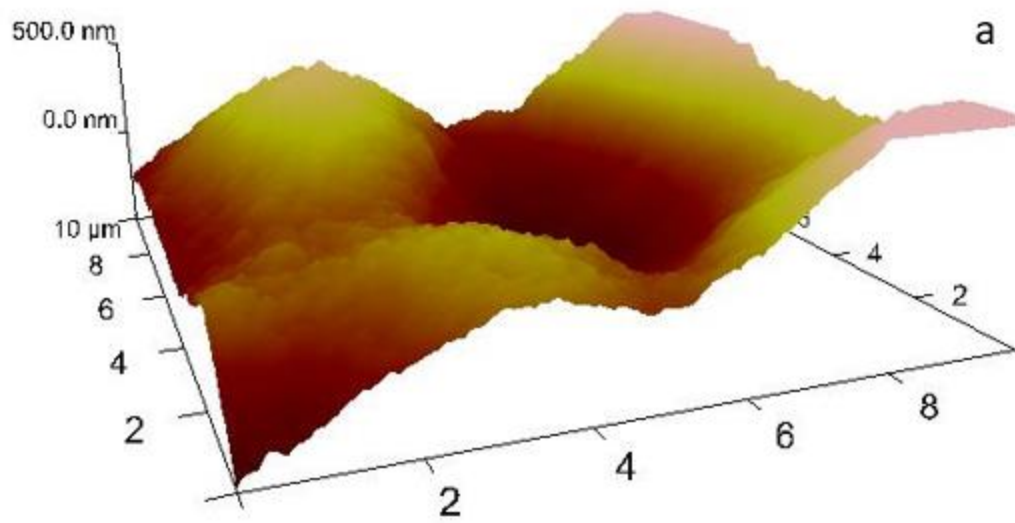
**Figure 4-3: (a) SEM images of the aggregated MWCNTs. (b) SEM images of the MWCNTs-COOH. (c) UV-vis absorption spectra of the MWCNTs solution and the MWCNTs-COOH solution. (d) FTIR of the MWCNTs and the MWCNTs-COOH.**

Compared with the non-modified MWCNTs, which aggregated easily on the substrate due to its hydrophobic property (Figure 4-3(a)), the functionalized MWCNTs have a better distribution (Figure 4-3(b)). UV-vis absorption spectrums were further utilized to compare the improvement, as shown in Figure 4-3(c). Both CNT solutions (5 mg/ml) were filtered by 0.2  $\mu\text{m}$  filter due to the requirement of ink printability. The absorbance of filtered non-modified MWCNT solution was almost same with the buffer solution ( $\sim 0$ ) meaning that most of the MWCNTs were filtered away due to severe aggregation. The absorbance of the filtered modified MWCNT solution showed a regular increasing tendency towards lower wavelength demonstrating the high dispersion property after functionalization [26]. The characteristic peaks at 3438 and 1610  $\text{cm}^{-1}$  in the FTIR transmission spectrum of MWCNTs-COOH indicated that the stretching vibrations of O-H and C=O of carboxyl groups (Figure 4-3(d)) [27]. Occurrence of these peaks in the FTIR spectrum suggested the successful inclusion of -COOH groups on the external surface of MWCNTs [28].

### 4.3.2 Comparison of functionalization performance between of drop-casting and inkjet-printing methods



**Figure 4-4: Schematic of the drying process of the droplet on the electrode, side view and top view of the particle distribution status by (a) drop casting method and (b) inkjet printing method.**



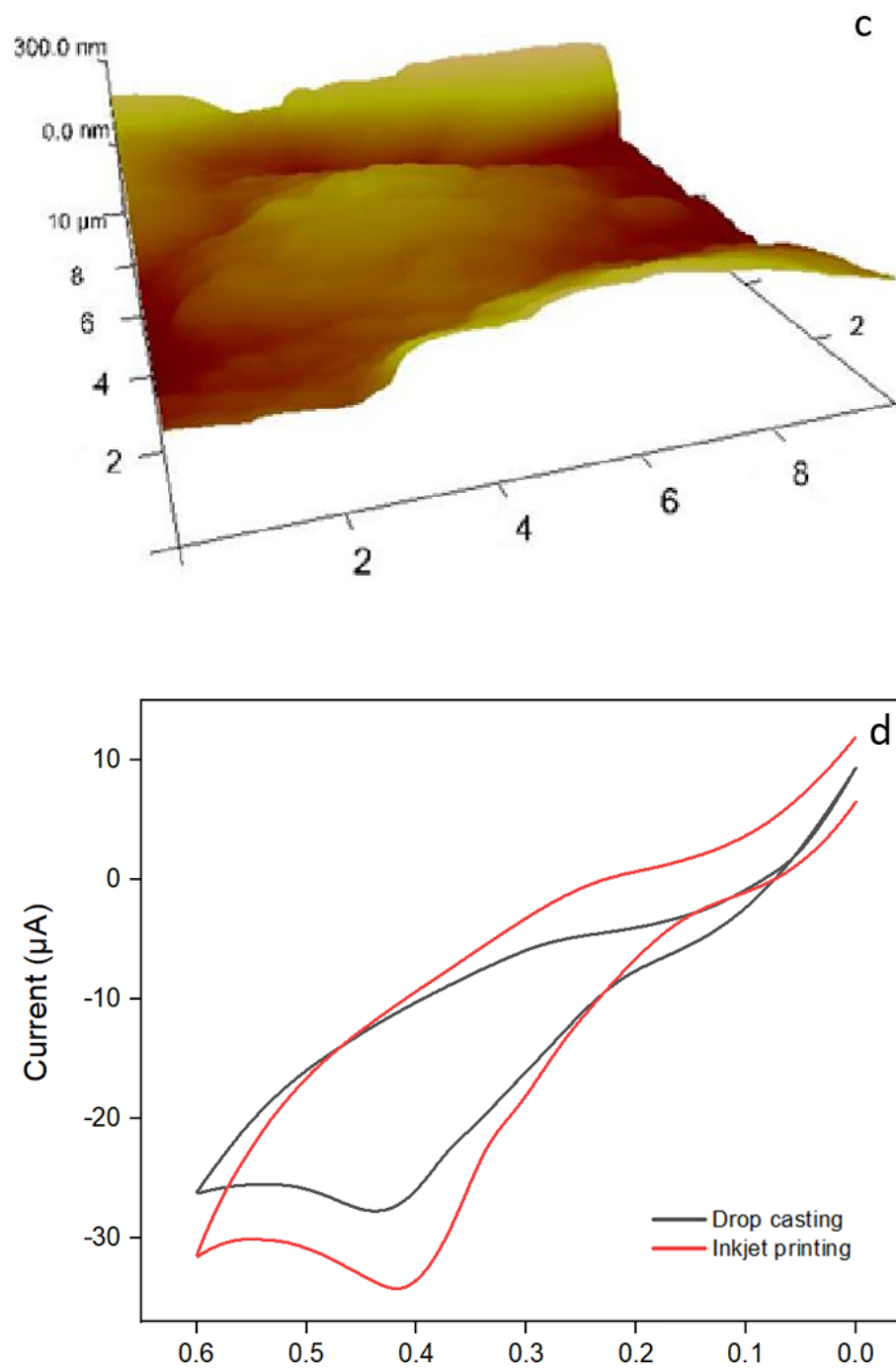


**Figure 4-5: (a) AFM image of the “coffee ring” effect by drop casting method. (b) AFM image of an area between the center and the “coffee ring” on the working electrode by drop casting method. (c) AFM image of the same area with (b) by**



**inkjet printing method. (d) CV curves of the functionalized electrode fabricated by drop casting method and inkjet printing method in the presence 2 mM phosphate. Scan rate: 50 mV/s.**

Inkjet printing method can effectively eliminate the “coffee ring” effect that is always occurred during traditional drop casting method. [29]. AFM was used to demonstrate the improvement by comparing the surface roughness. A schematic illustration of the drying process and characterization results were shown in Figure 4-4, and Figure 4-5 separately. When the ink was drop-casted on the working electrode, the ingredients of the ink would be pushed to the edge of the drop due to capillary flow during evaporation, causing a “coffee ring” on the edge (Figure 4-5(a)). Figure 4-5(a) proved the formation of the “coffee ring” showing the height different at the outer side of the electrode. The middle part of the drop-casted electrode showed a bumpy morphology that indicated less particle distribution (Figure 4-5(b)). Compared to drop casting method, inkjet printing deposited micro-droplets and the droplets evaporated separately on the electrode which largely decrease the particle aggregation phenomenon (Figure 4-4(a)). It is also proved by the AFM that the coffee ring effect was largely mitigated by our inkjet printing method (Figure 4-5(c)). The mitigation effect can be interpreted by the smaller droplet size (decrease the coffee ring size [30]), substrate heating procedure (accelerate evaporation time [22]) and the inclusion of surfactant (increase Marangoni flow [31]).

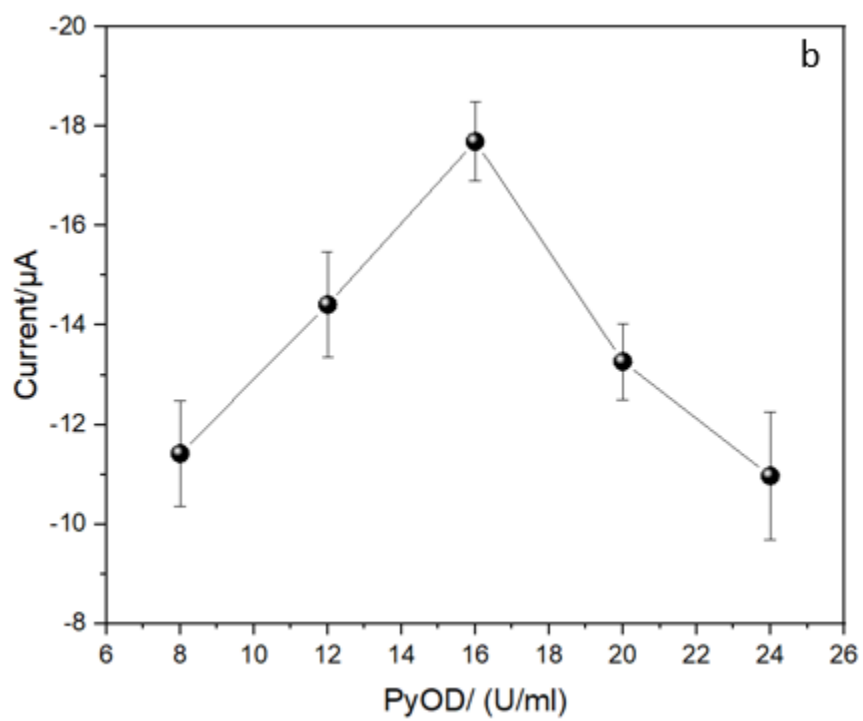
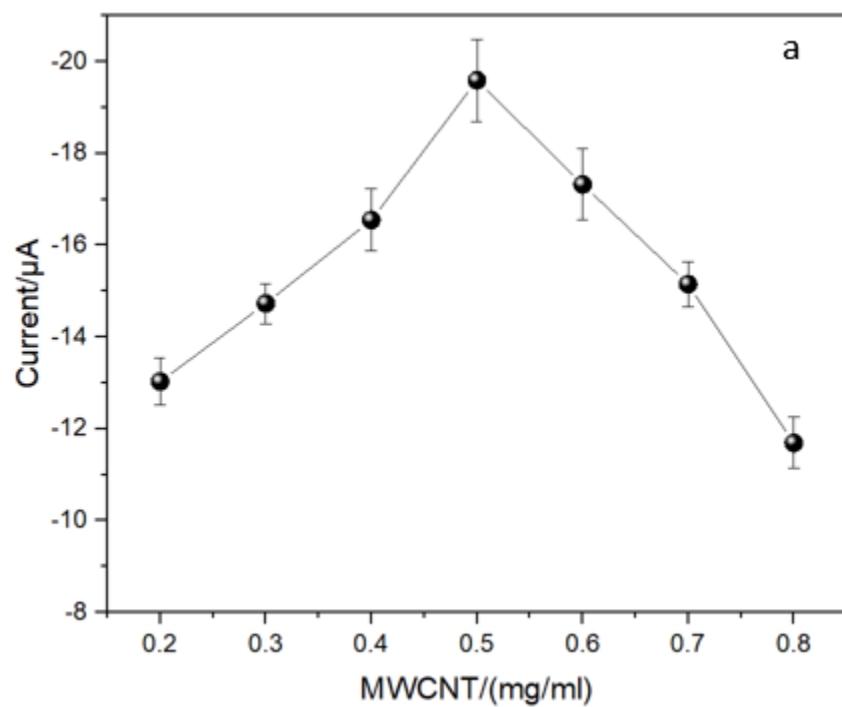
CV responses of the functionalized electrode by drop casting and inkjet printing were included in Figure 4-5(d) to compare their effects on the analytical performance. Higher

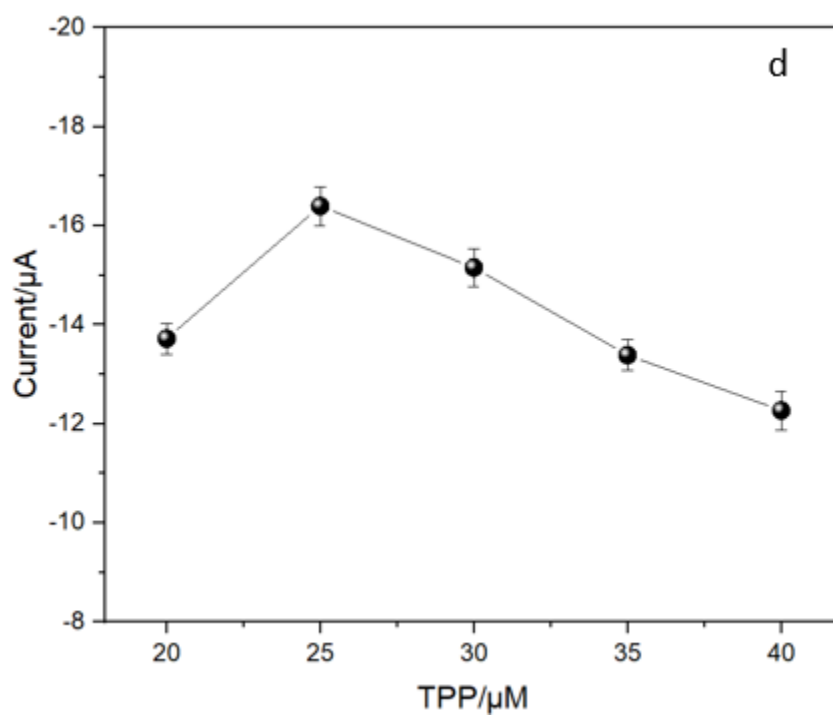
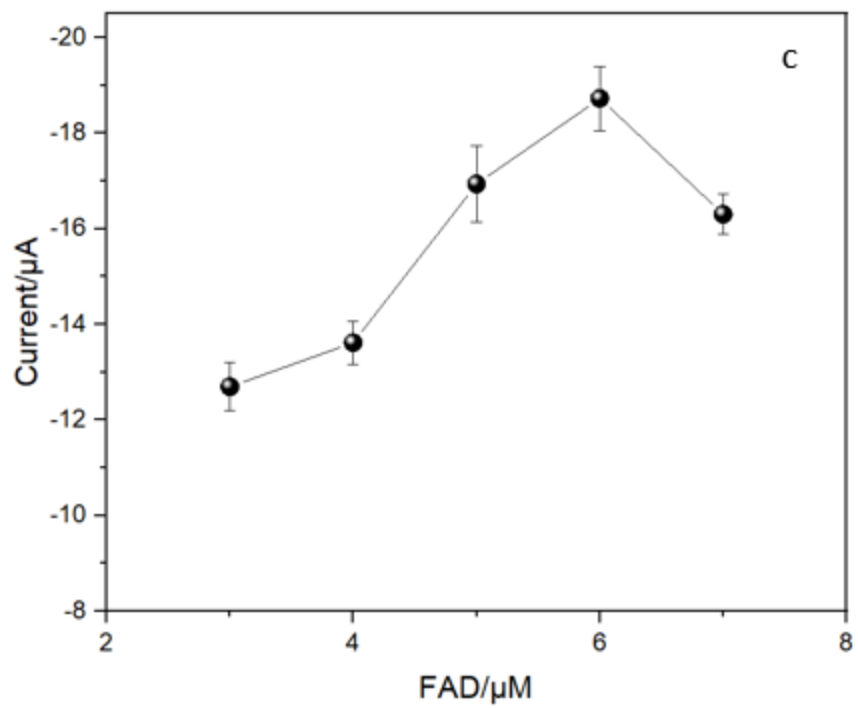
and more evident oxidation peak was shown by inkjet printing method. The effective surface area of electrode can be obtained by Randles-Servick equation [32, 33]:

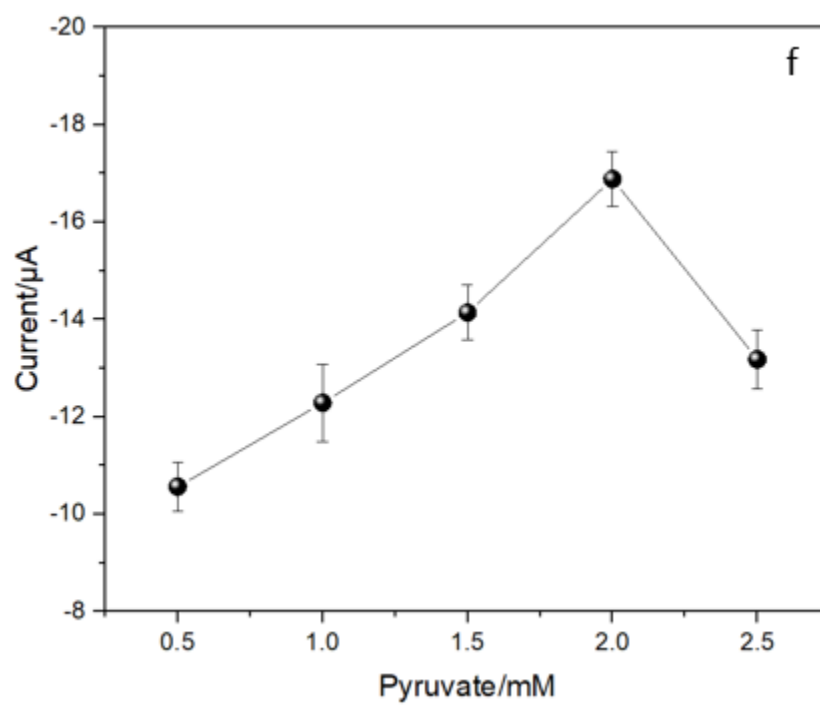
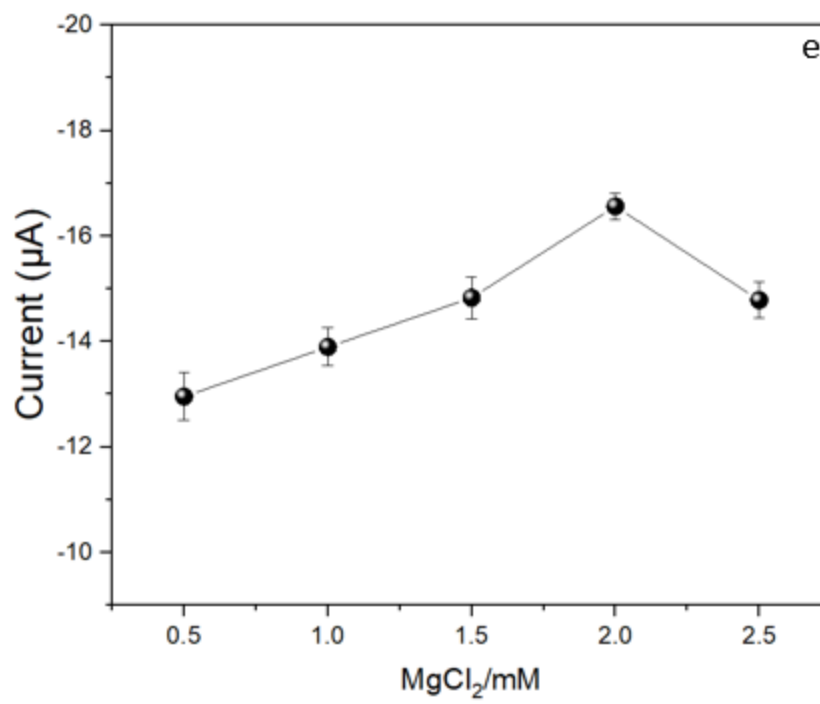
$$I_p = 268600n^{3/2}AD^{1/2}C\nu^{1/2} \quad (1)$$

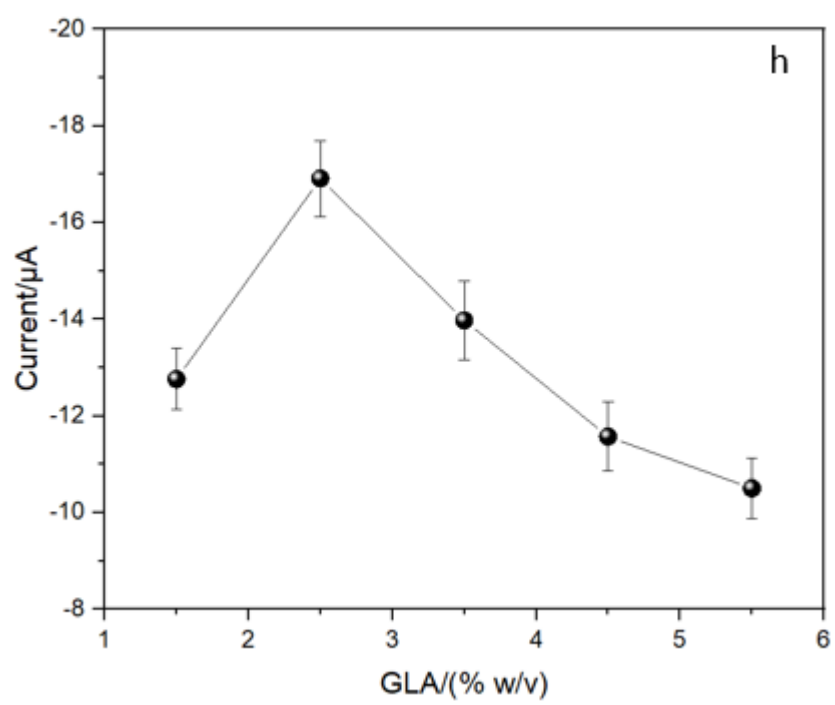
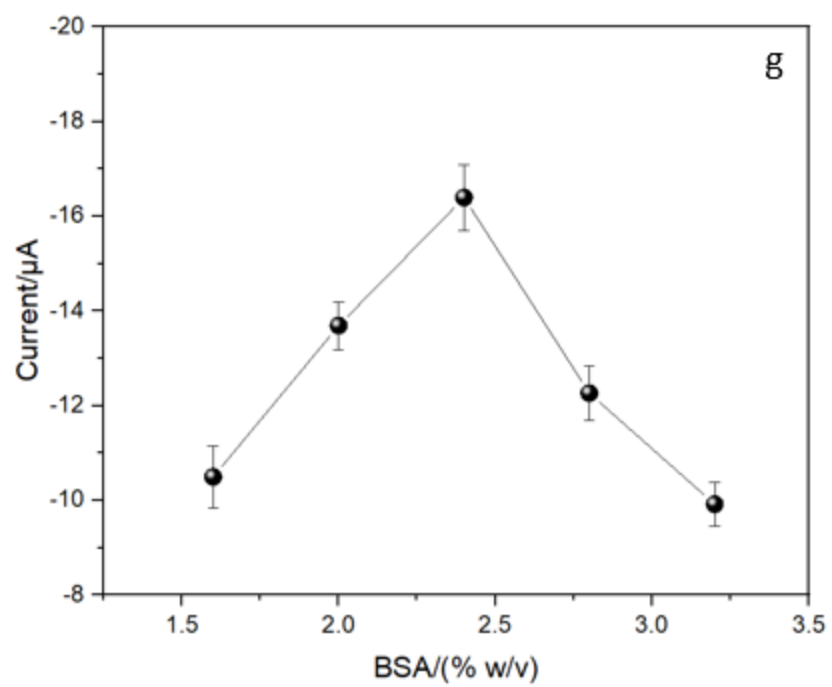
Where  $I_p$  is the peak current,  $n$  is the electron transfer number,  $A$  is the electroactive surface area,  $D$  is the diffusion coefficient of the electrolyte,  $C$  is the electrolyte concentration and  $\nu$  is the scan rate. With other parameters being constant in the equation,  $I_p$  is proportional to the effective surface area  $A$ . The effective surface area of inkjet printing modified electrode was calculated to be around 1.5 times than the drop casted electrode, which suggested the superiority of inkjet printing technique for electrochemical measurement. Since the formation of uniformly functionalized working electrode was also required based on the fabrication reproducibility [7], the machine-controlled inkjet printing method was undoubtedly superior than the traditional drop-casted for the electrode modification.

### 4.3.3 Optimization of the sensor









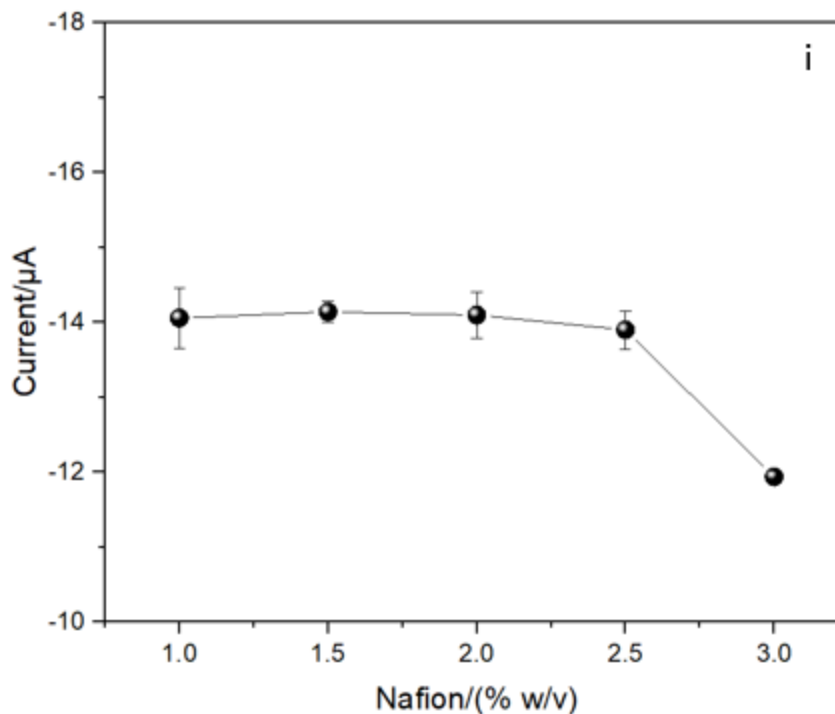


**Figure 4-6: Effects of the concentration of (a) MWCNTs-COOH, (b) PyOD, (c) FAD, (d) TPP, (e) MgCl<sub>2</sub>, (f) pyruvate, (g) BSA, (h) GLA, (i) Nafion on the oxidation peak current of the cyclic voltammogram obtained from the modified electrode. Phosphate concentration measured was 2 mM.**

The effect of functionalized MWCNTs-COOH on the electrochemical performance of the biosensor is shown in Figure 4-6(a). The concentration of functionalized MWCNTs was varied from 0.2 mg/ml to 0.8 mg/ml. The highest peak current was observed at 0.5 mg/ml. The functionalized MWCNTs as an electron transfer shuttle have great influence on the electrochemical reaction. At lower concentration of MWCNTs, the current response increased positively due higher MWCNTs-enzyme bounding. When MWCNTs concentration was too high, it caused the background interference and saturation of the

ink composite which impeded the reaction [34, 35]. 0.5 mg/ml functionalized MWCNTs was chosen to be used for all subsequent experiment.

The effect of pyruvate oxidase on the oxidation current is shown in Figure 4-6(b). The concentration of enzymes varied from 8 U/ml to 24 U/ml. The peak current increased with the enzyme concentration until reaching to the highest value at 16 U/ml. This is because low enzyme loading results in lower rate of enzyme catalysis and corresponding low current, while higher enzyme concentration created higher diffusion barrier that confined the current response [36].

Optimization for the concentration of cofactors (FAD, TPP,  $Mg^{2+}$ ) are shown in Figure 4-6 (c-e). These cofactors shared the same increasing and decreasing tendency upon the variations of peak current. The optimal concentrations of the cofactors are decided by the enzyme loading. Since cofactors bind with the enzyme around the active sites, the current will decrease since the concentrations of cofactors are too high to hinder the enzyme catalytic reaction. The maximum peak currents for FAD, TPP and  $Mg^{2+}$  were found at the concentration of 6  $\mu$ M, 25  $\mu$ M and 2 mM separately. All subsequent experiments were based on these values.

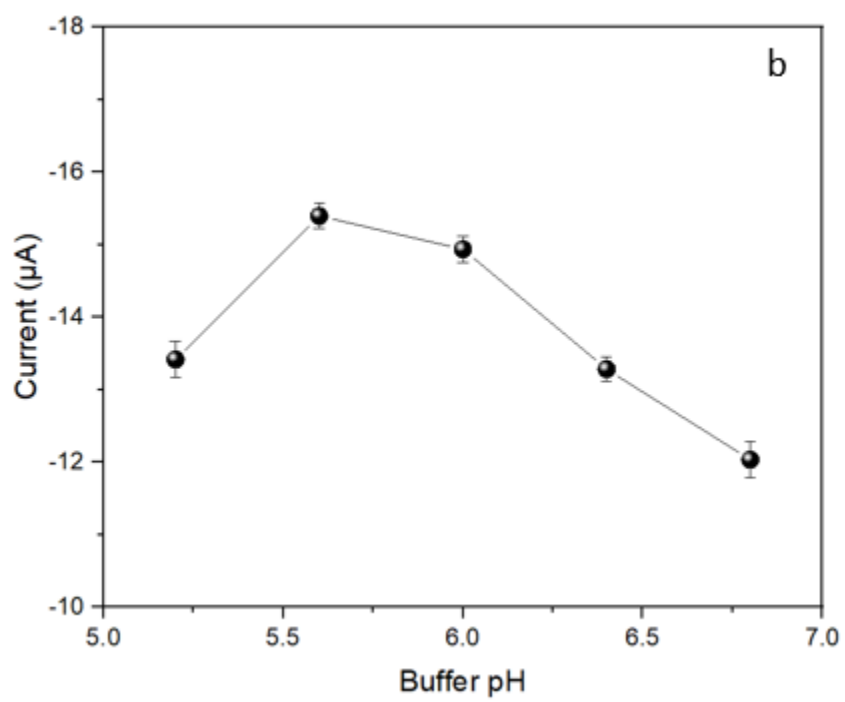
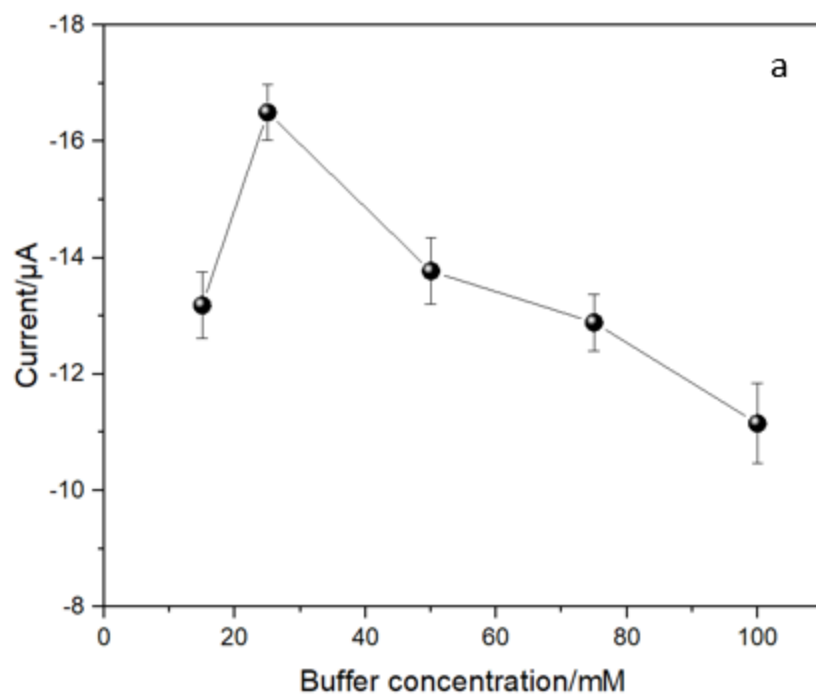
The effect of the concentration of the substrate (pyruvate) was investigated and the results are shown in Figure 4-6(f). The peak current reached the highest value at 2 mM and then begin to drop due to saturation. Thus, 2 mM pyruvate was selected for all subsequent experiments.

The concentration of crosslinking agents (BSA and GLA) was optimized as shown in Figure 4-3(g) and 4-3(h). As an inert lysine rich auxiliary protein and protective spacer,



the concentration of BSA is important for the effective enzyme crosslinking process [36, 37]. The concentration of BSA defines the spacing of enzyme molecules in the crosslinking composite. If the concentration of BSA is excessive, the response current decreases due to high protein content [38]. GLA plays an important role of crosslinking the bottom layer components to form a gel composite. Thus, deficient GLA resulted in peak current reduction due to insufficient crosslinking, while excessive GLA occupies the active sites of enzyme which hinders the reaction [39]. The optimized concentrations of BSA and GLA were 2.4% w/v and 2.5% w/v separately and were used in all subsequent experiments.

We also investigated the optimal concentration of Nafion (Figure 4-6(i)). The peak current for nafion presented a minimal change at low concentration range of 1.0% w/v to 2.5% w/v and begin to drop after 3% w/v because of increased diffusion barrier. 1.5 % w/v was chosen and used in all subsequent experiments due to a relative higher current response.



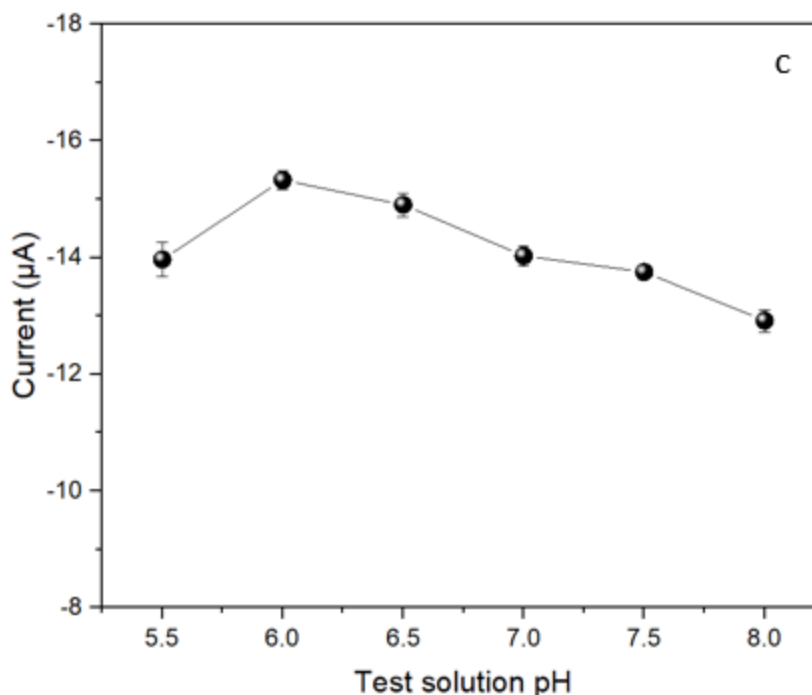
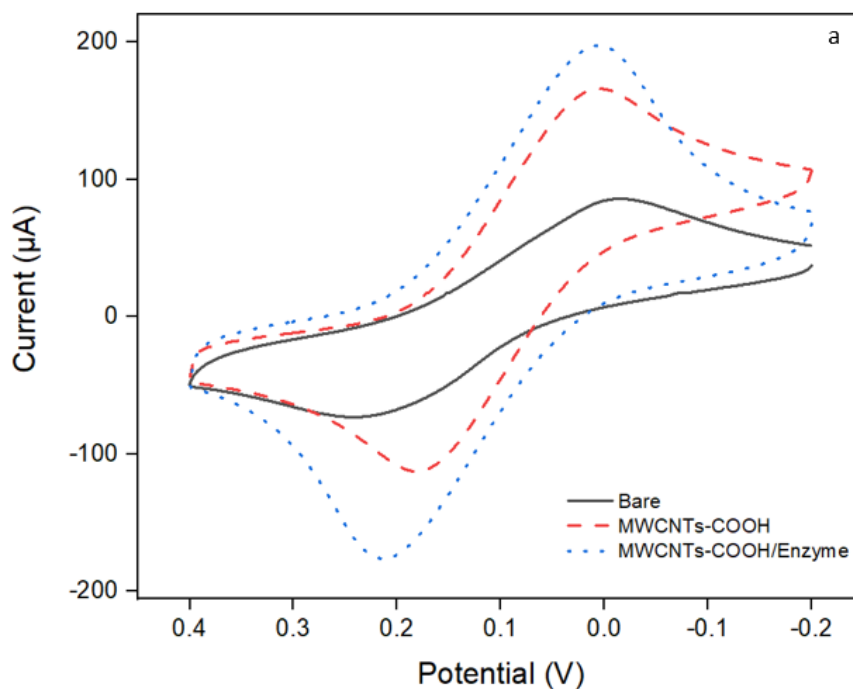


**Figure 4-7: Effects of the (a) the concentration of the citrate buffer, (b) the pH of the citrate buffer, (c) the pH of the test solution on the oxidation peak current of the cyclic voltammogram obtained from the modified electrode. Phosphate concentration measured was 2 mM.**

The concentration and pH of the citrate buffer for the enzyme ink were evaluated, as shown in Figure 4-7(a) and 4-7(b). The concentration of the buffer varied from 15 mM to 100 mM. Higher buffer concentration had higher buffering capacity but hindered the movement of  $\text{H}_2\text{O}_2$  and electron transfer to the electrode [36, 40]. The pH of the citrate buffer was investigated from 5.2 to 6.8. Highest peak current was obtained at pH 5.6. Decrease of the current at lower or higher pH resulted from the decrease of enzyme activity and potential enzyme denaturation [36, 41]. The concentration and pH of the citrate buffer were set to be 25 mM and 5.6 for all the subsequent experiments.

To optimize the pH of the test solution on the peak current, pH of the test solution was varied from 5.5 to 8. As shown in Figure 4-6(c), variation of the peak current within the pH range of 6 to 7 was relatively small (< 6.7%), indicating its potential use for the body fluid phosphate detection.

#### 4.3.4 Evaluation of the modified working electrode



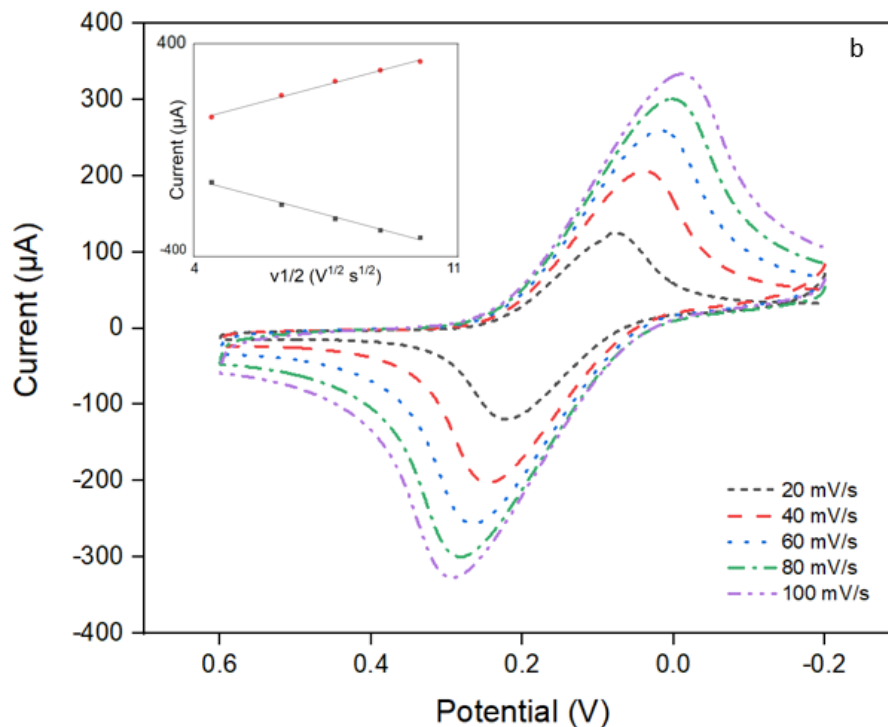
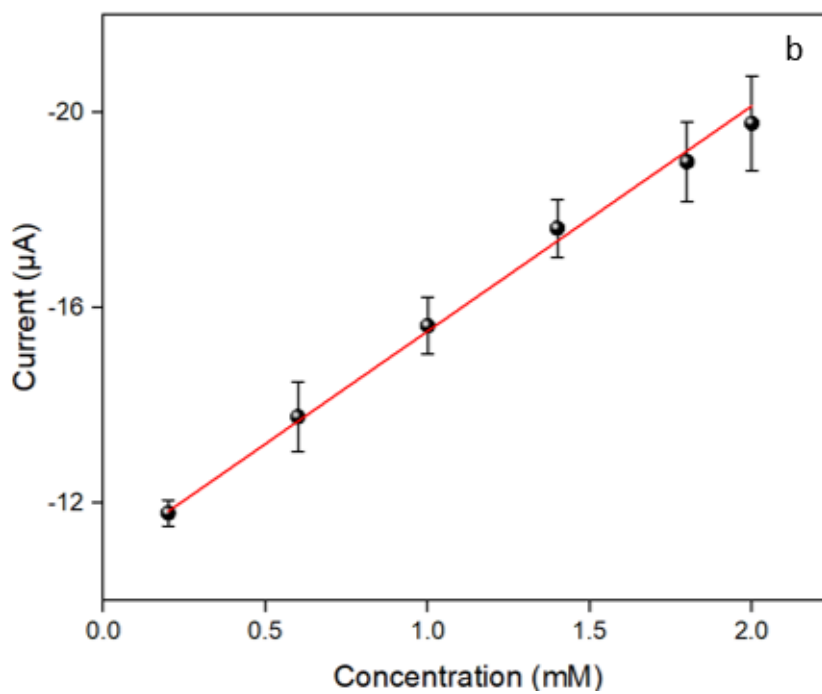
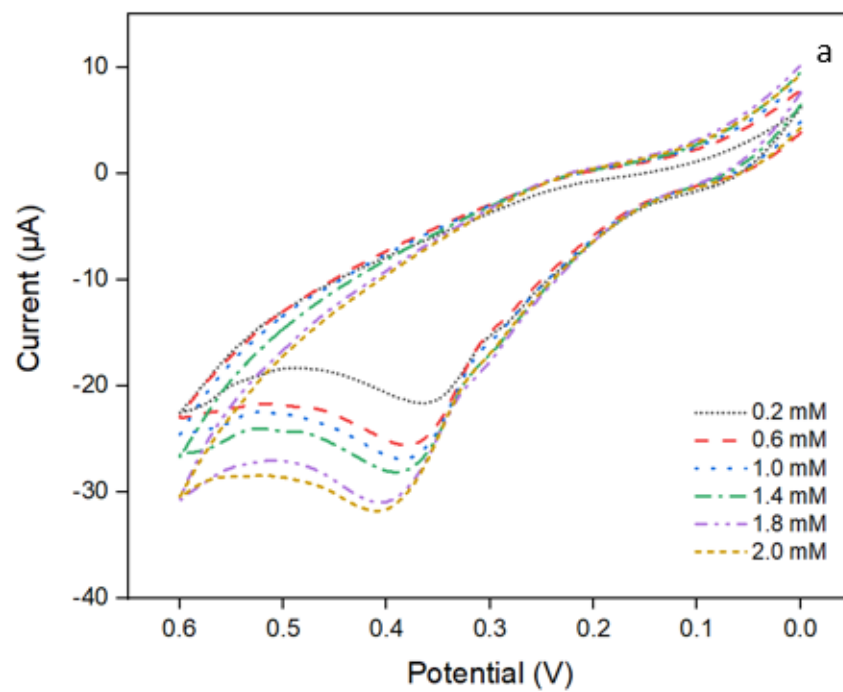


**Figure 4-8: CV curves of bare electrode (solid line), MWCNTs-COOH/substrate/cofactor electrode (dash line), MWCNTs-COOH/enzyme/substrate/cofactor electrode (dot line) in 0.1 M KCl which contained 10 mM  $\text{K}_3\text{Fe}(\text{CN})_6$ . Scan rate: 50 mV/s.**

CV responses of different electrodes to the  $\text{K}_3\text{Fe}(\text{CN})_6$  solution (Figure 4-8(a)) showed that the addition of MWCNTs facilitated the electron transfer process. The presence of MWCNTs-COOH (dash line) decreased the peak-peak separation and increased the peak current (about three times than the bare electrode) which suggested the evident improvement for the electron transfer kinetic [42]. The combination of MWCNTs-COOH and enzyme electrode (dot line) showed even higher peak current than MWCNTs-COOH electrode, which is resulted from the syngenic effect of MWCNTs-COOH and enzyme for electron transfer. As seen in Figure 4-8(b), both anodic/cathodic peak current and

peak-peak separation increased with the scan rate from 20 to 100 mV/s. This suggested that the electrode reaction was a surface-confined and diffusional-controlled process [36]. A linear relationship of the peak current and the square root of the scan rate was acquired (see inset of Figure 4-8(b)), which indicates that the electron transfer process was quasi-reversible.

## 4.3.5 Phosphate detection by cyclic voltammetry



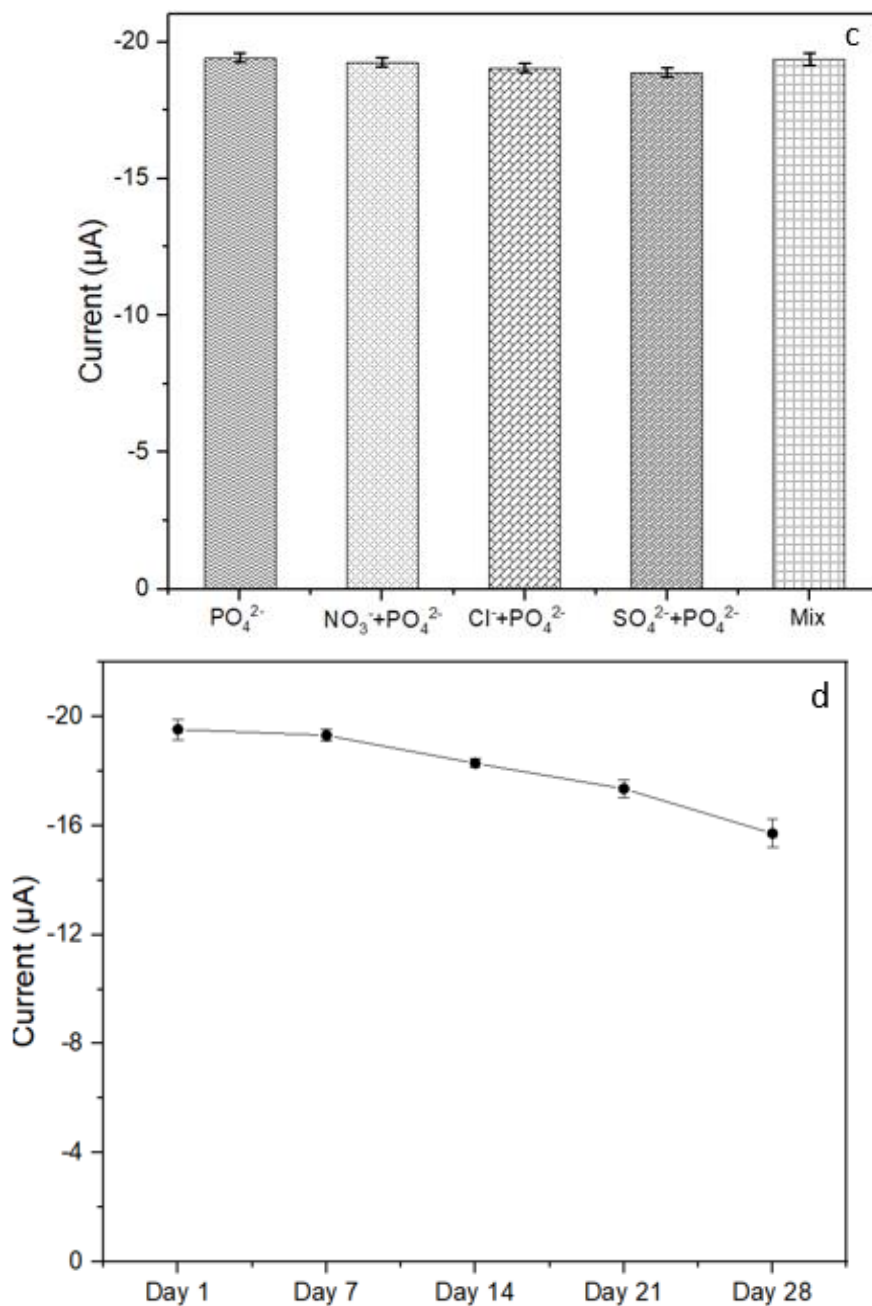


**Figure 4-9: Potentiometric responses of the sensor to different concentration of phosphate. (a) Concentration increased with the direction of the orange arrow (0.2 to 2.0 mM). (b) Calibration curve for different concentration of phosphate. (c) Interference test. (d) Sensor stability test.**



Figure 4-9(a) showed the peak current increased proportionally with the phosphate concentration. The anodic peak current of modified electrode appeared at around the potential of 0.4 V, in agreement with the literature [43]. A wide linear range of 0.2 mM to 2.0 mM ( $R^2 = 0.997$ ) with 0.13 mM detection limit was obtained by the proposed biosensor (see Figure 4-9(b)). The comparison with different electrochemical sensors from the aspects of electrode composition, sensor linear range, use of reagents and manufacturing method are listed in Table 4-1. As for the cost effective manufacturing, inkjet printing is superior to the photolithography method [44]. For the realization of reagentless measurement using SPE sensor, substrate preloading was achieved in this work, which excels other biosensors that required additional reagents [39, 45, 46]. Compared with the drop casting electrode modification [47] for phosphate detection, our inkjet printing method demonstrates highly probability for future mass production. From the aspect of POC testing, the use of SPE in our sensor is evidently superior than the traditional electrochemical cell sensing platform [48-50]. For the same enzyme crosslinking method, our proposed biosensor has a wider linear range compared to 12.5-1000  $\mu$ M achieved by AuNWs [36] and 0.248-1.456 mM achieved by Pt/Au alloy [37]. The improvement is attributed to the uniform modification of the electrode surface achieved by the utilization of inkjet printing method. In addition, the inclusion of functionalized MWCNTs also facilitate the rapid electron transfer during reaction.

**Table 4-1: Comparison of electrochemical sensors reported in literature for phosphate detection.**

Electrode	Composition	Linear range	Reagents addition	Manufacturing method	Ref
Co microelectrodes	e-beam evaporator of Au and Cobalt	0.01-10 mM	Potassium hydrogen phthalate	Photolithography	[44]
GLA/PyOD/Co PC/SPE	PyOD cross-linked with GLA	2.5-130 $\mu$ M	MOPS, pyruvic acid, MgSO <sub>4</sub> , NaCl	Drop cast	[39]
CB/SPE	CB	0.5-100 $\mu$ M	Molybdate, H <sub>2</sub> SO <sub>4</sub> , KCL	Drop cast	[45]
CB/SPE	CB and reaction substrate	10-300 $\mu$ M	None	Drop cast	[47]
PyOD/SPE	Gel-entrapment of PyOD	7.5-625 $\mu$ M	Pyruvic acid, FAD, TPP, MgCl <sub>2</sub> , citrate buffer	Drop cast	[46]
PyOD/MWCNT /GCE	Gel-entrapment of PyOD and MWCNT	1-100 $\mu$ M	Sodium pyruvate, TPP, FAD, Mg <sup>2+</sup>	Drop cast	[48]
Polyelectrolyte/PyOD/CE	Physical adsorption of polyelectrolyte and PyOD on the carbon electrode	0.05-1.25 mM	Pyruvate and HEPES buffer	Drop cast	[49]
Multienzyme/carbon paste	Three kinds of enzymes and carbon paste electrode	2-250 mM	NAD <sup>+</sup> , MgCl <sub>2</sub> , Os(1,10-phenanthroline-5,6-dione)2Cl <sub>2</sub> , Tris buffer	Drop cast	[50]
AuNWs/cofactor/BSA/PyOD/GLA	Crosslinking of cofactors and PyOD by BSA and GLA	12.5-1000 $\mu$ M	Pyruvic acid, MgCl <sub>2</sub> , citrate buffer	Drop cast	[36]
Pt/Au/cofactor/BSA/PyOD/GLA	Crosslinking of cofactors and PyOD by BSA and GLA	0.248-1.456 mM	Sodium pyruvate, MgCl <sub>2</sub> , NaOH, citrate buffer	Electrodeposition Drop cast	[37]
MWCNT-COOH/cofactor/substrate/BSA/PyOD/GLA/SPE	Crosslinking of MWCNTs, cofactors, substrate and PyOD by BSA and GLA	0.2-2 mM	None	Inkjet printing	This work

Sensor selectivity test was investigated and was shown in Figure 4-9(c). Interference species ( $\text{NO}_3^-$ ,  $\text{Cl}^-$ ,  $\text{SO}_4^{2-}$  and the mixture of them) was included respectively to the phosphate solution. It was observed that the inclusion of interferents rarely affect the response caused by phosphate, suggesting a negligible effect ( $< 2\%$ ) of the interferents on the sensor. These results indicated the proposed sensor had satisfactory selectivity. Stability test was explored and shown in Figure 4-9(d). A batch of optimized sensors were vacuum sealed and stored at  $4^\circ\text{C}$  before use. The result showed that the sensor retained 89% of the initial response after three weeks, indicating a good stability of the prepared biosensor. The reproducibility of the proposed biosensor was also evaluated, and five biosensors were prepared under the optimized condition. The peak current responses to 2 mM phosphate showing a relative standard deviation of less than 4%, which indicates the reproducibility of the fabrication.

Three artificial serum samples of different concentration were prepared and measured to validate the applicability of the proposed sensor (see Table 4-2). The recovery of biosensor ranged from 98.9% to 103% suggesting the proposed biosensor had great potential for the serum phosphate detection. In addition, the cost for the proposed electrochemical biosensor is less than 1.34 USD (see Appendix 4-2) indicating the feasibility of mass fabrication.

**Table 4-2: Detection of phosphate in the artificial serum (n=3).**

Phosphate concentration in sample/ mM	Founded phosphate / mM	Recovery/%	RSD/%
1.50	1.49	99.1	1.7
1.25	1.24	98.9	3.3
1.00	1.03	103	6.4

#### 4.4 Conclusions

In this study, a simple and effective surface functionalization strategy was developed to achieve enzyme crosslinking through inkjet printing technique for the construction of a reagentless enzyme-based biosensor. This method avoids any other post-treatment but only involves printing procedures, allowing more uniform deposition and enhanced analytical performance than those produced by drop casting method. Ink formula and printing route of multiple functionalization layers for sensor fabrication were presented; the results give references to other inkjet-printed biosensors. In addition, the applicability of the developed strategy was proven by successfully detecting the phosphate in the artificial serum. Together with the substrate preloading strategy, the constructed biosensor has potential to be industrialized for on-site analyte detection with minimum samples (30  $\mu$ l). More importantly, as a simple, affordable, labour-free and reagentless approach, this sensor fabrication practice can be easily applied to fabricate other enzyme-based biosensors by simply modifying the enzyme in the ink components.

## References

1. da Silva, E.T.S.G., D.E.P. Souto, J.T.C. Barragan, J. de F. Giarola, A.C.M. de Moraes, and L.T. Kubota, *Electrochemical Biosensors in Point-of-Care Devices: Recent Advances and Future Trends*. ChemElectroChem, 2017. **4**(4): p. 778-794.
2. Ispas, C.R., G. Crivat, and S. Andreescu, *Review: Recent Developments in Enzyme-Based Biosensors for Biomedical Analysis*. Analytical Letters, 2012. **45**(2-3): p. 168-186.
3. Walter, P., B. Podsiadły, B. Wałpuski, and M. Jakubowska. *Common configurations and challenges in screen-printed enzymatic electrochemical biosensors*. in *Photonics Applications in Astronomy, Communications, Industry, and High-Energy Physics Experiments 2018*. 2018. SPIE.
4. Rocchitta, G., A. Spanu, S. Babudieri, G. Latte, G. Madeddu, G. Galleri, S. Nuvoli, P. Bagella, M.I. Demartis, V. Fiore, R. Manetti, and P.A. Serra, *Enzyme Biosensors for Biomedical Applications: Strategies for Safeguarding Analytical Performances in Biological Fluids*. Sensors (Basel, Switzerland), 2016. **16**(6): p. 780.
5. Mohamad, N.R., N.H.C. Marzuki, N.A. Buang, F. Huyop, and R.A. Wahab, *An overview of technologies for immobilization of enzymes and surface analysis techniques for immobilized enzymes*. Biotechnology, biotechnological equipment, 2015. **29**(2): p. 205-220.
6. Sassolas, A., L.J. Blum, and B.D. Leca-Bouvier, *Immobilization strategies to develop enzymatic biosensors*. Biotechnology advances, 2012. **30**(3): p. 489-511.
7. Kaliyaraj Selva Kumar, A., Y. Zhang, D. Li, and R.G. Compton, *A mini-review: How reliable is the drop casting technique?* Electrochemistry Communications, 2020. **121**: p. 106867.
8. Kit-Anan, W., A. Olarnwanich, C. Sriprachuabwong, C. Karuwan, A. Tuantranont, A. Wisitsoraat, W. Srituravanich, and A. Pimpin, *Disposable paper-based electrochemical sensor utilizing inkjet-printed Polyaniline modified screen-printed carbon electrode for Ascorbic acid detection*. Journal of Electroanalytical Chemistry, 2012. **685**: p. 72-78.
9. Cinti, S., F. Arduini, D. Moscone, G. Palleschi, and A.J. Killard, *Development of a hydrogen peroxide sensor based on screen-printed electrodes modified with inkjet-printed Prussian blue nanoparticles*. Sensors, 2014. **14**(8): p. 14222-14234.
10. Khan, N.I., A.G. Maddaus, and E. Song, *A Low-Cost Inkjet-Printed Aptamer-Based Electrochemical Biosensor for the Selective Detection of Lysozyme*. Biosensors (Basel), 2018. **8**(1).

11. Cinti, S., F. Arduini, D. Moscone, G. Palleschi, L. Gonzalez-Macia, and A.J. Killard, *Cholesterol biosensor based on inkjet-printed Prussian blue nanoparticle-modified screen-printed electrodes*. Sensors and Actuators B: Chemical, 2015. **221**: p. 187-190.
12. Li, Y.-G., Y.-X. Zhou, J.-L. Feng, Z.-H. Jiang, and L.-R. Ma, *Immobilization of enzyme on screen-printed electrode by exposure to glutaraldehyde vapour for the construction of amperometric acetylcholinesterase electrodes*. Analytica Chimica Acta, 1999. **382**(3): p. 277-282.
13. Moreno-Cortez, I.E., J. Romero-García, V. González-González, D.I. García-Gutierrez, M.A. Garza-Navarro, and R. Cruz-Silva, *Encapsulation and immobilization of papain in electrospun nanofibrous membranes of PVA cross-linked with glutaraldehyde vapor*. Materials Science and Engineering: C, 2015. **52**: p. 306-314.
14. Gdor, E., S. Shemesh, S. Magdassi, and D. Mandler, *Multienzyme Inkjet Printed 2D Arrays*. ACS Applied Materials & Interfaces, 2015. **7**(32): p. 17985-17992.
15. Cinti, S., D. Moscone, and F. Arduini, *Preparation of paper-based devices for reagentless electrochemical (bio) sensor strips*. Nature protocols, 2019. **14**(8): p. 2437-2451.
16. Forano, C., H. Farhat, and C. Mousty, *Recent trends in electrochemical detection of phosphate in actual waters*. Current Opinion in Electrochemistry, 2018.
17. Juan, E.C.M., M.M. Hoque, M.T. Hossain, T. Yamamoto, S. Imamura, K. Suzuki, T. Sekiguchi, and A. Takénaka, *The structures of pyruvate oxidase from Aerococcus viridans with cofactors and with a reaction intermediate reveal the flexibility of the active-site tunnel for catalysis*. Acta crystallographica. Section F, Structural biology and crystallization communications, 2007. **63**(Pt 11): p. 900-907.
18. Basiaga, M., Z. Paszenda, W. Walke, P. Karasiński, and J. Marciniak, *Electrochemical Impedance Spectroscopy and corrosion resistance of SiO<sub>2</sub> coated cpTi and Ti-6Al-7Nb alloy*, in *Information Technologies in Biomedicine, Volume 4*. 2014, Springer. p. 411-420.
19. Chiang, Y.-C., W.-H. Lin, and Y.-C. Chang, *The influence of treatment duration on multi-walled carbon nanotubes functionalized by H<sub>2</sub>SO<sub>4</sub>/HNO<sub>3</sub> oxidation*. Applied Surface Science, 2011. **257**(6): p. 2401-2410.
20. Noordadi, M., F. Mehrnejad, R.H. Sajedi, M. Jafari, and B.J.P.o. Ranjbar, *The potential impact of carboxylic-functionalized multi-walled carbon nanotubes on trypsin: A Comprehensive spectroscopic and molecular dynamics simulation study*. 2018. **13**(6): p. e0198519.

21. Bai, Y., D. Zhang, Q. Guo, J. Xiao, M. Zheng, and J. Yang, *Study of the Enzyme Activity Change due to Inkjet Printing for Biosensor Fabrication*. ACS Biomaterials Science & Engineering, 2021.
22. Soltman, D. and V. Subramanian, *Inkjet-Printed Line Morphologies and Temperature Control of the Coffee Ring Effect*. Langmuir, 2008. **24**(5): p. 2224-2231.
23. Gupta, S., C. Murthy, and C.R. Prabha, *Recent advances in carbon nanotube based electrochemical biosensors*. International journal of biological macromolecules, 2018. **108**: p. 687-703.
24. Sheldon, R.A. and S. van Pelt, *Enzyme immobilisation in biocatalysis: why, what and how*. Chemical Society Reviews, 2013. **42**(15): p. 6223-6235.
25. Du, X., C.J. Durgan, D.J. Matthews, J.R. Motley, X. Tan, K. Pholsena, L. Árnadóttir, J.R. Castle, P.G. Jacobs, and R.S. Cargill, *Fabrication of a flexible amperometric glucose sensor using additive processes*. ECS journal of solid state science and technology: JSS, 2015. **4**(4): p. P3069.
26. Wang, Z., Q. Liu, H. Zhu, H. Liu, Y. Chen, and M.J.C. Yang, *Dispersing multi-walled carbon nanotubes with water-soluble block copolymers and their use as supports for metal nanoparticles*. 2007. **45**(2): p. 285-292.
27. NB, R.K., V. Crasta, B. Praveen, and M.J.N.R. Kumar, *Studies on structural, optical and mechanical properties of MWCNTs and ZnO nanoparticles doped PVA nanocomposites*. 2015. **4**(5): p. 457-467.
28. Vuković, G.D., A.D. Marinković, M. Čolić, M.Đ. Ristić, R. Aleksić, A.A. Perić-Grujić, and P.S. Uskoković, *Removal of cadmium from aqueous solutions by oxidized and ethylenediamine-functionalized multi-walled carbon nanotubes*. Chemical Engineering Journal, 2010. **157**(1): p. 238-248.
29. Li, H., D. Buesen, R. Williams, J. Henig, S. Stapf, K. Mukherjee, E. Freier, W. Lubitz, M. Winkler, and T.J.C.s. Happe, *Preventing the coffee-ring effect and aggregate sedimentation by in situ gelation of monodisperse materials*. 2018. **9**(39): p. 7596-7605.
30. Shen, X., C.-M. Ho, and T.-S. Wong, *Minimal Size of Coffee Ring Structure*. The Journal of Physical Chemistry B, 2010. **114**(16): p. 5269-5274.
31. Mampallil, D. and H.B. Eral, *A review on suppression and utilization of the coffee-ring effect*. Advances in Colloid and Interface Science, 2018. **252**: p. 38-54.
32. He, B. and H. Liu, *Electrochemical biosensor based on pyruvate oxidase immobilized AuNRs@ Cu<sub>2</sub>O-NDs as electroactive probes loaded poly (diallyldimethylammonium chloride) functionalized graphene for the detection of phosphate*. Sensors and Actuators B: Chemical, 2020. **304**: p. 127303.

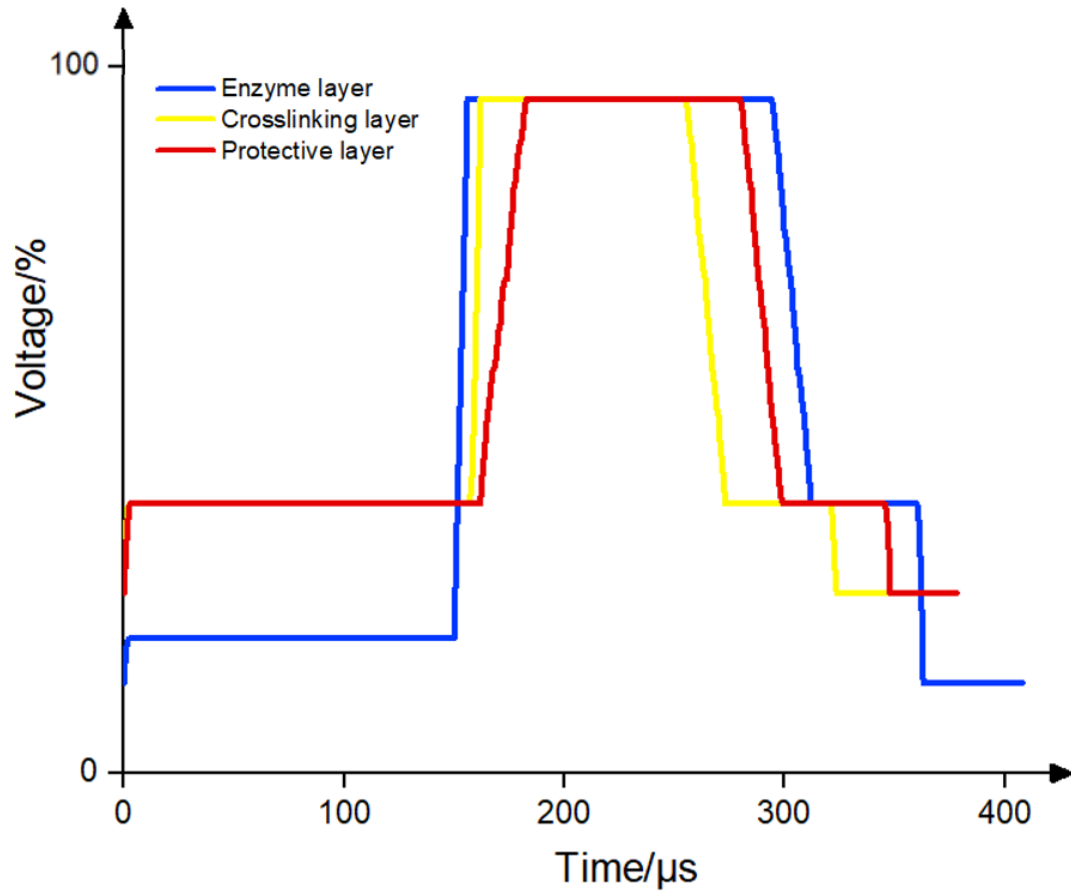
33. de Rooij, M.J.A.-C.M. and Materials, *Electrochemical methods: Fundamentals and applications*. 2003.
34. Yao, L., J. Teng, M. Zhu, L. Zheng, Y. Zhong, G. Liu, F. Xue, and W. Chen, *MWCNTs based high sensitive lateral flow strip biosensor for rapid determination of aqueous mercury ions*. *Biosensors and Bioelectronics*, 2016. **85**: p. 331-336.
35. Guan, W.-J., Y. Li, Y.-Q. Chen, X.-B. Zhang, and G.-Q. Hu, *Glucose biosensor based on multi-wall carbon nanotubes and screen printed carbon electrodes*. *Biosensors and Bioelectronics*, 2005. **21**(3): p. 508-512.
36. Ogabiela, E., S.B. Adeloju, J. Cui, Y. Wu, and W. Chen, *A novel ultrasensitive phosphate amperometric nanobiosensor based on the integration of pyruvate oxidase with highly ordered gold nanowires array*. *Biosensors and Bioelectronics*, 2015. **71**: p. 278-285.
37. Cui, J., E.E. Ogabiela, J. Hui, Y. Wang, Y. Zhang, L. Tong, J. Zhang, S.B. Adeloju, X. Zhang, and Y. Wu, *Electrochemical Biosensor based on Pt/Au Alloy Nanowire Arrays for Phosphate Detection*. *Journal of The Electrochemical Society*, 2015. **162**(3): p. B62-B67.
38. Adeloju, S.B. and A.T. Lawal, *Fabrication of a bilayer potentiometric phosphate biosensor by cross-link immobilization with bovine serum albumin and glutaraldehyde*. *Analytica Chimica Acta*, 2011. **691**(1): p. 89-94.
39. Gilbert, L., A.T.A. Jenkins, S. Browning, and J.P. Hart, *Development of an amperometric, screen-printed, single-enzyme phosphate ion biosensor and its application to the analysis of biomedical and environmental samples*. *Sensors and Actuators B: Chemical*, 2011. **160**(1): p. 1322-1327.
40. Lawal, A.T. and S.B. Adeloju, *Polypyrrole based amperometric and potentiometric phosphate biosensors: A comparative study B*. *Biosensors and Bioelectronics*, 2013. **40**(1): p. 377-384.
41. Luo, X.-L., J.-J. Xu, Y. Du, and H.-Y. Chen, *A glucose biosensor based on chitosan–glucose oxidase–gold nanoparticles biocomposite formed by one-step electrodeposition*. *Analytical Biochemistry*, 2004. **334**(2): p. 284-289.
42. Wang, J. and M. Musameh, *Carbon nanotube screen-printed electrochemical sensors*. *Analyst*, 2004. **129**(1): p. 1-2.
43. Rahman, M.A., D.-S. Park, S.-C. Chang, C.J. McNeil, and Y.-B. Shim, *The biosensor based on the pyruvate oxidase modified conducting polymer for phosphate ions determinations*. *Biosensors and Bioelectronics*, 2006. **21**(7): p. 1116-1124.



44. Zou, Z., J. Han, A. Jang, P.L. Bishop, and C.H. Ahn, *A disposable on-chip phosphate sensor with planar cobalt microelectrodes on polymer substrate*. *Biosensors and Bioelectronics*, 2007. **22**(9): p. 1902-1907.
45. Talarico, D., F. Arduini, A. Amine, D. Moscone, and G. Palleschi, *Screen-printed electrode modified with carbon black nanoparticles for phosphate detection by measuring the electroactive phosphomolybdate complex*. *Talanta*, 2015. **141**: p. 267-272.
46. Kwan, R.C., H.F. Leung, P.Y. Hon, J.P. Barford, and R. Renneberg, *A screen-printed biosensor using pyruvate oxidase for rapid determination of phosphate in synthetic wastewater*. *Appl Microbiol Biotechnol*, 2005. **66**(4): p. 377-83.
47. Cinti, S., D. Talarico, G. Palleschi, D. Moscone, and F. Arduini, *Novel reagentless paper-based screen-printed electrochemical sensor to detect phosphate*. *Analytica Chimica Acta*, 2016. **919**: p. 78-84.
48. Norouzi, P., M. Pirali-Hamedani, F. Faridbod, and M.J.I.J.E.S. Ganjali, *Flow Injection Phosphate Biosensor Based on PyOx-MWCNTs Film on a Glassy Carbon Electrode Using FFT Continuous Cyclic Voltammetry*. 2010. **5**(9): p. 1225-1235.
49. Gavalas, V.G. and N.A. Chaniotakis, *Phosphate biosensor based on polyelectrolyte-stabilized pyruvate oxidase*. *Analytica Chimica Acta*, 2001. **427**(2): p. 271-277.
50. Fernández, J.J., J.R. López, X. Correig, and I. Katakis, *Reagentless carbon paste phosphate biosensors: preliminary studies*. *Sensors and Actuators B: Chemical*, 1998. **47**(1): p. 13-20.

## Appendices

**Appendix 4-1: Printing waveforms for enzyme layer (blue line), crosslinking layer (yellow line), and protective layer (red line).**



**Appendix 4-2: Cost breakdown of the serum phosphate sensor (materials and reagents)**

Material	Stock volume/Amount	Price (\$)	Estimated volume/Amount for each sensor	Estimated price for each sensor (\$)
<b>Screen printed sensor</b>	Pack of 25	30.58	1	1.22
<b>Triton X-100</b>	500 ml	44.69	0.02 $\mu$ l	< 0.01
<b>GLA</b>	500 ml	31.20	0.72 $\mu$ l	< 0.01
<b>Pyruvate oxidase</b>	1 KU	300	0.10 U	< 0.01
<b>Puruvic acid</b>	500 ml	100.25	< 0.01 $\mu$ l	< 0.01
<b>MgCl<sub>2</sub></b>	1 kg	40.87	< 0.01 mg	< 0.01
<b>FAD</b>	25 mg	50.78	< 0.001 mg	< 0.01
<b>TPP</b>	5 g	54.83	< 0.001 mg	< 0.01
<b>BSA</b>	10 g	59.51	0.19 mg	< 0.01
<b>MWCNT</b>	100 g	27.52	0.004 mg	< 0.01
<b>Citric acid</b>	500 g	44.85	0.04 mg	< 0.01
<b>Sodium Citrate dihydrate</b>	1000 g	54.60	< 0.01 mg	< 0.01
<b>Nafion</b>	25 ml	106.08	0.01 $\mu$ l	< 0.01
				Total < 1.34

## Chapter 5

### 5 An inkjet-printed smartphone-based electrochemical biosensor system for reagentless point-of-care analyte detection

In this work, we developed an inkjet-printed electrochemical enzyme-based biosensor system which can work with the smartphone for the point-of-care analyte detection. Inkjet printing technique was applied to functionalize electrodes. Multi-walled carbon nanotubes were used as the enzyme carrier to enhance the enzyme loading. Enzyme immobilization was realized through layer-by-layer printing strategy by crosslinking ink components (BSA and glutaraldehyde) between printing layers. Reagents for the enzyme catalyzed reaction were preloaded onto the working electrode to eliminate the use of traditional electrochemical cell. In addition, a versatile smartphone Android application was developed for real-time data processing on multiple occasions. Phosphate in the artificial saliva was measured to demonstrate the feasibility of the proposed biosensor system. The miniaturized biosensor system presents a wide linear range with rapid response time (less than 10 s). High selectivity and stability of the sensor demonstrate its practical use for saliva test. The proposed biosensor system can be applicable for various analyte detection by exchanging the sensing elements and reagents. And the biosensor system can be easily operated by users without specific training. In all, this novel integrated biosensor system has great potentiality for point-of-care applications. Our proposed sensor system demonstrates a reliable and reproducible biosensor fabrication route that has meaningful reference for similar point-of-care biosensor systems.

## 5.1 Introduction

Recently, point-of-care (POC) diagnostic devices are continuously being demanded in the healthcare field due to the advantages of low-cost, easy-to-use, rapid and on-site detection. With the convenience of smartphones, optical sensors based on colorimetric or fluorescent measurement, surface plasmon resonance biosensors and electrochemical sensors evolve to an instrument-independent, use-friendly and inexpensive point-of-care devices [1]. Among various kinds of smartphone-supported biosensors, electrochemical biosensors are superior to the others due to the merits of miniaturization simplicity, fast analysis and high selectivity nature to the sensing analytes [2, 3]. Most electrochemical sensors employ the three-electrode configuration consisting of a working electrode (WE), counter electrode (CE) and reference electrode (RE). Upon the potential applied between the working electrode and counter electrode, the electrochemical biosensors convert the biological response occurring on the transducer electrodes into a quantifiable electric signal [4]. The miniaturization of electrochemical transducers and readout instruments are the major subjects in the development of POC electrochemical devices.

In recent years, a few point-of-care smartphone-supported electrochemical biosensors have been developed by researchers [5-8]. As the sensing and transducing unit, screen printed electrodes (SPEs) have been involved to take their full advantage of small size, lightness, ease of modification [9-11]. Various diagnostic biomarkers can be detected through modifying the working SPEs using certain biological entities. For most studies, drop casting is widely used as a simple, easy and rapid method for surface modification of the SPE. However, drop casting method is not applicable for mass production of the proposed POC biosensors. Also, the inevitable coffee ring occurring on the drop-casted

SPEs greatly limits the reproducibility and electrochemical performance of the biosensors [12, 13].

To overcome the problems of drop casting method, inkjet printing as a prevailing tool for its capability of customization, accurate deposition and pico-liter volumes delivery is facile to achieve high reproducibility with low cost [14]. Moreover, researchers have confirmed that through modulating the printing parameters, uniform modification of the electrode can be achieved to highly mitigate the coffee ring effect during the drying process [15, 16]. Utilization of the inkjet printing technique is highly recommended for the batch manufacturing of high performance POC electrochemical biosensors.

Though the miniaturized structure of the screen-printed electrochemical biosensors boosts the POC application, the limited sensing area confines the loading of biological recognition elements. To solve this problem, nanomaterials have attracted great interests from researchers due to the high specific surface area, nano-scaled size, varied internal structure and superior electrical properties in the analytical chemistry. Various nanomaterials (nanoparticles, nanowires and nanotubes; metal nanomaterials, carbon nanomaterials and polymer nanomaterials) have been employed to functionalize enzyme electrodes with ability to achieve satisfactory electrical signal between the active site of the enzyme and the electrode [17-19].

Herein, a smartphone-supported inkjet-printed nanomaterial-modified biosensor for point-of-care analyte detection is developed. A commercialized three-electrode configuration was functionalized by layer-by-layer inkjet printing strategy for enzyme immobilization. Functionalized multi-walled carbon nanotubes were introduced in the

printing ink to increase the surface area and maximize the loading of enzyme. A portable wireless potentiostat was connected with the smartphone to execute signal processing, transducing and exporting. An Android application (App) was developed to interpret the electrochemical signal through real-time analyte measurement. To assess the sensitivity and specificity of the proposed biosensor system as a point-of-care device, a clinically informative biomarker in an easily obtained biofluid is recommended to use. Saliva as a clinically important, non-invasive and readily available biofluid are perfectly suitable in the development of point-of-care biosensors. Saliva phosphate (SP), as an commonly used standard indicator of many physiological conditions such as hyperphosphatemia in chronic kidney disease, hyperphosphatemia in hemodialysis patients, ovulation condition for female infertility, uremia status, occurrence of dental caries, is highly recommended in the clinical applications for disease diagnosis and monitoring [20-25]. To demonstrate the validity of our biosensor system, artificial saliva with different concentration of phosphate was used in our research. Our fabrication route of the point-of-care biosensor system advances other sensor systems in terms of high feasibility of customization, great reproducibility and potential of mass production. The exclusion of traditional electrochemical cell and the application of the user-friendly App have demonstrated the practical use for future point-of-care analyte detection.

## 5.2 Materials and methods

### 5.2.1 Chemicals and reagents

Pyruvate oxidase from *microorganism* (PyOD, E.C.1.2.3.3) was purchased from Toyobo (New York, USA). Multi-walled carbon nanotubes (MWCNTs, L-MWNT-1020) were purchased from Shenzhen Nanotech Port Co., Ltd (Shenzhen, China). Bovine serum

albumin (BSA), Triton X-100, hydrochloric acid (1 mol/l), nitric acid, sulfuric acid, potassium ferricyanide (III) ( $K_3Fe(CN)_6$ ), glutaraldehyde (GLA), Nafion<sup>®</sup> (5 wt. %), citric acid and sodium citrate dihydrate were obtained from Sigma-Aldrich. Thiamine pyrophosphate (TPP), flavin adenine dinucleotide (FAD), magnesium chloride ( $MgCl_2$ ), pyruvate acid, sodium chloride, calcium chloride, potassium chloride, potassium nitrate, potassium phosphate monobasic, potassium phosphate dibasic and urea were purchased from TCI. All other reagents were of analytical grade and used as received. All solutions were prepared in the deionized water ( $18.2M\Omega \cdot cm^{-1}$ ). The disposable screen-printed electrode (SPE, C10) as a novel electro-analytical electrode were purchased from Mxense Bio-Tech Co., Ltd. (Shanghai, China). The substrate of the SPE is polyethylene terephthalate (PET) with three-dimensions of  $5 \times 15 \times 0.8$  mm (L×W×H). It has a three electrode configuration: a carbon working electrode (diameter  $d = 2.50$  mm) and a counter electrode using carbon electrodes and a Ag/AgCl electrode used as a reference electrode [26].

Phosphate stock solution (50 mM, pH 6.0) and Citrate buffer (25 mM, pH 5.6) were prepared according to normal lab procedures. MWCNTs were functionalized for the attachment of -COOH group on the surface based on the method reported by Yu-Chun Chiang *et.al.* [27]. The functionalized MWCNTs were kept dry and stored at room temperature. Basic artificial saliva solution for sensor validity study was made by mixing 13.2 mg sodium chloride, 96.4 mg potassium chloride, 17.2 mg calcium chloride, 20.4 mg urea, and 17.4 mg lactic acid together in 100 ml DI water and stored in 4°C [28, 29]. Then, different concentration of phosphate solution was prepared with the basic artificial solution.



### 5.2.2 Functionalization of the screen-printed electrode

Experiments for electrode functionalization were carried out using Fujifilm DIMATIX Materials Printer Dmp-2831 (FUJIFILM Dimatix, Inc., USA) with the customized ink cartridge DMC-11610. Driving waveforms of printhead piezo-element were controlled through Graphical User Interface (GUI) application software. Prior to working electrode functionalization, bare SPE were ultrasonically cleaned in ethanol and water (1:1) for 30 min and dried under a stream of nitrogen. Three kinds of ink including enzyme layer (Ink 1), GLA layer (Ink 2) and nafion layer (Ink 3) were prepared (See Table S1 for detailed ink formula), and then layer-by-layer printed to functionalize the working electrode as the crosslinking layer, and protective ion selective layer. Optimized printing waveforms were applied in each printing layer. The optimized voltage and frequency settings for enzyme layer, GLA layer, and nafion layer were 6 kHz 28V, 8kHz 30V and 8kHz 32V separately. The drop number for each layer was programmed through Pattern Editor Module. The enzyme layer GLA layer and nafion layer were designed with 459,330 counts (~ 3.0622  $\mu$ l), 229,665 counts, (~1.5311  $\mu$ l) and 229,665 counts (~1.5311  $\mu$ l) respectively. The substrate was heated to 30°C to enhance the ink evaporation during the printing process. The drop spacing was set for 20  $\mu$ m for uniform drop deposition.

### 5.2.3 APP development

Android App based on Android Studio 4.1.1. was developed for processing the experiment results and outputting the measured sample information. Logical design and page design were realized by using Java language. A user-friendly graphic user interface (GUI) was developed for parameter settings and results presentation. Code for the APP can be found in the Appendix B&C.

#### 5.2.4 Testing of the proposed biosensor system.

Electrochemical experiments on sensor performance and sensor prototyping were conducted at room temperature using CHI potentiostat (Shanghai Chen Hua Instrument Co., Ltd., Shanghai, China) and Xenstat potentiostat (Mxense Bio-Tech Co., Ltd., Shanghai, China) separately. For CHI potentiostat, all the experiment parameters were set on computer through USB-connection. For experiments performed on the Xenstat potentiostat, parameter settings were input and wirelessly transmitted from the smartphone App. For both cyclic voltammetry (CV) or chronoamperometry experiments, 30  $\mu$ l of sample solution were dropped on to the working electrode of the biosensor. For CV experiments, potential range comprised between 0 and 0.6V at scan rate of 50 mV/s were used. For chronoamperometry experiments, potential was set at 0.4V vs Ag/AgCl with time range of 10 seconds for CHI and 60 seconds for Xenstat potentiostat. All experiments were performed based on the above settings unless otherwise stated.

### 5.3 Results and discussion

#### 5.3.1 Design of the biosensor system

The proposed biosensor system consisted of a functionalized SPE, a portable potentiostat and an Android App. Figure 5-1 shows the user interaction with the biosensor system where the users can use the smartphone to set the experiment parameters on the App. The instructions are transmitted through Bluetooth to the portable potentiostat where a functionalized SPE with detection sample is loaded. Herein, the potentiostat executes the electrochemical experiments, and transmits the results back to the smartphone App which conducts the data processing according to the user settings. The result will be displayed

on the smartphone in a straightforward way to the users, seen in Figure 5-2(d) for the screenshot of the result page.

The SPE was functionalized aiming to detect the analyte. Three kinds of layer were inkjet-printed on the working electrode in a sequence. The first layer is deposited with biological entities, BSA and reagents for enzyme catalyzed reaction. Then, GLA was printed to form a crosslinking layer, on which a protective layer was deposited on to encapsulate the sensor. It is noted that the proposed functionalization procedures can be applied to other screen-printed biosensors through simply modifying the components of the ink and settings of the printing parameters.

The portable potentiostat was connected with an Android smartphone and controlled on a lab-made App. (Figure 5-2(a)). The proposed biosensor system was designed with two operating modes which consist of two kinds of commonly used electrochemical experiments - differential pulse voltammetry (DPV) and chronoamperometry experiments. After selecting the experiment mode and setting the operating parameters (*e.g.* scan rate, voltage, time, *etc.*) on the smartphone App, the instructions can be wirelessly transmitted by Bluetooth to the potentiostat. The experiment results will be displayed as a dynamic curve on the smartphone.

The App on the smartphones was developed to analyze the electrochemical curves obtained from the connected potentiostat in real time. The parameters can be directly set through the user-friendly graphic user interface (GUI). The App of current version can process the results using differential pulse voltammetry (DVP) method and Chronoamperometry method. The obtained results can be fitted linearly or

logarithmically according to the experiment conditions (Figure 5-2(b)). For chronoamperometry results, specific time is set as a constant of steady state value for the data processing (Figure 5-2(c)). Once the parameters were set, the next experiment will automatically load the previous settings. With the help of our App, users even without professional training can easily obtain the analyte information of interest from the measurement. The users can simply touch the “start” button on the smartphone, and the results will be processed and displayed on the screen instantly. In addition, the obtained results can also be saved and uploaded in the cloud server.

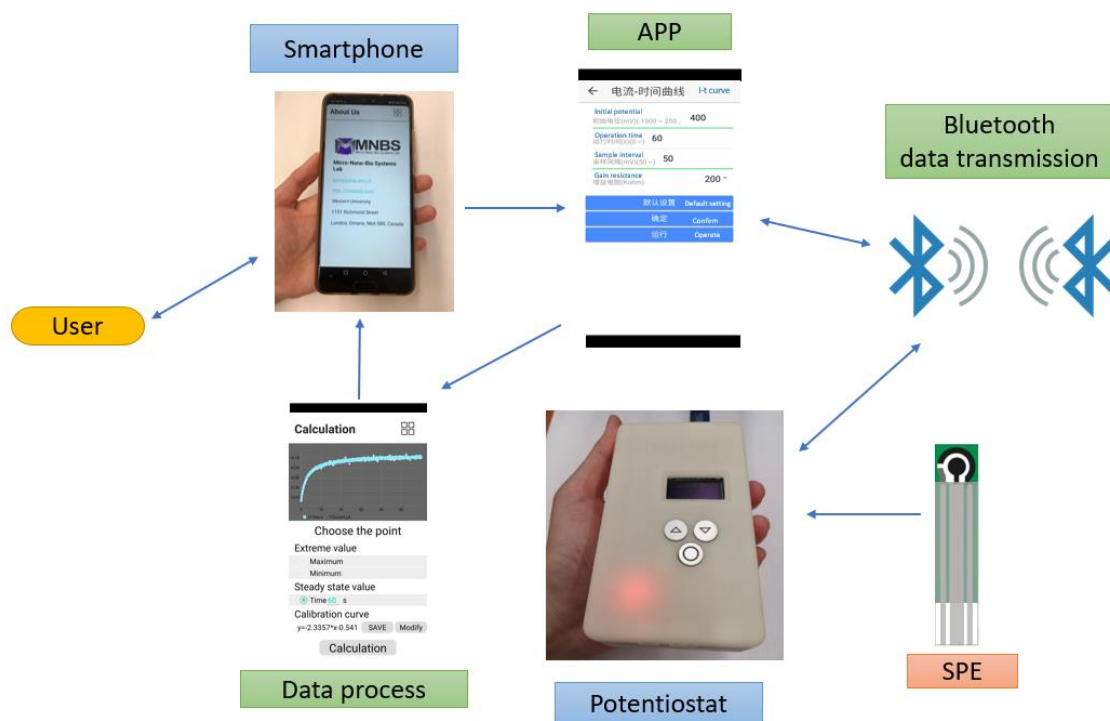


**Figure 5-1: User interaction with the proposed biosensor system**

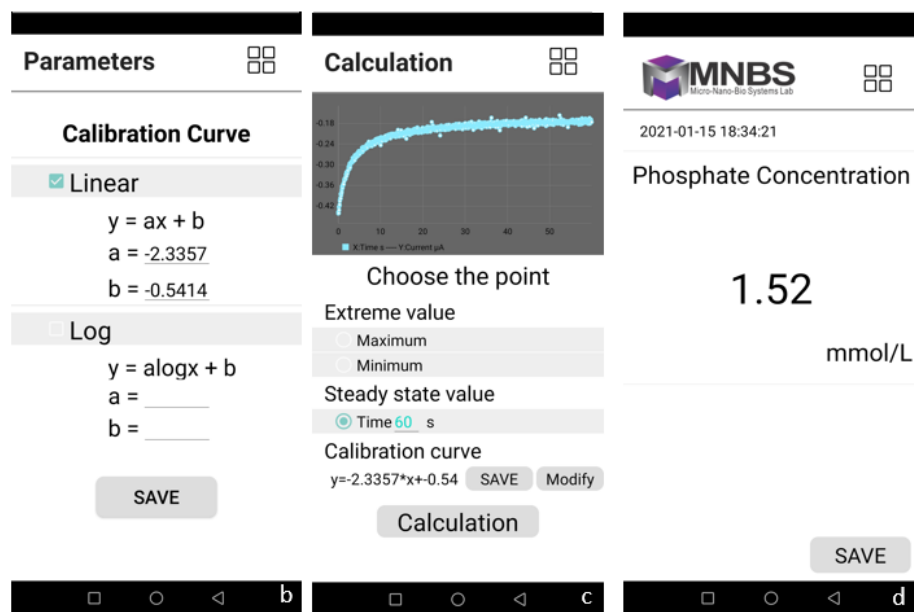
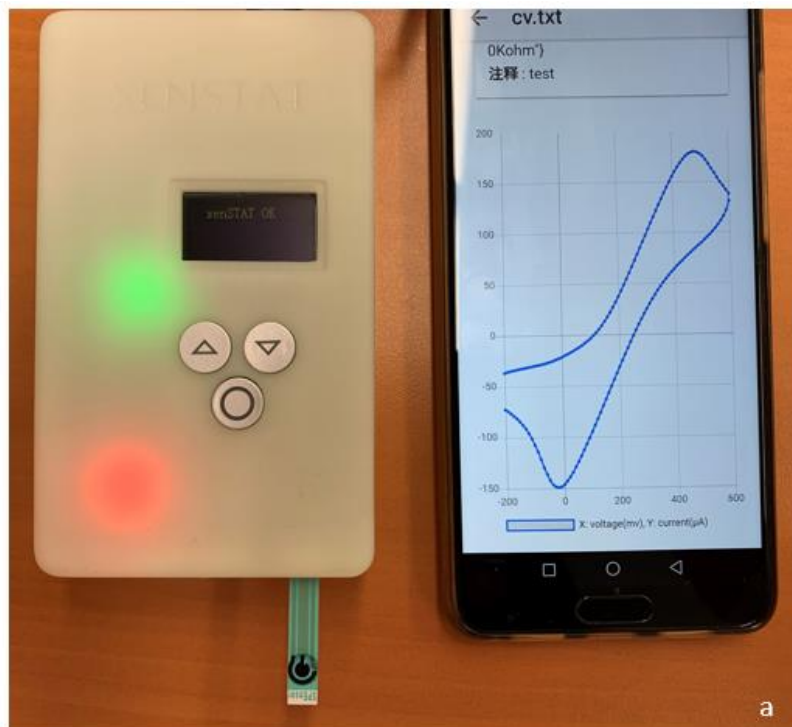


**Figure 5-2:** (a) Electrochemical measurement using wireless portable potentiostat. The biosensor system includes a smartphone displaying a dynamic curve for the real-time data received through Bluetooth, a portable potentiostat and a modified

**SPE for analyte detection. (b) Parameter settings for the calibration curve. (c) Settings of the data processing method for the obtained data. (d) The App displays the real-time saliva phosphate concentration on the smartphone.**

### 5.3.2 Design and evaluation of the functionalized working electrode

Figure 5-3 shows the functionalization process of the SPE. Three steps are involved as determination of the printing strategy, ink formula and finalization of the printing parameters. For our SPE functionalization practice, we chose layer-by-layer printing strategy and different functional layers were printed on the working electrode in sequence. Ink formula for each layer was developed based on four considerations, namely the rheological requirement (viscosity and surface tension) for printing, the components of electrochemical reactions, the sufficient loading and stability maintenance of the sensing materials and the analytical performance of the sensor. To print the bottom enzyme layer, the functionalized multi-walled carbon nanotubes were introduced in the printing ink as enzyme carrier to enhance the enzyme loading [30, 31]. TritonX-100 as a non-ionic surfactant were used to adjust the surface tension of the ink, and can also preserve the functional state of proteins and accelerate the electron transfer process [32]. Cofactors were added in the ink to support the enzyme reaction. The reaction substrates were also included to exclude the needs of traditional electrochemical cell [33]. BSA was added in the ink as a spacer agent in the next crosslinking procedure, in which GLA was the major component of the crosslinking layer. Together with the pre-deposited layer, a BSA-glutaraldehyde-enzyme crosslinking gel mixture was formed to obtain high stability and strong connection between the enzyme and the electrode [34, 35]. The top protective layer was formed by the nafion to encapsulate the sensor.

The printing parameters were set and optimized after finalizing the ink formula. The printing waveforms for each layer were optimized based on drop formation requirements of stable and round droplets in the Drop Watcher window for each printing layer (see Appendix 5-1 stable droplet array). Printing parameters (voltage & frequency) for enzyme layer were optimized according to previous studies to ensure highest enzyme activity [36]. The number of drops to be delivered on the working electrode for each layer were programmed through Pattern Editor Module to ensure the defined amount of material based on the requirements of the electrochemical experiments. Fiducial Camera was used to check out the relative position of adjacent printed drops and the drop spacing was set 20  $\mu\text{m}$  for all three layers.

After the completion of the SPE modification, electrochemical experiments were conducted to evaluate the performance of the functionalized electrode (see Appendix 5-2). Appendix 5-2(a) shows the CV responses of different electrodes in the  $\text{K}_3\text{Fe}(\text{CN})_6$  solution. Without the help of MWCNTs, the enzyme/substrate/cofactor electrode (red line) had the lowest the peak current which suggested the unfavorable environment for electron transfer reactions. After the addition of the MWCNTs, the peak-peak separation decreased, and the significantly increased peak current suggested the evident improvement for the electron transfer kinetic [37]. In Appendix 5-2(b), both the cathodic and anodic peaks increased proportionally with the scan rate from 40 to 100 mV/s, indicating a surface confined electrode process [38, 39]. The peak-peak separation also increased linearly with the scan rate and the peak current was linear to the square root of the scan rate (see inset of Appendix 5-2(b)), suggesting that the electrode process was a diffusion control and quasi-reversible electron transfer process [33, 38, 40].

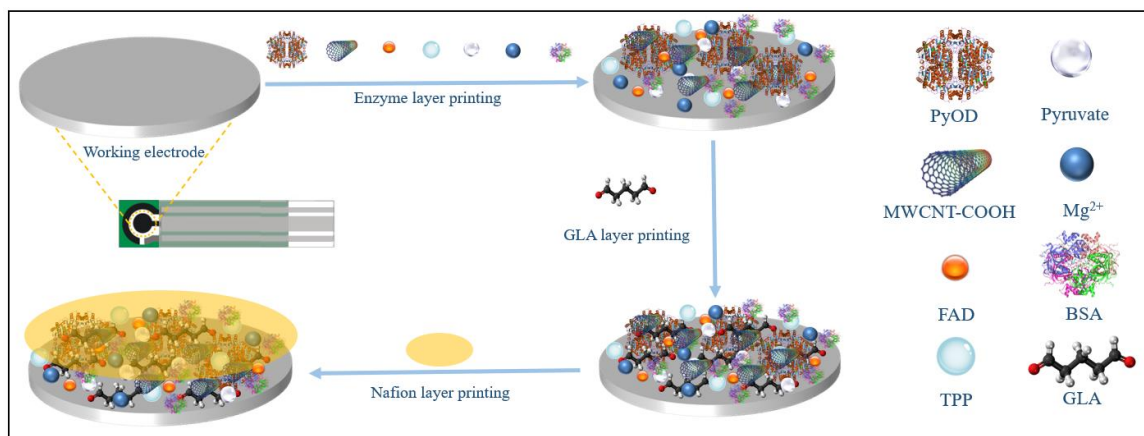


**Figure 5-3: Schematic of the functionalized process of the screen-printed electrodes.**

### 5.3.3 Sensing principle and electrochemical performance of the SPE sensor

To demonstrate the feasibility of the proposed biosensor system, phosphate in the artificial saliva was selected as the biomarker of interest. Figure 5-4 illustrates the sensing principle of the saliva phosphate sensor. When the sensing area of the SPE is exposed to the sample solution which contains the phosphate ion, a chemical reaction between the working electrode surface and the phosphate will happen upon the application of the voltage potential. Then the sensor will transfer the signal of the chemical reaction into a readable electrochemical current curve that reflects the phosphate concentration.



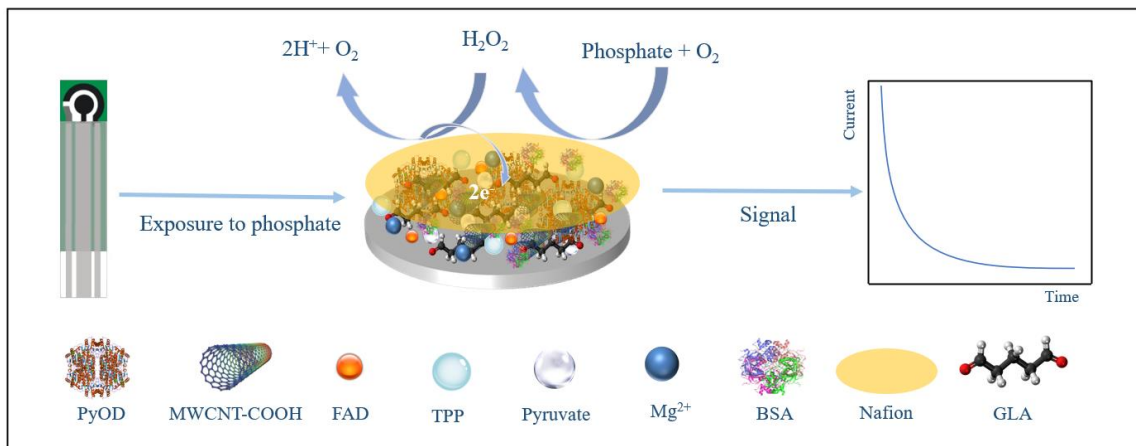


**Figure 5-4: Illustration of the detection mechanism of the proposed biosensor system for saliva phosphate detection.**

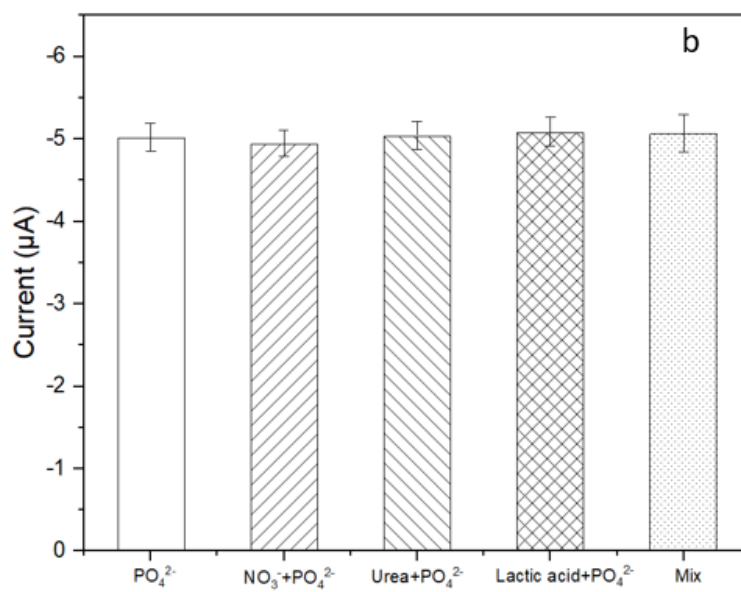
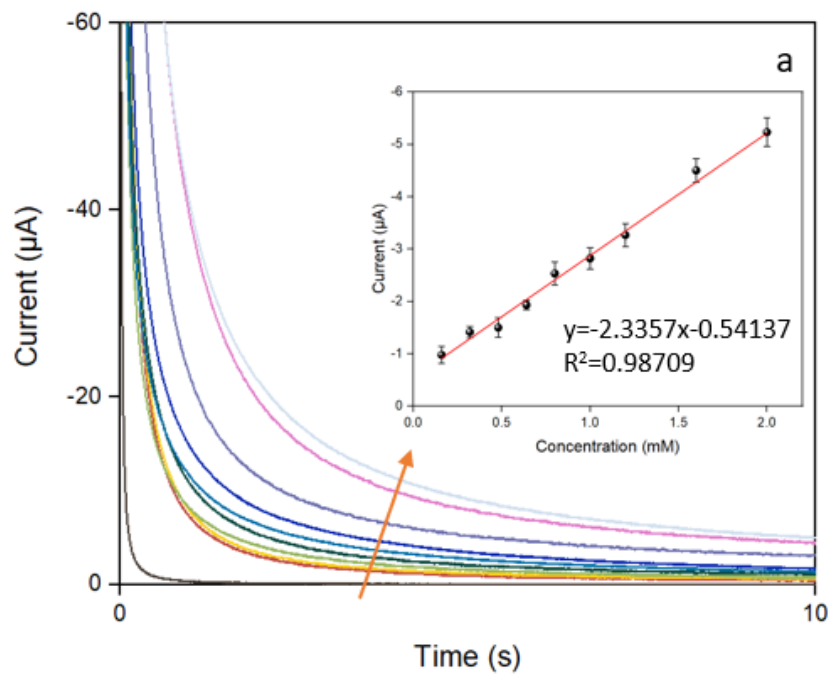
To evaluate the analytical performance of the inkjet-printed SPE sensor, a series of chronoamperometry experiments with different concentrations of the phosphate were performed to obtain the linear range of the sensor. The amperometric responses increased with the increasing of the phosphate concentration, and the evident exponential decay curves were plotted. The phenomenon can be fitted by Cottrell equation (Figure 5-5(a)) [41]. Once the double layer between the electrode and the solution was charged, the current decayed exponentially until it arrived a steady state, which we could use as the Faradaic current/reaction current. To obtain the steady state value of the response current rather than the end-point measurement, we fitted individual amperometric response empirically with an exponential decay equation:

$$I = I_0 \exp(-t/t_0) + I_\infty \quad (1)$$

Here  $I$  is response current,  $t$  is the time,  $I_0$  is the double layer charging current when  $t = 0$ ,  $t_0$  is a characteristic time scale representing the decay time,  $I_\infty$  the reaction current which

can be measured at steady state. After the curve fit, we extracted  $I_{\infty}$  and plotted the concentration-current relationship in the inset of Figure 5-5(a). The current and phosphate concentration displayed a good linear correlation from 0.16 to 2.0 mM ( $y = -2.3357x - 0.5414$ ,  $R^2 = 0.9879$ ) with 38  $\mu\text{M}$  detection limit. Selectivity of the proposed biosensor was evaluated by the addition of different interferences in the saliva (Figure 5-5(b)). All interference had little effect for the phosphate amperometric measurement which demonstrated the feasibility of the actual saliva test.

Storage condition of the biosensor was evaluated by different temperature and seal condition (Figure 5-6(c)). The sensor reserved highest response current (91.41%) when sealed under vacuum and stored at 4 °C. The room temperature of 25 °C is detrimental for sensor storage which may result from the increased enzyme denaturation rate under higher temperature. The packing method had little effect (~2% difference) for the sensor which attribute to the storage time of 14 days (short to identify the difference). The stability of the sensor was evaluated and shown in Figure 5-6(d). The current response remained 84.88% of its initial response after storing for three weeks. The results suggested the good stability of the sensor. The reproducibility of the sensor was also evaluated by using five sensors measuring 2 mM phosphate (pH = 6). A standard deviation of 3.5% was obtained, which implied excellent reproducibility of the proposed sensor. Comparison between the proposed sensor with other works for saliva phosphate detection was listed in Table 5-1. The inkjet-printed SPE sensor has gained sufficient improvement from the aspect of measuring time, ease of measurement, linear range extension than the existing electrochemical sensor [42] for saliva phosphate detection.



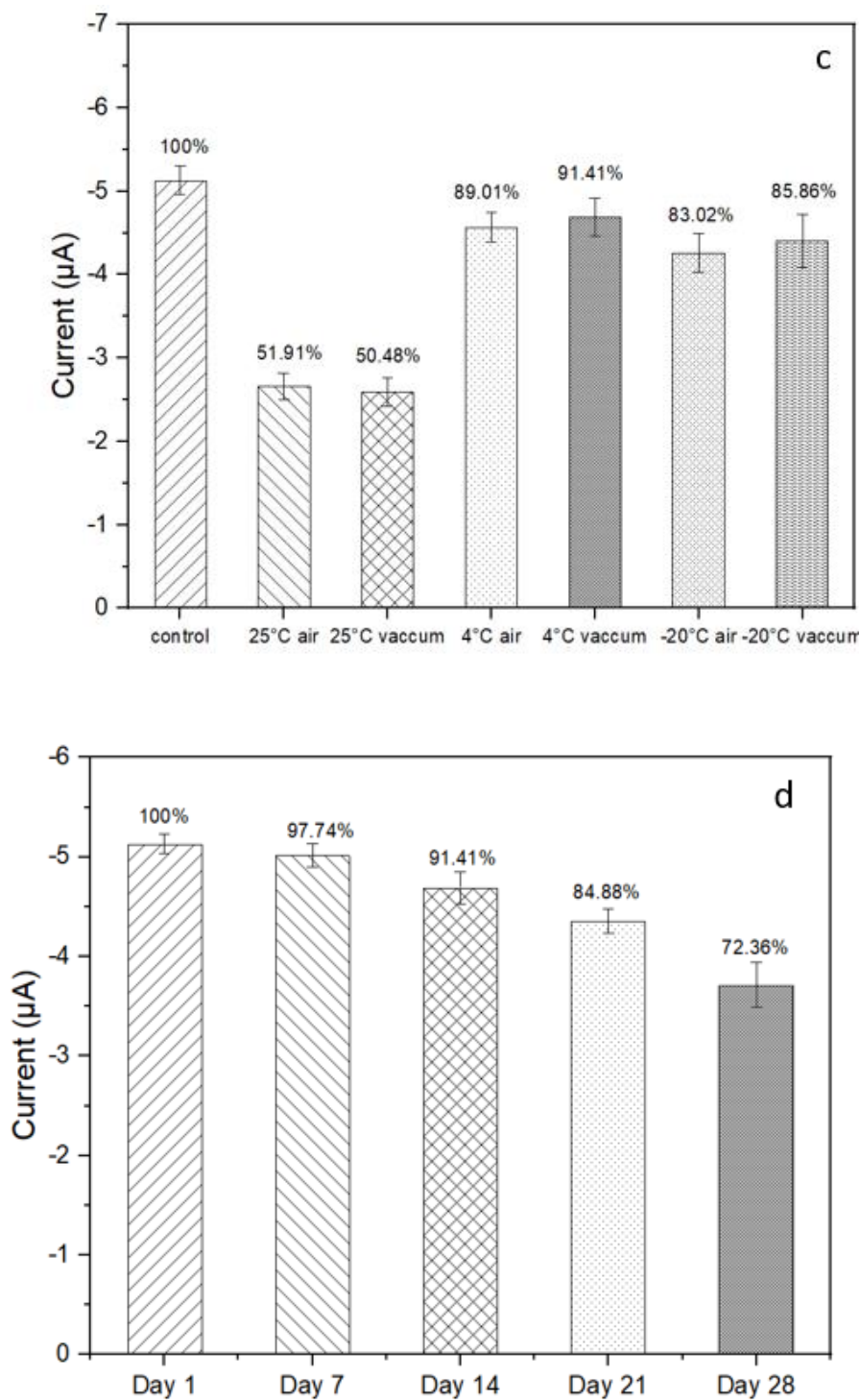


**Figure 5-5: (a) Amperometric responses of the sensor to different concentration of phosphate. Concentration increased with the direction of the orange arrow (from 0**

mM to 2 mM). Inset is the calibration curve for different concentration of phosphate. (b) Anti-interference of the biosensor with the existence of  $\text{NO}_3^-$ , Urea, lactic acid and the mixture in the phosphate solution. (c) Different storage condition after 14 days (control group is the current response on the first day). (d) Stability study of the sensor.

**Table 5-1: Comparison of sensors reported in literature for saliva phosphate detection.**

Type	Testing platform	Methods	Testing platform	Display unit	Linear range/ $\mu\text{M}$	Measuring time	Ref
Chemical sensor	UV/vis spectrometer	Colorimetric assay	UV/vis spectrometer	Computer	24-480	-	[43]
Electrochemical Sensor	Desktop potentiostat	Chronoamperometry	Desktop potentiostat	Computer	7.5-625	4 min	[42]
Optical sensor	Photoluminescence spectrometer	Fluorometric titration	Photoluminescence spectrometer	Computer	1440-8640	30 min	[44]
Electrochemical Sensor	Desktop/portable potentiostat	Chronoamperometry	Desktop/portable potentiostat	Computer/Smartphone	160-2000	10/60 s	This work

#### 5.3.4 Demonstration of the proposed biosensor system

To demonstrate the point-of-care use of the proposed biosensor, we integrated the functionalized screen-printed electrode into our proposed biosensor system. During the demonstration test of saliva phosphate measurement, chronoamperometric method was used. Calibration curve of linear fit was selected and the fitting equation obtained from

the last section was set in the APP. 60 seconds was set for Xenstat potentiostat measurement and end-point value of the chronoamperometric result was selected as the steady state and data processing value. Three concentrations of artificial saliva were tested by using the Xenstat potentiostat (see Table 4-2). The recovery of the biosensor ranged from 89.7% to 94.0% suggesting the potential use of proposed biosensor system for the practical saliva test. The proposed biosensor system is versatile for the detection of other analytes by simply exchanging the sensing elements and adjusting the calibration curve in the settings of the App. The nature of easy operation and miniature size of the sensor system have demonstrated its feasibility of point-of-care analyte detection. Our study will be meaningful for the development of other POC sensor systems.

**Table 5-2: Detection of phosphate using Xenstat portable potentiostat (n=3).**

Sample	Phosphate concentration in sample/mM	Founded phosphate /mM	Recovery/%
Artificial saliva	2.0	1.82	91.0%
	1.75	1.57	89.7%
	1.5	1.41	94.0%

## 5.4 Conclusions

An inkjet-printed and reagentless electrochemical biosensor system was developed for point-of-care application. The proposed system has four components: a smartphone, an Android App, a portable potentiostat and a functionalized screen-printed electrode. Compared with the conventional electrochemical biosensors, the reaction substrate was

preloaded into this system to eliminate the use of electrochemical cell, which is the key strategy to achieve a reagentless and portable system. The layer-by-layer printing strategy offers a novel method for enzyme crosslinking through inkjet printing. The combination of the inkjet printing technique and screen-printed electrode gives the feasibility of customization, high reproducibility and mass production. Through the APP offered by the system, the whole data processing function was automated for the experiment results that an untrained people can easily operate and read the results. Researchers can easily adjust the codes that we provided based on their experiment requirements or simply change the input parameters on the APP. The prototyping biosensor showed a wide linear range (three times than other electrochemical sensors [42]) with quick response time. Good anti-interference property and high stability were achieved. In addition, the recovery rate of as high as 94.0% was achieved through artificial saliva test, suggesting the feasibility of the practical use for the proposed biosensor system.

Our developed biosensor system demonstrated a reliable and reproducible biosensor fabrication route for the reference of POC applications. For future directions to improve this study, real-life application of the proposed biosensor system using natural saliva will be further explored. The functions of the proposed biosensor system can be further extended by exchanging the sensing elements for detection of different analytes and adjusting the calibration curve in the App. Especially, the application of carbon nanotubes has greatly enhanced the performance, thus, utilizing the latest nanomaterials can potentially deliver better analytical performance. The present biosensor framework could result in a lighter and smaller system for a more convenient and practical POC application after further integration.

## References

1. Zarei, M., *Portable biosensing devices for point-of-care diagnostics: Recent developments and applications*. TrAC Trends in Analytical Chemistry, 2017. **91**: p. 26-41.
2. Sun, A.C. and D.A.J.E. Hall, *Point - of - care smartphone - based electrochemical biosensing*. Electroanalysis, 2019. **31**(1): p. 2-16.
3. Kou, X., L. Tong, Y. Shen, W. Zhu, L. Yin, S. Huang, F. Zhu, G. Chen, and G. Ouyang, *Smartphone-assisted robust enzymes@MOFs-based paper biosensor for point-of-care detection*. Biosensors and Bioelectronics, 2020. **156**: p. 112095.
4. Grieshaber, D., R. MacKenzie, J. Vörös, and E. Reimhult, *Electrochemical Biosensors - Sensor Principles and Architectures*. Sensors, 2008. **8**(3): p. 1400.
5. Zhang, L., W. Yang, Y. Yang, H. Liu, and Z. Gu, *Smartphone-based point-of-care testing of salivary  $\alpha$ -amylase for personal psychological measurement*. Analyst, 2015. **140**(21): p. 7399-7406.
6. Shen, X., F. Ju, G. Li, and L.J.S. Ma, *Smartphone-Based Electrochemical Potentiostat Detection System Using PEDOT: PSS/Chitosan/Graphene Modified Screen-Printed Electrodes for Dopamine Detection*. Sensors, 2020. **20**(10): p. 2781.
7. Cai, X., Q. Gao, S. Zuo, H. Zhao, and M.J.E. Lan, *Smartphone - coupled Electrochemical Analysis of Cellular Superoxide Anions Based on  $Mnx(PO_4)_y$  Monolayer Modified Porous Carbon*. Electroanalysis, 2020. **32**(3): p. 598-605.
8. Aronoff-Spencer, E., A.G. Venkatesh, A. Sun, H. Brickner, D. Looney, and D.A. Hall, *Detection of Hepatitis C core antibody by dual-affinity yeast chimera and smartphone-based electrochemical sensing*. Biosens Bioelectron, 2016. **86**: p. 690-696.
9. Jiang, H., J. Yang, K. Wan, D. Jiang, and C. Jin, *Miniaturized Paper-Supported 3D Cell-Based Electrochemical Sensor for Bacterial Lipopolysaccharide Detection*. ACS Sensors, 2020. **5**(5): p. 1325-1335.
10. Loncaric, C., Y. Tang, C. Ho, M.A. Parameswaran, and H.-Z. Yu, *A USB-based electrochemical biosensor prototype for point-of-care diagnosis*. Sensors and Actuators B: Chemical, 2012. **161**(1): p. 908-913.
11. Bihar, E., S. Wustoni, A.M. Pappa, K.N. Salama, D. Baran, and S. Inal, *A fully inkjet-printed disposable glucose sensor on paper*. npj Flexible Electronics, 2018. **2**(1): p. 30.



12. Kaliyaraj Selva Kumar, A., Y. Zhang, D. Li, and R.G. Compton, *A mini-review: How reliable is the drop casting technique?* *Electrochemistry Communications*, 2020. **121**: p. 106867.
13. Li, H., D. Buesen, R. Williams, J. Henig, S. Stapf, K. Mukherjee, E. Freier, W. Lubitz, M. Winkler, and T.J.C.s. Happe, *Preventing the coffee-ring effect and aggregate sedimentation by in situ gelation of monodisperse materials*. 2018. **9**(39): p. 7596-7605.
14. Delaney, J.T., P.J. Smith, and U.S. Schubert, *Inkjet printing of proteins*. *Soft Matter*, 2009. **5**(24): p. 4866-4877.
15. Soltman, D. and V. Subramanian, *Inkjet-Printed Line Morphologies and Temperature Control of the Coffee Ring Effect*. *Langmuir*, 2008. **24**(5): p. 2224-2231.
16. Shen, X., C.-M. Ho, and T.-S. Wong, *Minimal Size of Coffee Ring Structure*. *The Journal of Physical Chemistry B*, 2010. **114**(16): p. 5269-5274.
17. Wang, J., *Nanomaterial-based electrochemical biosensors*. *Analyst*, 2005. **130**(4): p. 421-426.
18. Maduraiveeran, G., M. Sasidharan, and V. Ganesan, *Electrochemical sensor and biosensor platforms based on advanced nanomaterials for biological and biomedical applications*. *Biosensors and Bioelectronics*, 2018. **103**: p. 113-129.
19. Arduini, F., L. Micheli, D. Moscone, G. Palleschi, S. Piermarini, F. Ricci, and G. Volpe, *Electrochemical biosensors based on nanomodified screen-printed electrodes: Recent applications in clinical analysis*. *TrAC Trends in Analytical Chemistry*, 2016. **79**: p. 114-126.
20. Savica, V., L.A. Calo, A. Granata, R. Caldarella, A. Cavaleri, D. Santoro, P. Monardo, R. Savica, U. Muraca, and G. Bellinghieri, *A new approach to the evaluation of hyperphosphatemia in chronic kidney disease*. *Clin Nephrol*, 2007. **68**(4): p. 216-21.
21. Savica, V., L.A. Calo, R. Caldarella, A. Cavaleri, A. Granata, D. Santoro, R. Savica, U. Muraca, A. Mallamace, and G. Bellinghieri, *Phosphate salivary secretion in hemodialysis patients: implications for the treatment of hyperphosphatemia*. *Nephron Physiol*, 2007. **105**(3): p. p52-5.
22. Ben-Aryeh, H., S. Filmar, D. Gutman, R. Szargfl, and E. Paldi, *Salivary phosphate as an indicator of ovulation*. *American Journal of Obstetrics & Gynecology*, 1976. **125**(6): p. 871-874.
23. Alagendran, S., G. Archunan, E.O. Armando, and R.G. Guzman, *Evaluation of salivary electrolytes during normal menstrual cycle with special reference to ovulation*. *American Journal of Applied Sciences*, 2010. **7**(8): p. 1066.

24. Blum, M., S. Zurkowsky, J. Gilad, and A. Aviram, *Salivary phosphate and calcium concentrations in uremia*. *Clinical nephrology*, 1979. **12**(4): p. 191-192.
25. Larsen, M. and E. Pearce, *Saturation of human saliva with respect to calcium salts*. *Archives of Oral Biology*, 2003. **48**(4): p. 317-322.
26. Yang, L., D. Chen, X. Wang, B. Luo, C. Wang, G. Gao, H. Li, A. Li, and L.J.R.A. Chen, *Ratiometric electrochemical sensor for accurate detection of salicylic acid in leaves of living plants*. 2020. **10**(64): p. 38841-38846.
27. Chiang, Y.-C., W.-H. Lin, and Y.-C. Chang, *The influence of treatment duration on multi-walled carbon nanotubes functionalized by H<sub>2</sub>SO<sub>4</sub>/HNO<sub>3</sub> oxidation*. *Applied Surface Science*, 2011. **257**(6): p. 2401-2410.
28. Gal, J.-Y., Y. Fovet, and M. Adib-Yadzi, *About a synthetic saliva for in vitro studies*. *Talanta*, 2001. **53**(6): p. 1103-1115.
29. Bao, C., M. Kaur, and W.S. Kim, *Toward a highly selective artificial saliva sensor using printed hybrid field effect transistors*. *Sensors and Actuators B: Chemical*, 2019. **285**: p. 186-192.
30. Verma, M.L., M. Naebe, C.J. Barrow, and M. Puri, *Enzyme Immobilisation on Amino-Functionalised Multi-Walled Carbon Nanotubes: Structural and Biocatalytic Characterisation*. *PLOS ONE*, 2013. **8**(9): p. e73642.
31. Prlainović, N.Ž., D.I. Bezbradica, J.R. Rogan, P.S. Uskoković, D.Ž. Mijin, and A.D. Marinković, *Surface functionalization of oxidized multi-walled carbon nanotubes: Candida rugosa lipase immobilization*. *Comptes Rendus Chimie*, 2016. **19**(3): p. 363-370.
32. Wang, T., C. Cook, and B. Derby. *Fabrication of a Glucose Biosensor by Piezoelectric Inkjet Printing*. in *2009 Third International Conference on Sensor Technologies and Applications*. 2009.
33. Cinti, S., D. Talarico, G. Palleschi, D. Moscone, and F. Arduini, *Novel reagentless paper-based screen-printed electrochemical sensor to detect phosphate*. *Analytica Chimica Acta*, 2016. **919**: p. 78-84.
34. Sassolas, A., L.J. Blum, and B.D. Leca-Bouvier, *Immobilization strategies to develop enzymatic biosensors*. *Biotechnology advances*, 2012. **30**(3): p. 489-511.
35. Sheldon, R.A. and S. van Pelt, *Enzyme immobilisation in biocatalysis: why, what and how*. *Chemical Society Reviews*, 2013. **42**(15): p. 6223-6235.
36. Bai, Y., D. Zhang, Q. Guo, J. Xiao, M. Zheng, and J. Yang, *Study of the Enzyme Activity Change due to Inkjet Printing for Biosensor Fabrication*. *ACS Biomaterials Science & Engineering*, 2021.

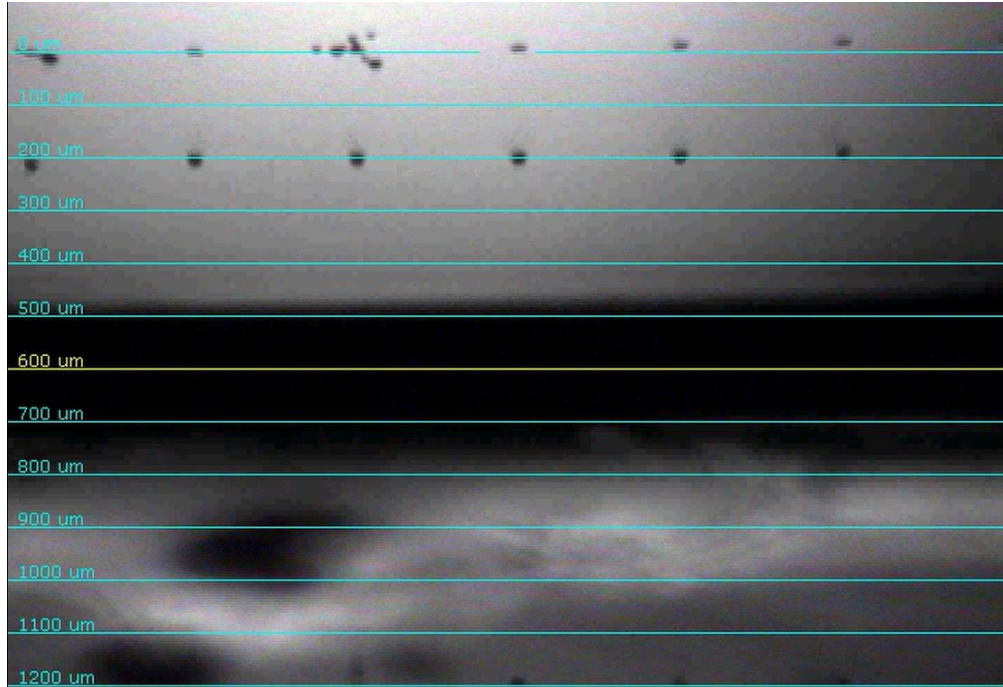
37. Wang, J. and M. Musameh, *Carbon nanotube screen-printed electrochemical sensors*. *Analyst*, 2004. **129**(1): p. 1-2.
38. Ogabiela, E., S.B. Adeloju, J. Cui, Y. Wu, and W. Chen, *A novel ultrasensitive phosphate amperometric nanobiosensor based on the integration of pyruvate oxidase with highly ordered gold nanowires array*. *Biosensors and Bioelectronics*, 2015. **71**: p. 278-285.
39. Rahman, M.A., D.-S. Park, S.-C. Chang, C.J. McNeil, and Y.-B. Shim, *The biosensor based on the pyruvate oxidase modified conducting polymer for phosphate ions determinations*. *Biosensors and Bioelectronics*, 2006. **21**(7): p. 1116-1124.
40. Cui, J., E.E. Ogabiela, J. Hui, Y. Wang, Y. Zhang, L. Tong, J. Zhang, S.B. Adeloju, X. Zhang, and Y. Wu, *Electrochemical Biosensor based on Pt/Au Alloy Nanowire Arrays for Phosphate Detection*. *Journal of The Electrochemical Society*, 2015. **162**(3): p. B62-B67.
41. Wang, J. and Z.J.T.T.P. Zhang, *Analytical chemistry*. 1994.
42. Kwan, R.C.H., H.F. Leung, P.Y.T. Hon, H.C.F. Cheung, K. Hirota, and R. Renneberg, *Amperometric biosensor for determining human salivary phosphate*. *Analytical Biochemistry*, 2005. **343**(2): p. 263-267.
43. Tobey, S.L. and E.V. Anslyn, *Determination of Inorganic Phosphate in Serum and Saliva Using a Synthetic Receptor*. *Organic Letters*, 2003. **5**(12): p. 2029-2031.
44. Saikia, G. and P.K. Iyer, *A Remarkable Superquenching and Superdequenching Sensor for the Selective and Noninvasive Detection of Inorganic Phosphates in Saliva*. *Macromolecules*, 2011. **44**(10): p. 3753-3758.

## Appendices

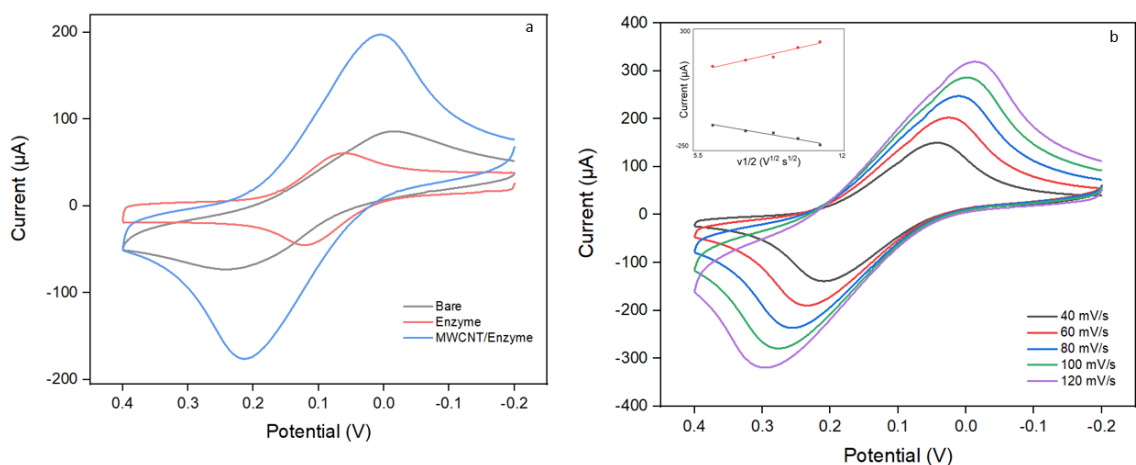
### Appendix 5-1: Ink formula and composition for each printing layer.

Ink	Formula	Concentration	Solvent
1	Pyruvate	16 U/ml	CB
	TPP	25 $\mu$ M	
	FAD	6 $\mu$ M	
	MgCl <sub>2</sub>	2.0 mM	
	Pyruvate acid	2.0 mM	
	MWCNT	0.5 mg/ml	
	BSA	2.5 % w/v	
	Triton X-100	0.0075 % v/v	
2	GLA	2.5 % w/v	DI
	Triton X-100	0.006 % v/v	
3	Nafion	1.7 % w/v	DI
	Triton X-100	0.005 % v/v	

**Appendix 5-2: Stable droplet array (Nozzles are positioned at the 0-micron mark, perfect round droplets are shown at the 200-micron mark).**



**Appendix 5-3: (a) CV curves of bare electrode (black line), enzyme/substrate/cofactor electrode (red line) and MWCNT-COOH/enzyme/substrate/cofactor electrode (blue line) in 0.1 M KCl which contained 10 mM  $K_3Fe(CN)_6$ . Scan rate: 50 mV/s. (b) Cyclic voltammograms of modified electrode in 0.1M KCL which contained 10 mM  $K_3Fe(CN)_6$  at scan rate of 40, 60, 80 100, 120 mV/s (inset: the plot of peak current vs. square root of scan rates).**



#### Appendix 5-4: Code of the parameter page for settings of the calibration curve

```

/**
 * Code of the parameter page for settings of the calibration curve
 */

@Nullable
@Override

/**
 * Define variables
 */

public View onCreateView(@NonNull LayoutInflater inflater, @Nullable ViewGroup
container, @Nullable Bundle savedInstanceState) {

    View view = inflater.inflate(R.layout.parameters_fragment, container, false);

    mSideIcon = view.findViewById(R.id.side_icon);

    mSave = view.findViewById(R.id.save);

    mLinerInputA = view.findViewById(R.id.liner_input_a);

    mLinerInputB = view.findViewById(R.id.liner_input_b);

    mLogInputA = view.findViewById(R.id.log_input_a);

    mLogInputB = view.findViewById(R.id.log_input_b);

    mSideIcon.setOnClickListener(this);

    mSave.setOnClickListener(this);

    mCheckBoxLinear = view.findViewById(R.id.checkbox_linear);

```

```

    mCheckBoxLog = view.findViewById(R.id.checkbox_log);

    mCheckBoxLinear.setOnCheckedChangeListener(this);

    mCheckBoxLog.setOnCheckedChangeListener(this);

/**
 * Display the previous settings
 */

    type = Integer.parseInt(Tools.readerLocalMessage(getActivity(), "type", "0"));
    if (type == 1) {
        mCheckBoxLinear.setChecked(true);

        mLinerInputA.setText(Tools.readerLocalMessage(getActivity(), "a", "0"));
        mLinerInputB.setText(Tools.readerLocalMessage(getActivity(), "b", "0"));
    } else if (type == 2) {
        mCheckBoxLog.setChecked(true);

        mLogInputA.setText(Tools.readerLocalMessage(getActivity(), "a", "0"));
        mLogInputB.setText(Tools.readerLocalMessage(getActivity(), "b", "0"));
    }

    return view;
}

@Override

/**
 * Set and save the parameters of the calibration curve
 */

    public void onClick(View v) {

```



```

switch (v.getId()) {
    case R.id.side_icon:
        openSideMenu();
        break;
    case R.id.save:
        if (type == 0) {
            Toast.makeText(getActivity(), getActivity().getString(R.string.selectType),
Toast.LENGTH_SHORT).show();
        } else if (type == 1) {
            if (TextUtils.isEmpty(mLinerInputA.getText().toString()) ||
TextUtils.isEmpty(mLinerInputB.getText().toString())) {
                Toast.makeText(getActivity(), getActivity().getString(R.string.inputNum),
Toast.LENGTH_SHORT).show();
                return;
            } else {
                Tools.putLocalMessage(getActivity(), "type", type + "");
                Tools.putLocalMessage(getActivity(), "a", mLinerInputA.getText().toString());
                Tools.putLocalMessage(getActivity(), "b", mLinerInputB.getText().toString());
                Toast.makeText(getActivity(), getActivity().getString(R.string.save_success),
Toast.LENGTH_SHORT).show();
            }
        } else if (type == 2) {
            if (TextUtils.isEmpty(mLogInputA.getText().toString()) ||

```

```

TextUtils.isEmpty(mLogInputB.getText().toString()) {
    Toast.makeText(getActivity(), getActivity().getString(R.string.inputNum),
Toast.LENGTH_SHORT).show();

    return;
} else {
    Tools.putLocalMessage(getActivity(), "type", type + "");
    Tools.putLocalMessage(getActivity(), "a", mLogInputA.getText().toString()
    Tools.putLocalMessage(getActivity(), "b", mLogInputB.getText().toString()
    Toast.makeText(getActivity(), getActivity().getString(R.string.save_success),
Toast.LENGTH_SHORT).show();
    }
}
break;
}
}
@Override

/**
 * Change the fitting method
 */
public void onCheckedChanged(CompoundButton buttonView, boolean isChecked) {
    if ("Linear".equals(buttonView.getText().toString()) && isChecked) {
        type = 1;
        mCheckBoxLog.setChecked(false);

```

```
}  
  
if ("Log".equals(buttonView.getText().toString()) && isChecked) {  
    type = 2;  
    mCheckBoxLinear.setChecked(false);  
}  
  
if (!mCheckBoxLinear.isChecked() && !mCheckBoxLog.isChecked()) {  
    type = 0;  
}  
}
```

**Appendix 5-5: Code for the Calculation page**

```

/**
 * Code for the Calculation page
 */
{
    @Nullable
    @Override

/**
 * Define variables
 */

    public View onCreateView(@NonNull LayoutInflater inflater, @Nullable ViewGroup
container, @Nullable Bundle savedInstanceState) {

        View view = inflater.inflate(R.layout.calculate_fragment, container, false);

        mSideIcon = view.findViewById(R.id.side_icon);

        mListview = view.findViewById(R.id.listview);

        mCalculation = view.findViewById(R.id.calculation);

        mModify = view.findViewById(R.id.modify);

        mSave = view.findViewById(R.id.save);

        mInput_time = view.findViewById(R.id.input_time);

        mRadioButtonMax = view.findViewById(R.id.max);

        mRadioButtonMin = view.findViewById(R.id.min);

        mRadioButtonTime = view.findViewById(R.id.time);

        mCalibration_curve = view.findViewById(R.id.calibration_curve);

```

```

mChart = view.findViewById(R.id.chart);

mSideIcon.setOnClickListener(this);

mCalculation.setOnClickListener(this);

mSave.setOnClickListener(this);

mModify.setOnClickListener(this);

mPointList = new ArrayList<>();

resulteJson = new JSONObject();

mType = Tools.readerLocalMessage(getActivity(), "type", "0");

mRadioButtonMax.setOnCheckedChangeListener(this);

mRadioButtonMin.setOnCheckedChangeListener(this);

mRadioButtonTime.setOnCheckedChangeListener(this);

mListView.setOnClickListener(new AdapterView.OnItemClickListener() {

    @Override

    public void onItemClick(AdapterView<?> parent, View view, int position, long id) {

/**

 * Choose the file that needs to be analyzed

 **/

        mPointList.clear();

        String data = readTxtFile(mFileList.get(position));

        try {

            JSONObject jsonObject = new JSONObject(data);

            Date date = new Date();

            String strDateFormat = "yyyy-MM-dd HH:mm:ss";

```

```

SimpleDateFormat sdf = new SimpleDateFormat(strDateFormat);
Tools.putLocalMessage(getActivity(), "time", sdf.format(date));
Tools.putLocalMessage(getActivity(), "fileName",
JSONObject.getString("fileName"));

Tools.putLocalMessage(getActivity(), "note", JSONObject.getString("note"));
JSONArray jsonArray = JSONObject.getJSONArray("data");
for (int i = 0; i < jsonArray.length(); i++) {
    Point point = new Point(jsonArray.getJSONArray(i).getDouble(0),
JSONArray.getJSONArray(i).getDouble(1));

    entries.add(new Entry((float) point.getX(), (float) point.getY()));
    mPointList.add(point);
}
String label;

/**
 * Draw the electrochemical curve according to different experiments
 */

if ("it".equals(JSONObject.getString("method"))) {
    label = "X:Time s    Y:Current  $\mu$ A";
} else {
    label = "X:Potential mV    Y:Current  $\mu$ A";
}

LineDataSet dataSet = new LineDataSet(entries, label);
LineData lineData = new LineData(dataSet);

```

```

        mChart.setData(lineData); // insert the data in the chart

        mChart.invalidate(); // update the chart

        mChart.setContentDescription("");

        XAxis xAxis = mChart.getXAxis();

        xAxis.setPosition(XAxis.XAxisPosition.BOTTOM);

        YAxis yAxis = mChart.getAxisRight();

        yAxis.setEnabled(false);

        mListView.setVisibility(View.GONE);

        mChart.getDescription().setEnabled(false);

        setDefaultValue();

    } catch (JSONException e) {

        e.printStackTrace();

    }

}

});

setFileList();

return view;

}

@Override

public void onResume() {

    super.onResume();

}

/**

* Display the equation of the calibration curve for data processing

```



```

**/

String type = Tools.readerLocalMessage(getActivity(), "type", "0");
String tempA = Tools.readerLocalMessage(getActivity(), "a", "9999");
String tempB = Tools.readerLocalMessage(getActivity(), "b", "9999");

if (type.equals("0")) {
    Toast.makeText(getActivity(), getActivity().getString(R.string.selectCaluType),
    Toast.LENGTH_SHORT).show();
    else if (type.equals("1")) {
        if (Double.parseDouble(tempB) < 0) {

mCalibration_curve.setText(getActivity().getResources().getString(R.string.linear_format_0,
tempA, tempB));
        else {
mCalibration_curve.setText(getActivity().getResources().getString(R.string.linear_format,
tempA, tempB));
        }
    } else if (type.equals("2")) {
        if (Double.parseDouble(tempB) < 0) {

mCalibration_curve.setText(getActivity().getResources().getString(R.string.log_format_0,
tempA, tempB));
        else {
mCalibration_curve.setText(getActivity().getResources().getString(R.string.log_format,

```



```

tempA, tempB));
    }
}
}
/**
 * Read the data in the selected file
 **/

private void setDefaultValue() {
    String selectXY = Tools.readerLocalMessage(getActivity(), "selectXY", "0");
    if (mPointList.size() > 0) {
        tempPonit = mPointList.get(0);
    } else {
        Toast.makeText(getActivity(), getActivity().getString(R.string.NoPoint),
Toast.LENGTH_SHORT).show();

        return;
    }
    if (selectXY.equals("1")) {
        setMaxValue();
        mRadioButtonMax.setChecked(true);
    } else if (selectXY.equals("2")) {
        setMinValue();
        mRadioButtonMin.setChecked(true);
    } else if (selectXY.equals("3")) {

```

```

        setTimeValue();

        mRadioButtonTime.setChecked(true);
    }
}

private void setFileList() {
    File file = new File(Environment.getExternalStorageDirectory().getPath() + "/xenstat");

    mFileList = new ArrayList<>();
    File[] array = file.listFiles();

    if (array == null) {
        TextView textView = new TextView(getActivity());
        textView.setText("No Date");
        textView.setTextColor(Color.parseColor("#000000"));
        textView.setTextSize(24);

        mListView.setEmptyView(textView);

        return;
    }

    for (int i = 0; i < array.length; i++) {
        File temp = array[i];

        mFileList.add(temp);
    }

    MyAdapter myAdapter = new MyAdapter(getActivity(), mFileList, new CallBack() {
        @Override

```

```

    public void callback(int index) {
        mFileList.remove(index);
    }
});

mListView.setAdapter(myAdapter);
}

@Override

public void onClick(View v) {
    switch (v.getId()) {
        case R.id.side_icon:
            openSideMenu();
            break;
        case R.id.save:
/**
 * Save the calibration curve
 */
            if (!mRadioButtonMin.isChecked() && !mRadioButtonMax.isChecked() &&
!mRadioButtonTime.isChecked()) {
                Toast.makeText(getActivity(), getString(R.string.selectPoint),
Toast.LENGTH_SHORT).show();
            } else {
                if (tempPonit != null) {
                    Tools.putLocalMessage(getActivity(), "X", tempPonit.getX() + "");

```

```

        Tools.putLocalMessage(getActivity(), "Y", tempPonit.getY() + "");
        Toast.makeText(getActivity(), getString(R.string.save_data),
Toast.LENGTH_SHORT).show();
    }
}
break;

/**
 * Process the data file according to the calibration curve
 */

    case R.id.modify:
        ((MainActivity) getActivity()).showParametersFragment();
        break;

/**
 * Modify the calibration curve
 */

    case R.id.calculation:
        String selectXY = Tools.readerLocalMessage(getActivity(), "selectXY", "0");
        if ("3".equals(selectXY)) {
            setTimeValue();
        }
        if (tempPonit == null) {
            Toast.makeText(getActivity(), getActivity().getString(R.string.selectType),
Toast.LENGTH_SHORT).show();

```

```

    }
    try {
        String type = Tools.readerLocalMessage(getActivity(), "type", "0");
        if ("0".equals(type)) {
            Toast.makeText(getActivity(), getActivity().getString(R.string.selectType),
Toast.LENGTH_SHORT).show();

            return;
        }
        String tempA = Tools.readerLocalMessage(getActivity(), "a", "9999");
        String tempB = Tools.readerLocalMessage(getActivity(), "b", "9999");
        double a = Double.parseDouble(tempA);
        double b = Double.parseDouble(tempB);
        double resultX = 0;
        if (type.equals("1")) { // "y = ax + b"
            if (a != 0) {
                resultX = (tempPonit.getY() - b) / a;
            } else {
                Toast.makeText(getActivity(), getActivity().getString(R.string.errorA),
Toast.LENGTH_SHORT).show();
            }
        }
        } else if (type.equals("2")) { // x = 10^((y-b)/a)
            resultX = Math.pow(10, (tempPonit.getY() - b) / a);
        }
    }
}

```

```

        DecimalFormat df = new
DecimalFormat(getActivity().getString(R.string.reslut_num));

        Tools.putLocalMessage(getActivity(), "resultX", df.format(resultX) + "");
        Tools.putLocalMessage(getActivity(), "X", tempPonit.getX() + "");
        Tools.putLocalMessage(getActivity(), "Y", tempPonit.getY() + "");
        ((MainActivity) getActivity()).showResultFragment();
    } catch (Exception e) {
        e.printStackTrace();
    }
    break;
}
}
/**
 * Save the results
 */
private void setMinValue() {
    Tools.putLocalMessage(getActivity(), "selectXY", "2");
    for (int i = 0; i < mPointList.size(); i++) {
        if (tempPonit.getY() > mPointList.get(i).getY()) {
            tempPonit = mPointList.get(i);
        }
    }
}
}
}

```

```

private void setMaxValue() {
    Tools.putLocalMessage(getActivity(), "selectXY", "1");
    for (int i = 0; i < mPointList.size(); i++) {
        if (tempPonit.getY() < mPointList.get(i).getY()) {
            tempPonit = mPointList.get(i);
        }
    }
}

private void setTimeValue() {
    boolean obtainValue = false;
    Tools.putLocalMessage(getActivity(), "selectXY", "3");
    for (int i = 0; i < mPointList.size(); i++) {
        if (!TextUtils.isEmpty(mInput_time.getText().toString())) {
            if (Double.parseDouble(mInput_time.getText().toString()) ==
mPointList.get(i).getX()) {
                tempPonit = mPointList.get(i);
                obtainValue = true;
            }
        }
    }
    if (!obtainValue) {
        tempPonit = null;
    }
}

```

```
}  
  
private boolean getState(RadioButton radioButton, String tag) {  
    return tag.equals((String) (radioButton.getTag()));  
}  
  
}
```



## Chapter 6

### 6 Thesis summary and further direction

This thesis focuses on inkjet printing biosensors for point-of-care applications in the following three important aspects:

- (1) the effect of mechanical stress on enzymes during inkjet printing process;
- (2) multi-functional layer printing strategy for sensor fabrication;
- (3) the built-up of the inkjet-printed smartphone-supported biosensor platform for point-of-care analyte detection.

They are summarized according to the thesis structures as follows. Subsequently, contributions of this thesis and the future directions are discussed.

#### 6.1 Thesis summary

The effect of wave propagation induced mechanical stress on the activity of pyruvate oxidase is studied in Chapter 3. It is found that pyruvate oxidase activity was positively influenced by the mechanical stress. The change in protein conformation was caused by mechanical activation or mild proteolysis. It is also found that the printing frequency had less effect on the catalytic ability of pyruvate oxidase since a limited change of wave superposition was induced. The mechanical stress induced by printing voltage had a significant effect on the catalytic efficiency of pyruvate oxidase, and low shear stress tended to create higher enhancement for the activity. Partial denaturation and mechanical

activation of the enzymes occurred simultaneously when higher mechanical stress was induced. Protein structural change varied due to the property of the different protein.

Chapter 4 presents a simple and effective surface functionalization strategy to achieve enzyme crosslinking through inkjet printing technique for the construction of a reagentless enzyme-based biosensor. This study combined the drop-on-demand inkjet printing technique with easily mass-produced screen-printed electrode. The proposed sensor system can be industrialized for on-site phosphate detection with minimum sample required (30  $\mu$ l) when coupled with substrate preloading strategy. Ink formula and printing strategy of multiple functionalization layers for sensor fabrication were demonstrated. It is found that electrode functionalized method by inkjet printing achieved more uniform deposition and enhanced analytical performance than that of drop casting method. The applicability of the developed printing strategy for sensor fabrication was proven by successfully detecting the phosphate in the artificial serum. A wide linear range was achieved that covered the physiological range of serum phosphate (0.2–2.0 mM). Excellent anti-interference performance towards common anions, satisfactory reproducibility and stability indicated the practical use of the proposed sensor. The validity test achieved an excellent recovery of 98.9-103% with a cost of less than 1.34 USD. Our proposed novel surface functionalization method avoids any other post-treatment and only involves printing procedures. More importantly, as a simple, affordable, labour-free and reagentless approach, this sensor fabrication practice can be easily applied to fabricate other enzyme-base biosensors by simply modifying the enzyme in the ink components.

In Chapter 5, an inkjet-printed reagentless electrochemical biosensor system was developed for point-of-care application. The proposed system consists of a smartphone, an Android APP, a portable potentiostat and a functionalized screen-printed electrode. The reaction substrate was preloaded into this system to eliminate the use of electrochemical cell. The combination of the inkjet printing technique and screen-printed electrode gives the feasibility of customization, high reproducibility and mass production. Through the APP offered by the system, the whole data processing function was automated for the experiment results, so that an untrained people can easily operate and read the results. The prototyping biosensor showed a wide linear range (three times than other electrochemical sensors) with quick response time. High selectivity and stability of the sensor demonstrate its practical use for saliva test. In addition, the recovery of as high as 94.0% can be achieve, suggesting the potentiality of the proposed biosensor system in real life application. The proposed biosensor system can be applicable for various analyte detection by exchanging the sensing elements and reagents. This novel integrated biosensor system has great potentiality for point-of-care applications. Our proposed sensor system demonstrates a reliable and reproducible biosensor fabrication route that has meaningful reference for similar point-of-care biosensor systems.

## 6.2 Thesis contribution

Three major contributions of this thesis are summarized as:

1. The influence of printing parameters from the aspect of the pressure wave propagation mechanism on the biological materials of enzymes were studied to meet the gap in the bioprinting area. The results of this paper are favorable for the fabrication of future biosensors to increase their sensitivity and stability. This study points out that ink formula

and printing parameters for enzyme ink need to be adjusted based on not only the requirement of drop formation but also the stability of the enzyme in the ink. The practice of correlating the pressure wave propagation and the corresponding mechanical stress with the change in the enzyme activity is meaningful for other studies about enzyme printing.

2. A simple and universal surface functionalization strategy for reagentless enzyme-based biosensor was developed through a novel inkjet printing assisted enzyme crosslinking method. The proposed ink formula and printing strategy of multiple functionalization layers for sensor fabrication would be useful for other inkjet printing biosensor manufacturing in pursuit of high reproducibility and high stability. As a simple, affordable, labor-free and reagentless approach, this sensor fabrication practice can be easily applied to measure other analytes of interest by simply modifying the ink components.

3. An inkjet-printed electrochemical enzyme-based biosensor system was developed to work with the smartphone for the point-of-care analyte detection. The proposed biosensor system can be applicable for various analyte detection by exchanging the sensing elements and reagents. And the biosensor system can be easily operated by users without specific training. In all, this novel integrated biosensor system has great potentiality for point-of-care applications.

### 6.3 Future direction

The studies about effect of ink printing on the enzymes have been reviewed and further studied in chapter 3. Current studies mainly based on correlations between enzyme

activity and printing parameters (for previous studies) or applied stress/forces (in this thesis). Further investigation can be achieved by studies the change of enzyme structure after printing at the molecular level using cryoelectron microscopy (Cryo-ET). A more universal model for enzyme activity change after printing is expected to adapt to various kinds of enzymes for a broad future application of bioprinting.

Also, the multi-functional layer printing strategy for biosensor construction as mentioned in chapter 4 can inspire and promote research in the fabrication of many other inkjet-printed biosensors. Further improvement of this printing strategy is achievable. For example, the application of carbon nanotubes in the enzyme layer can be exchanged by the latest nanomaterials in pursuit of enhanced analytical performance of the biosensor.

The proposed biosensor system demonstrated in chapter 5 can be widely applicable for detection of various analytes, especially in detection and monitoring disease-related biomarkers in the body fluid. The functions of the proposed biosensor system can be further extended by exchanging the sensing elements for detection of different analytes and adjusting the calibration curve in the APP. In addition, real-life application for point-of-care testing using natural saliva or body fluid is expected for further improvement of the proposed biosensor system, since only artificial saliva was used in the thesis to verify the sensor. At last, with the development of compact and integrated potentiostat or analyzing chip, the present biosensor framework could result in a lighter and smaller system for a more convenient and practical POC application.

## Curriculum Vitae

**Name:** Yang Bai

**Post-secondary Education and Degrees:**

University of Science and Technology Beijing (USTB)  
Beijing, China  
2010-2014 B.A. in Metallurgical Engineering

University of Science and Technology Beijing (USTB)  
Beijing, China  
2011-2014 B.A. in English

University of Chinese Academy of Sciences (UCAS)  
Beijing, China  
2014-2017 M.A. in Materials Engineering

The University of Western Ontario (UWO)  
London, Ontario, Canada  
2017-2021 Ph.D. in Biomedical Engineering

**Honours and Awards:**

People's Scholarship  
2012, 2013

Triple-A Student  
2013, 2016

School's Academic Scholarship  
2014-2017

Outstanding student leader award  
2016-2017

Chinese scholarship council (CSC) scholarship  
2017-2021

**Related Work Experience**

Teaching Assistant  
The University of Western Ontario  
2017-2021

### Publications:

**Yang Bai**, Qiuquan Guo, Junfeng Xiao, Mingyue Zheng, Dongxing Zhang, and Jun Yang. "An inkjet-printed smartphone-supported electrochemical biosensor system for reagentless point-of-care analyte detection." *Sensors & Actuators, B: Chemical*, available online 16 July 2021, 130447.

**Yang Bai**, Dongxing Zhang, Junfeng Xiao, Mingyue Zheng, Qiuquan Guo, and Jun Yang. "An inkjet printing assisted surface functionalization method for enzyme immobilization to develop a reagentless enzyme-based biosensor." *Applied Materials Interfaces* (under review)

**Yang Bai**, Peipei Jia, Qiuquan Guo, Junfeng Xiao, Mingyue Zheng, Dongxing Zhang, and Jun Yang. "Highly sensitive phosphate sensor based on optical fiber surface plasmon resonance." *Applied Sciences* (in preparation)

**Yang Bai**, Dongxing Zhang, Qiuquan Guo, Junfeng Xiao, Mingyue Zheng, and Jun Yang. "Study of the Enzyme Activity Change due to Inkjet Printing for Biosensor Fabrication." *ACS Biomaterials Science & Engineering* 7, no. 2 (2021): 787-793.

Mingyue Zheng, Qiuquan Guo, Xiangyu Yin, Nuwansiri Nirosh Getangama, John R. de Bruyn, Junfeng Xiao, **Yang Bai**, Mei Liu, and Jun Yang. "Direct ink writing of recyclable and in situ repairable photothermal polyurethane for sustainable 3D printing development." *Journal of Materials Chemistry A* 9, no. 11 (2021): 6981-6992.

Dongxing Zhang, Junfeng Xiao, **Yang Bai**, Qiuquan Guo, Mingyue Zheng, Mei Liu, Carolyn Moorlag, and Jun Yang. "Introducing Bioinspired Initiator into Resins for In Situ Repairing of 3D-Printed Metallic Structures." *ACS Applied Materials & Interfaces* 12, no. 43 (2020): 49073-49079.

Jiajun Li, Bin Li, Yong-gang Zuo, Hao Liu, **Yang Bai**, Hwei Yuan, Zhenrui Li, Kai Xu, and Guang-chao Chen. "Application of dual radio frequency inductive coupled plasma into CVD diamond growth." *Vacuum* 154 (2018): 174-176.

Yonggang Zuo, Jiajun Li, **Yang Bai**, Hao Liu, Hwei Yuan, and Guangchao Chen. "Growth of nanocrystalline diamond by dual radio frequency inductively coupled plasma jet CVD." *Diamond and Related Materials* 73 (2017): 67-71.

**Yang Bai**, Yonggang Zuo, Jiajun Li, Hao Liu, Hwei Yuan, and Guangchao Chen. "Effect of water-cooling and sheath gas-cooling in a jet driven by RF-ICP studied by means of numerical simulation." *Diamond and Related Materials* 73 (2017): 72-79.

Jiajun Li, Hao Liu, Yonggang Zuo, **Yang Bai**, Hwei Yuan, Qiyu He, Long Jiang, Hui Guo, Zhenlu Sun, and Guangchao Chen "Analysis of Adhesive Strength between Magnetron Sputtered Copper Films and Substrate." *Chinese Journal of Materials Research*. 30.8 (2016): 634-640.

Yanchao Shi, Bin Li, Jiajun Li, Yonggang Zuo, **Yang Bai**, Hao Liu, Zhanfeng Sun, Dianli Ma, and Guangchao Chen. Deposition of Diamond by RF Plasma Jet CVD and Doping of Ni-N Complex. *Journal of Synthetic Crystals*, 44.10 (2015): 2670-2678.